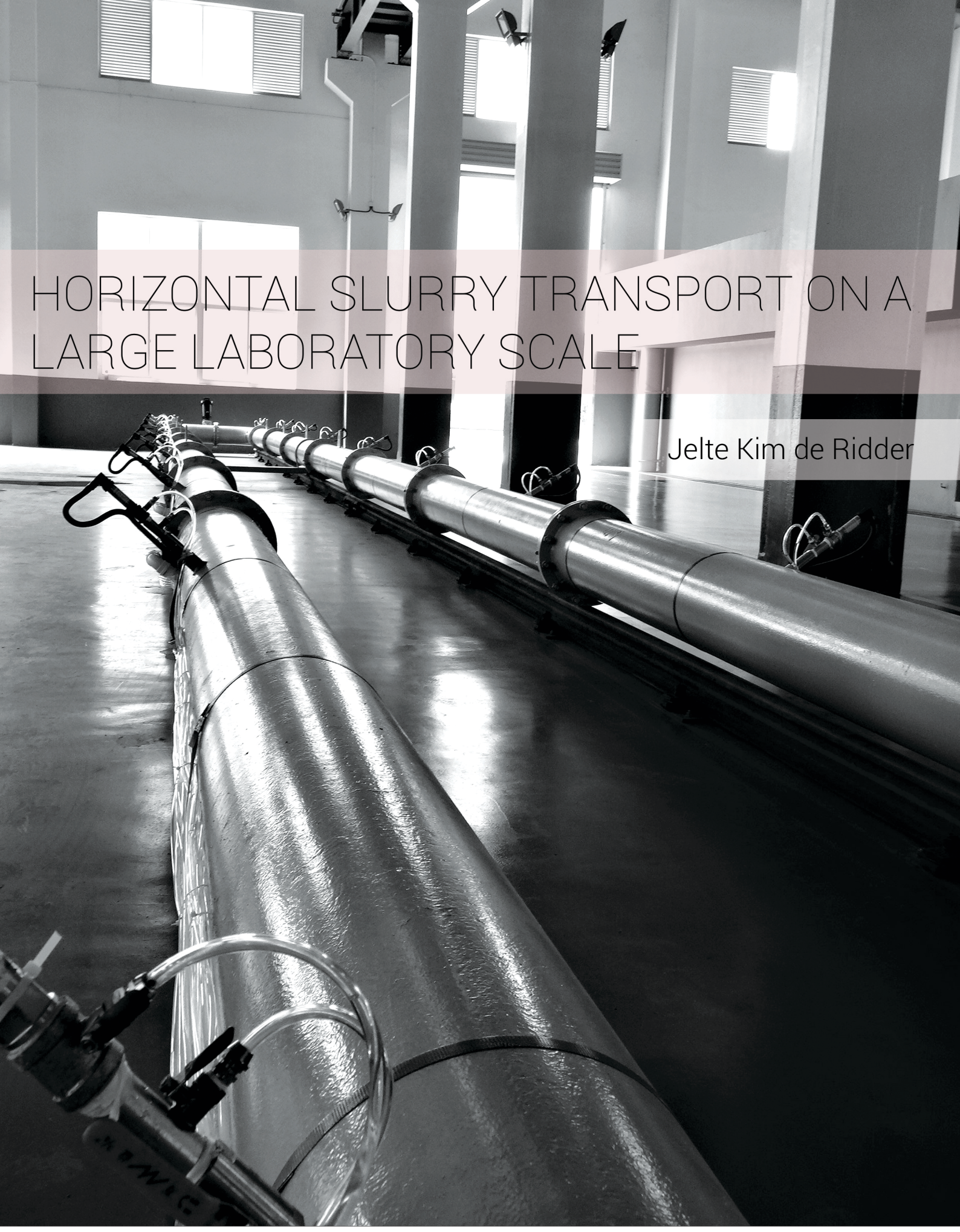

HORIZONTAL SLURRY TRANSPORT ON A LARGE LABORATORY SCALE

Jelte Kim de Ridder

TU Delft Delft University of Technology

Challenge the future

HORIZONTAL SLURRY TRANSPORT ON A LARGE LABORATORY SCALE

by

Jelte Kim de Ridder

to obtain the degree of Master of Science at the Delft University of Technology, to be defended publicly on Tuesday April 24, 2018 at 01:30 PM.

Student number:	4175271	
Project duration:	December 6, 2016 – January 1, 2018	
Thesis committee:	Prof. dr. ir. C. van Rhee,	TU Delft, chairman
	Dr. Ir. A. M. Talmon,	TU Delft, supervisor
	Dr. Ir. F. Wang,	CCCC NERCD Co., Ltd, supervisor
	Dr. Ir. M. van Damme,	TU Delft

TU Delft Delft University of Technology

中交疏浚技术装备国家工程研究中心有限公司
CCCC NATIONAL ENGINEERING RESEARCH CENTER OF DREDGING TECHNOLOGY AND EQUIPMENT CO.,LTD

Preface

Where I grew up, people refer to China as ”the other side of the world”. Translated in the words of Dutch documentary producer Ruben Terlou [Terlou, 2016]: ”*China is one of the world’s greatest powers, but is hardly known by us. Let alone that we have an idea of how the ordinary Chinese lives and works or what he aspires or fears.*”. He alleges that for most inhabitants of the western world, the concept ”China” is something you can only grasp when you have experienced it.

I have to admit it also applied to me. I knew little or less about the country before I arrived there in April 2017. My knowledge was limited to films, books and documentaries. The first memory of China coming to mind is watching Walt Disney’s ”Mulan” [Cook et al., 1998], the first time my father treated me with a trip to the cinema. Intrigued by the foreign country my grandparents bought ”The Amazing Panda Adventure” [Rich et al., 1995]. A film I watched a dozens time from their settee. Growing older, but still a child, I saw China twice through the eyes of Tintin [Hergé, 1936, 1960]. An adventurous reporter drawn by the hand of Belgian artist George Remi.

My interest in China renewed when I started graduation at the end of 2016. Realising I would step into the footprints my favourite comic character, I started to prepare for the trip. Watching the documentary of Terlou [Terlou and Krijgsman, 2016], reading about their history in the book of Ransmayr [Ransmayr, 2017] and about their rise as a global power in politics and economy [Mees, 2016].

Now, looking back at it, I’m even more intrigued by what the country has to offer. From my arrival at Shanghai Pudong airport, awaited by Dr. Yin and Dr. Vivian, until the morning Mr Shu waved me goodbye after breakfast. I have had the opportunity to experience all of it with my own eyes. The contrast between the crowded streets of Shanghai and the small river towns, the museums filled with ancient artefacts of their rich history, from diners served at large round tables to the comfy street food and above all the unprecedented hospitality. Moved and touched by it, the other side of the world starts to feel very close.

Jelte Kim de Ridder
Delft, March 2018

Abstract

The first head loss prediction methods for hydraulic transport of solids in pipes, date back to the years '50 of last century. The principles are still applied today. Although it is observed that obtained results may differ from reality, when the circumstances do not represent the situation of the original experiment. To investigate this, the performance of various prediction models is analysed on a large scale laboratory test set-up.

In recent publications, several researchers observed disturbances in their expected flow patterns. Described as either 'unsteady flow', 'instability' or 'unexpected mechanism'. Talmon developed the theory that the occurrence of these events could be explained by transient processes in the pipe flow. It is recommended to use a test pipe with great length. To verify, by longitudinal pressure profile measurement, that equilibrium is measured, and that indicated transients are captured by the measuring system.

A laboratory test set-up is provided by the CCCC National Engineering Research Center of Dredging Technology and Equipment Co., Ltd (NERCD). In a joint research program with Delft University of Technology (TUD): the pressure drops for water and mixture flow over the pipeline length are analysed. This is done for horizontal hydraulic transport. The focus is on comparing test results with existing theories and find explanations to deviating results. If instabilities are observed, the gathered data can be used for further research on density waves in pipelines.

In the liquid flow experiment, three prediction methods derived from the Colebrook-White equation are analysed: Darcy-Weisbach, Swamee & Jain and RangaRadju & Garde. Considering the pipeline to be smooth, the predicted values are similar. The difference between them is almost nil. Furthermore, the result shows good correspondence with the data acquired on the test set-up.

In the mixture experiment, four prediction methods are analysed: Durand, Führböter, Jufin & Lopatin and Wilson. They are compared with laboratory data of test conducted in a heterogeneous flow regime. With a velocity ranging from three to six meter per second and concentrations of: 4.4, 8.1, 12.3 and 14.6 percent. In a general approach, considering all transport velocities and concentrations. It is observed that the theoretical principle described by Durand shows the closest resemblance with the experimental data. When only the concentrations are considered, a distinction has to be made. For the two lowest mixture densities, the Führboter method gives the best fit. For the highest two, the best correlation is according to the Durand theory. The principles of Jufin & Lopatin and Wilson underestimate the pressure loss. Where the difference of the former is significantly larger in comparison to the latter.

For the lowest velocities of the twelve and fifteen percent slurry experiments, stationary waves over the pipeline length are observed. Due to the length of the test set-up, the transition to equilibrium flow is clearly visible. It demonstrates that longer flow loops give opportunity to conduct further research into the extent of waves.

Keywords: Hydraulic transport, pipeline, slurry flow, pressure gradient

List of Figures

3.1 Flow loop: line drawing . . . 7
3.2 U-loop configuration . . . 8
3.3 Pressure tap locations . . . 9
3.4 Measurement location . . . 9
3.5 Mixture and storage tank . . . 10
3.6 Equipment location . . . 11
3.7 Perspex section . . . 15
3.8 Flow loop: Delft University of Technology (2002) . . . 15
3.9 Flow loop: Delft Hydraulics (2004) . . . 16
3.10 Flow loop: Institute of Hydrodynamics Prague (2013) . . . 17
3.11 Flow loop: Delft University of Technology (2015) . . . 17

4.1 Grain size distribution . . . 21
4.2 180° turn . . . 23
4.3 Fitting loss . . . 24

5.1 Total pressure profile: water flow downstream bend . . . 29
5.2 Corrected total pressure profile: water flow downstream bend . . . 31
5.3 Corrected total pressure profile: water flow downstream bend . . . 31
5.4 Resistance curve: total pressure . . . 32
5.5 Pressure profile: water flow . . . 32
5.6 Hydraulic gradient: water flow . . . 33

6.1 Result mixture experiment: (C=4%) . . . 39
6.2 Result mixture experiment: (C=8%) . . . 40
6.3 Result mixture experiment: (C=12%) . . . 41
6.4 Result mixture experiment: (C=15%) . . . 41
6.5 Pressure profile: Durand (C=15%) . . . 42
6.6 Pressure profile: Führböter (C=15%) . . . 42
6.7 Pressure profile: Jufin-Lopatin (C=15%) . . . 43
6.8 Pressure profile: Wilson (C=15%) . . . 43
6.9 Resistance curve: Durand . . . 44
6.10 Resistance curve: Führböter . . . 44
6.11 Resistance curve: Jufin & Lopatin . . . 45
6.12 Resistance curve: Wilson . . . 45
6.13 Jufin-Lopatin Hydraulic gradient: C=4% . . . 46
6.14 Jufin-Lopatin Hydraulic gradient: C=12% . . . 46
6.15 Stationary wave: C=12%, V_m=3.7) . . . 47
6.16 Stationary wave: C=12%, V_m=3.7) . . . 48
6.17 Stationary wave: C=12%, V_m=3.7) . . . 48
6.18 Hydraulic gradient profile: C=12%, V_m=5.5) . . . 49
6.19 Stationary wave: C=15%, V_m=3.4) . . . 49
6.20 Stationary wave: C=15%, V_m=4.4) . . . 50
6.21 Stationary wave: C=15%, V_m=5.3) . . . 50
6.22 Hydraulic gradient profile: C=15%, V_m=4.2) . . . 51
6.23 Hydraulic gradient profile: C=15%, V_m=5.2) . . . 51

A.1 Flow loop: top view . . . 61
A.2 Flow loop: side view . . . 61

A.3 Flow loop: front view . . . 62
A.4 Laboratory: top view . . . 62
A.5 Laboratory: side view . . . 62
A.6 Pipeline: cross-section . . . 63
A.7 Connection of differential pressure transmitters . . . 63

B.1 Position: pressure taps . . . 65
B.2 Position: pressure tap interval . . . 65

C.1 Pump curve . . . 68

D.1 Temperature 07/31 . . . 69
D.2 Temperature 08/04 . . . 69
D.3 Temperature 08/03 . . . 70
D.4 Temperature 08/04 . . . 70
D.5 Temperature 08/04 . . . 70

F.1 Resistance curve: differential pressure . . . 73

G.1 Total pressure profile: water flow downstream vehicle lane . . . 75
G.2 Corrected total pressure profile: water flow downstream vehicle lane . . . 76

I.1 Result mixture experiment: (C=4%) . . . 83
I.2 Result mixture experiment: (C=8%) . . . 83
I.3 Result mixture experiment: (C=12%) . . . 84
I.4 Result mixture experiment: (C=15%) . . . 84

J.1 Pressure profile: Durand (C=4%) . . . 85
J.2 Pressure profile: Führböter (C=4%) . . . 86
J.3 Pressure profile: Jufin-Lopatin (C=4%) . . . 86
J.4 Pressure profile: Wilson (C=4%) . . . 87
J.5 Pressure profile: Durand (C=8%) . . . 87
J.6 Pressure profile: Führböter (C=8%) . . . 88
J.7 Pressure profile: Jufin-Lopatin (C=8%) . . . 88
J.8 Pressure profile: Wilson (C=8%) . . . 89
J.9 Pressure profile: Durand (C=12%) . . . 89
J.10 Pressure profile: Führböter (C=12%) . . . 90
J.11 Pressure profile: Jufin-Lopatin (C=12%) . . . 90
J.12 Pressure profile: Wilson (C=12%) . . . 91
J.13 Pressure profile: Durand (C=15%) . . . 91
J.14 Pressure profile: Führböter (C=15%) . . . 92
J.15 Pressure profile: Jufin-Lopatin (C=15%) . . . 92
J.16 Pressure profile: Wilson (C=15%) . . . 93

O.1 Concentration: C=12%, V_m=3.7 . . . 109
O.2 Concentration: C=12%, V_m=3.7 . . . 109
O.3 Concentration: C=12%, V_m=3.7 . . . 110
O.4 Concentration: C=15%, V_m=3.4 . . . 110
O.5 Concentration: C=12%, V_m=3.4 . . . 110
O.6 Concentration: C=12%, V_m=3.5 . . . 111

List of Tables

1 Nomenclature xiv

3.1 Specifications: Differential pressure transmitter 12
3.2 Specifications: Total pressure transmitter 12
3.3 Specifications: Ultrasonic concentration meter 13
3.4 Specifications: Electromagnetic flow meter 13
3.5 Specifications: Centrifugal pump 14
3.6 Temperature measurements 14
3.7 Flow loop comparison 18

4.1 Grain size distribution 22
4.2 Fittings: friction coefficient 23
4.3 General parameters 25

5.1 Test matrix: liquid flow 29
5.2 Flow loop correction coefficients 30

6.1 Particle settling parameter 37
6.2 Comparison of prediction models 38
6.3 Test matrix: mixture flow 39

B.1 Position of pressure taps 66
B.2 Position of pressure tap interval 66

E.1 Test matrix 72

Contents

Preface iii

Abstract v

List of Figures vii

List of Tables ix

Nomenclature xiii

1 Introduction 1

2 Problem definition 3
2.1 Problem analysis . . . 3
2.2 Objective . . . 3
2.3 Main challenges . . . 4
2.4 Literature review . . . 4
2.5 Hypothesis . . . 5

3 Experimental set-up 7
3.1 Flow loop . . . 7
3.2 Measurement equipment . . . 11
3.3 Comparison of the configuration . . . 15
3.4 Experimental protocol . . . 18

4 Preliminary calculations 21
4.1 Sediment . . . 21
4.2 Settling velocity . . . 22
4.3 Minor losses . . . 23
4.4 General parameters . . . 24

5 Analysis water flow experiment 27
5.1 Applicable theories . . . 27
5.2 Flow loop correction equation . . . 28
5.3 Pipe wall roughness . . . 31
5.4 Analysis . . . 32

6 Analysis mixture flow experiment 35
6.1 Applicable theories . . . 35
6.2 Comparison of the prediction models . . . 37
6.3 Result . . . 38
6.3.1 4% concentration . . . 39
6.3.2 8% concentration . . . 40
6.3.3 12% concentration . . . 40
6.3.4 15% concentration . . . 41
6.3.5 Resistance curves . . . 43
6.3.6 Analysis . . . 45
6.3.7 Stationary waves . . . 47

7 Conclusion 53

8 Recommendations 55

9 Acknowledgement 57

Appendices **59**
A Flow loop design 61
A.1 Line drawings 61
A.2 Ground plan 62
A.3 Various 63
B Position of pressure taps 65
C Pump characteristics 67
D Temperature measurements 69
E Test matrix 71
F Water flow: resistance curve 73
G Water flow: pressure profile downstream vehicle lane 75
H Water flow: pressure profile & hydraulic gradient 77
I Result mixture experiment: Führböter 83
J Mixture flow: pressure profiles 85
J.1 4% concentration 85
J.2 8% concentration 87
J.3 12% concentration 89
J.4 15% concentration 91
K Result: 4% concentration 95
L Result: 8% concentration 97
M Result: 12% concentration 101
N Result: 15% concentration 105
O Dynamic waves: ultrasonic concentration measurement 109

Bibliography **113**

Nomenclature

Nomenclature		
Symbol	Definition	Dimension
A	Area	$[m^2]$
a	Correction factor	$[-]$
b	Correction factor	$[-]$
C_{vd}	Delivered volumetric solids concentration	$[-]$
C_{vi}	In situ volumetric solids concentration	$[-]$
C_1, C_2	Ferguson and Church coefficients	$[-]$
d_{50}	Mass-median particle diameter	$[m]$
d_{mf}	Decisive particle diameter	$[mm]$
D_p	Pipe diameter	$[m]$
Fr_{vt}	Modified particle Froude number	$[-]$
f_s	Sampling frequency	$[Hz]$
g	Gravitational acceleration	$[m/s^2]$
h_{bend}	Head loss in bend	$[m]$
I_{bend}	Hydraulic gradient in bend	$[-]$
I_f	Hydraulic gradient for flow of fluid	$[-]$
I_m	Hydraulic gradient for flow of mixture	$[-]$
k	Absolute pipe wall roughness	$[m]$
L	Length	$[m]$
M	GSD sensitive empirical exponent	$[-]$
P	Pressure	$[kPa]$
P_a, P_b	Pressure at locations a & b	$[kPa]$
P_c	Corrected pressure	$[kPa]$
pi	Soil fraction	$[\%]$
Q	Flow rate	$[m^3/hour]$
r	Radius	$[m]$
R_e	Reynolds number	$[-]$
R_{sd}	Relative submerged density	$[-]$
S_f	Relative density of fluid	$[-]$
S_{kt}	Transport factor	$[m/s]$
S_s	Relative density of solids	$[-]$
T	Temperature	$[°C]$
t	Time	$[s]$
V	Mean liquid velocity	$[m/s]$
V_{50}	Velocity when one half of the transported sediment is in suspension	$[m/s]$
V_m	Mean mixture velocity	$[m/s]$
V_{min}	Minimum velocity	$[m/s]$
v_t	Terminal settling velocity of a single particle	$[m/s]$
z	Vertical distance	$[m]$

Nomenclature		
Symbol	Definition	Dimension
α	Angle	[°]
ΔL	Length of considered pipeline segment	$[m]$
ΔP	Pressure loss over distance ΔL	$[kPa]$
ΔT	Temperature difference over Δt	$[°C]$
Δt	Time interval	$[s]$
λ_f	Darcy-Weisbach friction coefficient	$[-]$
μ_s	Mechanical friction coefficient	$[-]$
Ψ^*	Particle settling parameter	$[-]$
υ_f	Kinematic viscosity of liquid	$[m^2/s]$
ξ	Resistance coefficient for fittings	$[-]$
ρ_f	Density of fluid	$[kg/m^3]$
ρ_m	Density of mixture	$[kg/m^3]$
ρ_s	Density of solids	$[kg/m^3]$

Table 1: Nomenclature

1 Introduction

Hydraulic transport of solid material in pipes is a widely documented subject in the dredging and mining research. The first head loss prediction methods, developed in the mid of last century, are still applied nowadays. The principles perform well in situations representing the original experiments. But if the circumstances change, the obtained result may differ from reality [Miedema, 2014]. To analyse their relevance, it is proposed to compare the prediction models with results obtained on a large scale laboratory experimental set-up.

In recent years, experiments [Matoušek and Krupička, 2013, Talmon, 2015] revealed the occurrence of pressure gradient variations downstream of a 180° bend. Symptoms of such disturbances; multiple peaked hydraulic resistance curves, have been observed on earlier occasions [Gu et al., 2007, Matoušek, 1997, 2002]. One of the main recommendations [Talmon, 2015] regarding future research is that experiments need to be conducted in longer flow loops. Reducing the risk to measure under non-equilibrium conditions.

Such a test set-up is present in the laboratory of the *CCCC National Engineering Research Center of Dredging Technology and Equipment Co., Ltd* (NERCD) in Shanghai. In December 2016 a joint research program with *Delft University of Technology* (DUT) was launched. It is agreed that the experimental part takes place in China and the data processing in the Netherlands. The current collaboration project focusses on the study of pressure drops in sand-water-mixture flow. Experiments are conducted for both horizontal and inclined hydraulic transport.

In both cases the focus is on documenting how hydraulic transport theories, for equilibrium condition, relate to test results on a large laboratory scale. This report discusses the horizontal experiments. Results of the inclined experiments are discussed in 'Hydraulic transport in inclined large diameter pipelines' by M.A. de Vreede [de Vreede, 2018].

The structure of the report is as follows. It start with the problem description and research questions in chapter 2. In chapter 3, the laboratory set-up and experimental protocol are discussed. Next is the determination of input parameters, regarding the prediction methods, in chapter 4. What follows is the explanation of the theoretical models with a discussion on the experiments. Therefore a distinction is made between tests with liquid and mixture flow. The former is described in chapter 5, the latter in chapter 6. The conclusion of this report is given in chapter 7 and recommendation are made in chapter 8.

2

Problem definition

This chapter describes the research topic in general. It starts with the problem analysis and is followed by the objective. The main research question is discussed and divided into sub questions. Subsequently the expected challenges are discussed. In the literature review the knowledge advancement, throughout recent history, on the subject is examined. It concludes with a hypothesis on the main research question.

2.1. Problem analysis

There is a broad variety of pressure drop prediction methods for slurry transport through pipelines. Some of them date back to years ’50 and ’60 of last century. Meanwhile, extra knowledge has been acquired about the subject. Recent publications recommend carrying out experiments on larger test set-ups. Which is necessary to prove some of the new discoveries.

In this context a longer flow loop can serve multiple purposes. First it can be used to analyse the relevance of the classic prediction models. Second it can provide more information to support the development of new theories.

2.2. Objective

For this specific project the NERCD decided to construct a large flow loop. Creating the opportunity to examine various new research topics. In this case it is decided to analyse the relevance of the classic prediction models. Considering this as the objective, the main research question is formed:

Q_{main}: *To what extent are the existing mathematical models applicable for slurry transport in a 300 millimetre diameter horizontal pipeline?*

Whilst searching for an answer, several subjects are encountered. Within this context the main question is divided in four sub questions. Each of them is a small step towards the conclusion. First, the focus is on gathering information about previous research in the field of horizontal hydraulic transport. This to create an overview of relevant models and recent developments. An answer to this question is given in chapter 2.4.

Q_1: *What are the existing models with regard to slurry transport in horizontal pipelines?*

When decided on the theoretical models to analyse, there is looked into the test set-up configuration. Lay-outs in relevant research are studied. Next the working principle of the own design is discussed, together with similarities, differences and why it is state-of-the-art. The information can be found in chapter 3.3.

Q_2: *Which test set-up is required to validate the prediction models in a large diameter pipeline?*

Next, the theoretical models that will be analysed are described. Predictions are made and the experimental research part can commence. The theory on water flow is discussed in chapter 5.1. Regarding mixture flow, information can be found in chapter 6.

Q_3: *What do the mathematical models predict for a pipeline of 300 millimetre diameter?*

The fourth and last sub question leads to a comparison between the existing models and the acquired experimental data. Their similarities and differences are discussed in order to form a conclusion and give answer to the main research question. The discussion can be found in chapter 7.

Q_4: *To what extent are the test results from the laboratory in agreement with expectations from the mathematical models?*

Nevertheless the objective, there is also the intention to look into the extent of stationary waves. Therefore an additional question is added to broaden the frame of the research. The goal of Q_A is not to give a physical description or explanation. It is to state whether the longer flow loop creates the opportunity to research the extent of waves, as recommended by Talmon[Talmon, 2015]. Hypothetically this is the case. When demonstrated it gives opportunity to future research on the topic. The answer can be found in chapter 6.3.7.

Q_A: *To which extent do stationary waves develop in a test set-up of greater length and greater pipe diameter?*

2.3. Main challenges

The main goal of this research is to create a trustworthy answer on main and sub questions. This comes with different challenges. One of them is to come up with realistic conditions and assumptions throughout the project process. As wrong conditions and assumptions could affect the conclusions credibility. Another possible risk is within the design of the experimental set-up. When not done properly, results will not be reliable. And if that is the case, the data cannot be compared with results from previous research. Furthermore it is key to have good communication between all parties in the joint research program.

2.4. Literature review

As stated in chapter 1, hydraulic transport through pipelines is often studied and documented. Resulting into multiple prediction methods for pressure loss in pipeline flow. Knowledge on the working principle of liquid flow is found in *'explicit equations for pipe flow problems'* [Swamee and Jain, 1976b]. The paper contains information about three computational techniques, derived from the Colebrook-White equation [Colebrook, 1939]. One of the examined principles, for the water-flow friction loss prediction ,is that of Churchill [Churchill, 1977].

Much more mathematical models are available regarding the slurry transport. One of the first, dating back to 1953, is by the hand of Durand [Durand, 1953]. The next decade the theories of Führböter [Führböter, 1961] and Jufin & Lopatin [Jufin and Lopatin, 1966] arose. After their publications multiple contributions have been made in this field of research. One of the most recent additions is delivered by Wilson [Wilson et al., 2006b], first published in 1992. These are the four prediction methods analysed in this report.

On two occasions these models are discussed together. In *'Slurry Transport Fundamental, A Historical Overview & The Delft Head Loss & Limit Deposit Velocity Framework'* [Miedema, 2016a], a historical overview of the slurry transport research is given by Miedema. He collected many publications and used them to develop his own theoretical model. The other reference treating multiple prediction methods is the *'Dredge Pumps and Slurry Transport'* reader [Matoušek, 2004b] by Matoušek.

In recent years, publications [Matoušek and Krupička, 2013, Talmon, 2015] revealed the occurrence of pressure gradient variations downstream of a 180° turn. Symptoms of such disturbances; multiple

peaked hydraulic resistance curves, had been observed on earlier occasions in Europe [Matoušek, 1997, 2002] and Asia [Gu et al., 2007].

Besides theory, the collected material also provides knowledge about test set-ups and measuring equipment. Publications show that comparable research facilities feature a U-loop in their test set-up design. The U-tube is used to determine the delivered volumetric solids concentration and the relative density of delivered mixture. The principle is proposed by Hagler [Clift and Clift, 1981]. Consulting the technical report on *'Standing Waves in Slurry Pipe Flow'* [van Es and Boone, 2015], a correction equation for the total pressure measurement along the horizontal pipe is developed. This is necessary to remove deviations, which are probably due to local imperfections at pressure taps or flanges.

The information in this section, gives answer to the first sub-question:

Q_1**:** *What are the existing models with regard to slurry transport in horizontal pipelines?*

For the considered principles, a summary on the development and proposed calculation method is given in chapter 6.1.

2.5. Hypothesis

Hypothetical no large deviations, between theory and result, are expected to show up. This statement is based on the argument that the mathematical prediction methods for pressure drops in a horizontal pipeline, analysed in this report, are common in this field of research. In the contention that some of the 60 year old models are still used today and are tested repeatedly, deviating results would rather give reason to doubt the result itself.

Furthermore, the Führböter prediction method is expected to give the most accurate fit. The reason behind it, is that it was developed for a 300 millimetre pipeline. Equal to the one used in this research.

3

Experimental set-up

The NERCD houses a 220 meter long open flow loop, see Figure 3.1. Considering the centrifugal pump (1) as the starting point, the 300 mm circuit features multiple sections: a U-loop (2), a cooling reservoir (3), a measurement section (4), a mixture and storage tank (5) and a water reservoir (6). In this chapter each section is discussed individually. Detailed information about the installed measurement equipment is given. A comparison is made with five other laboratory flow loop configurations and furthermore it informs on how the experimental research has been carried out. Additional figures showing the set-up layout are included in appendix A.

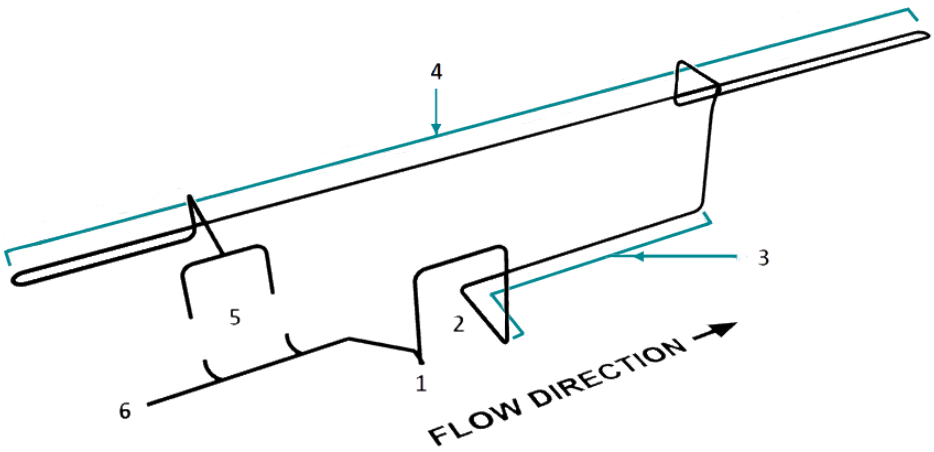

Figure 3.1: Flow loop: line drawing

3.1. Flow loop

U-loop
The U-loop is located immediately after the centrifugal pump. It is used to determine the relative density of the delivered slurry 'ρ_m' and delivered volumetric solids concentration 'C_{vd}'. The principle is first proposed by Hagler [Clift and Clift, 1981] and described by the *GIW Hydraulic Laboratory* [Wilson et al., 2006a].

The U-loop is equipped with two sets of differential pressure meters. One in the riser, the ascending limb of the tube, and the second in the downcomer, the descending limb of the tube. Their exact locations are displayed in Figure 3.2.

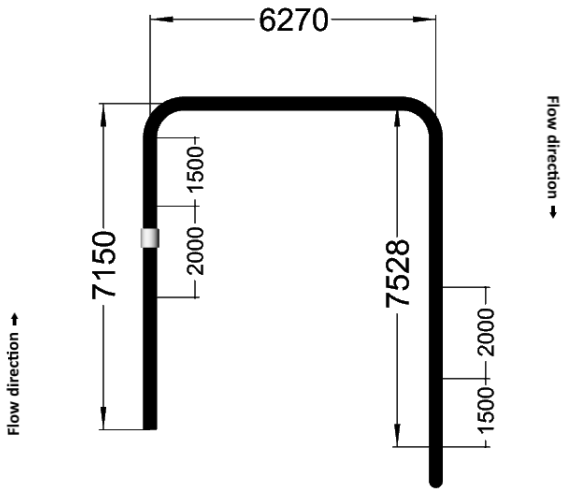

Dimensions are expressed in mm. The 2 meter distance indicates the differential pressure meter position, located 1.5 meter from the fittings. The grey rectangle in the riser represents the ultrasonic concentration meter.

Figure 3.2: U-loop configuration

The differential pressure meters give the input for equation 3.1, used to determine 'C_{vd}'. In the formula, 'ΔP_a' represents the pressure gradient measured by the pressure differential meters in the riser. The pressure differential measured in the downcomer is expressed as 'ΔP_b'. The outcome can be used in formula 3.2 to determine the mixture density 'ρ_m'.

$$C_{vd} = \frac{\Delta P_a + \Delta P_b - 2 * \rho_f * g * z}{2 * (S_s - 1) * g * z * \rho_f} \tag{3.1}$$

$$\rho_m = C_{vd} * (\rho_s - \rho_f) + \rho_f \tag{3.2}$$

Due to malfunction of the differential pressure meters, the U-loop was not operational in the described research.

Cooling section
Downstream of the U-loop a basin is located. When filled with water, it is used to cool a 21.4 meter long part of the pipeline. During the experimental research the cooling reservoir has not been punt into service. A discussion on the subject is found in section 3.2, under the heading: thermometer.

Measuring section
The material is transported out of the cooling basin through an up-going vertical tube. In this riser, the flow rate is measured. When a height of 4.8 meter above ground floor level is reached, the flow direction is altered and a vehicle lane is crossed horizontally. Next the material passes through a descending pipeline and enters the measurement section. This part of the flow loop has a total length of 123 meter and consists of 34 pressure taps, see Figure 3.3. The distance between two measurement locations is three meter, with exception of the ones that are situated in the bend (8-11) and at the flexible section (18-19). The exact positions, expressed in the distance too the starting point of the horizontal pipeline, are given in appendix B. Also included is information on the position of pressure tap intervals.

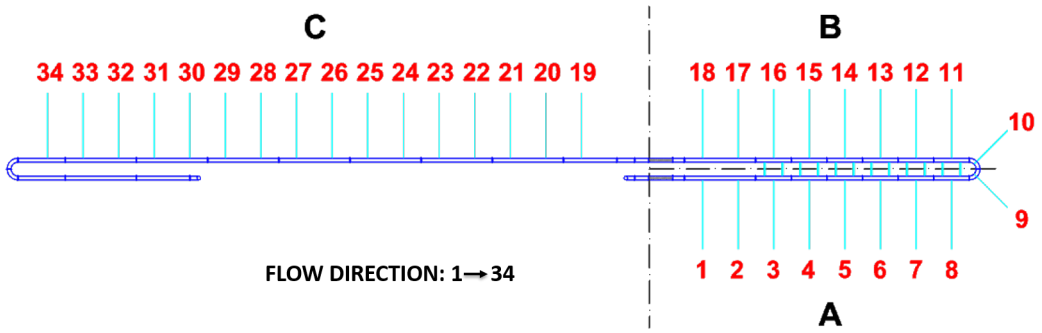

Figure 3.3: Pressure tap locations

Each location is equipped with a *Micro Sensor MPM4730* total and connected to a *Rosemount 3051D* differential pressure meter. Configured as can be seen in Figure 3.4. The taps, at a $45°$ angle of the pipeline crest, have a $25\ mm$ opening. Large of enough to fit the diameter of the total pressure meter (Table 3.2) and to guarantee water flow towards the Rosemount equipment. A figure of the cross-sectional area at a tap location is included in appendix A, together with a sketch of the differential pressure meter connection.

A: absolute pressure meter, B: air removal tube, C: impulse tube to differential pressure meter

Figure 3.4: Measurement location

The measurement section can be divided into two parts. The first one, 'A+B' (Figure 3.3), can be inclined. For the current lay-out of the set-up, the maximum achievable angle is $19.0°$. It is limited by the roof height of the laboratory. By shortening part 'A+B' larger angles, up to $45°$ can be reached. Between taps 9-10 a vent is installed to remove air trapped in the system.

The second part, 'C' (Figure 3.3), is a horizontal section of 52.6 meter. It is separated from the first part (A+B) by a flexible section, that is used to change the inclination angle. At this location no differential pressure measurement is carried out. The pressure drop over this section is calculated by extracting local pressures 18 and 19.

Mixing & storage tank

The mixture is transported towards a T-section. On both sides valves are installed. By operating them the slurry can be transported to the desired location, one of two reservoirs. The first a is storage basin, the second a mixing reservoir. Both have a volume of 100 m^3. The configuration is as can be seen in Figure 3.5, where the valves are the blue fragments on the pipeline.

Figure 3.5: Mixture and storage tank

In the current open loop design, the tanks can not be bypassed. That the mixture is discharged after one run through the pipe can cause complications. For constant operation, the fluidized material needs to re-enter fluidized into the inlet of the pipeline. Keeping the particles in suspension is achieved due to turbulence, created by discharging the mixture. Eventually the material flows back into the flow loop through the cone shaped bottom of the tank and suction of the centrifugal pump. At the bottom eight jets are installed. When necessary a good quality controlled fluidization can be achieved with this system.

Water reservoir
A water reservoir with a volume of 166 m^3 is attached to the loop. The supply of water to the system is controlled with a valve. At the end of a slurry experiment, liquid and solids are separated. In this way water can be re-used in an eco-friendly manner.

3.2. Measurement equipment

Drawing on the previous section, this part gives a more detailed description of the installed equipment and its specifications. Also special design features are highlighted. An overview of what is used and where it is located on the set-up is given in Figure 3.6.

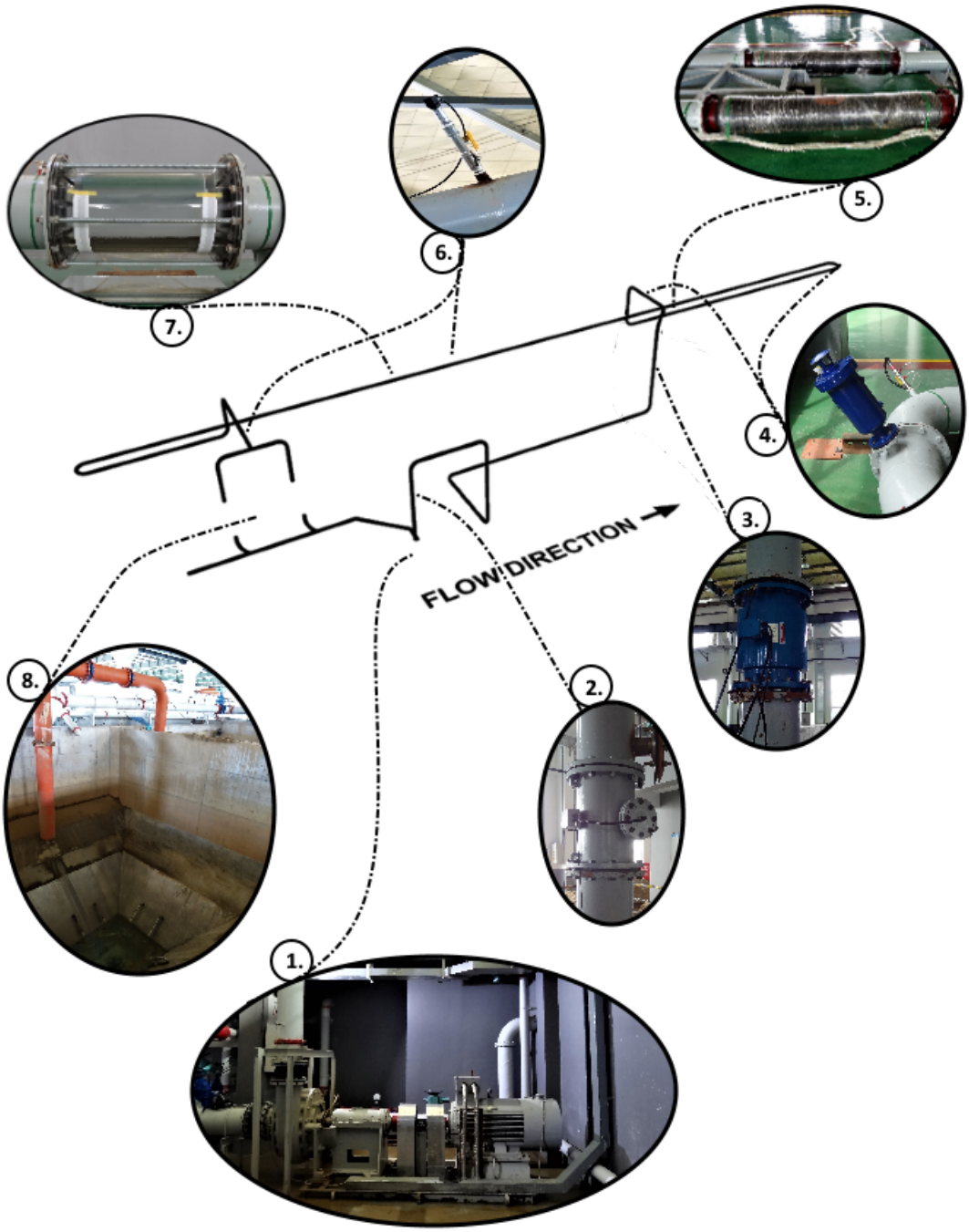

1: centrifugal pump, 2: ultrasonic concentration meter, 3: electromagnetic flow meter, 4: air vent, 5: flexible pipe, 6: temperature meter, 7: Perspex section and 8: storage and mixing tank.

Figure 3.6: Equipment location

Differential & Absolute pressure transmitter

As mentioned, in section 1 of chapter 3, each measurement location is equipped with two pressure transmitters. A differential and a total one. The specifications for both types can be found in respectively Table 3.1 and 3.2.

Table 3.1: Specifications: Differential pressure transmitter

Differential pressure transmitter		
Company **Type**	**Rosemount** **3051D**	
Diameter	–	$[m]$
Weight	–	$[kg]$
Accuracy	0.05	$[\%]$
Velocity range	–	$[m/s]$
Temperature range	-50 - 65	$[°C]$
Pressure range	0 - 10	$[KPa]$
Max. frequency	25	$[Hz]$

Table 3.2: Specifications: Total pressure transmitter

Total pressure transmitter		
Company **Type**	**Micro Sensor.,LTD** **MPM4730**	
Diameter	0.02	$[m]$
Weight	0.16	$[kg]$
Accuracy	0.1	$[\%]$
Velocity range	–	$[m/s]$
Temperature range	-10 - 80	$[°C]$
Pressure range	0 - 200	$[MPa]$
Max. frequency	20 - 5000	$[Hz]$

The availability of two independent measuring techniques is an advantage. When results are compared, any deviation can be quickly indicated. On one occasion, during the 4-8% concentration tests, a malfunction occurred. One of the signal receivers broke down and a spare part was not immediately available. Due to a tight schedule, the experiment had to be carried out. Causing that the differential pressure meter data could not be recorded.

Because of this incident, only the total pressure measurements are analysed in this report. It is the only option to compare the results in a correct manner. Results containing the differential pressure data are included in the appendices. Nevertheless, there is a good correspondence between the two measurement techniques.

Ultrasonic concentration meter

A *Tengine TPD* ultrasonic concentration meter is installed in the riser of the cooling basin. The exact location is visualised in Figure 3.6. Specifications of the equipment are given in Table 3.3.

Table 3.3: Specifications: Ultrasonic concentration meter

Ultrasonic concentration meter		
Company	**Tengine**	
Type	**TPD**	
Diameter	0.3	$[m]$
Weight	–	$[kg]$
Accuracy	2.5	[%]
Concentration range	0 - 40	[%]
Temperature range	0 - 50	$[°C]$
Pressure range	1	$[MPa]$
Max. frequency	60	$[Hz]$

After completion of the experimental research part, the U-loop became operational. At that point *M.A. de Vreede* started to use the set-up for a study on the frictional pressure drop during inclined sediment transport [de Vreede, 2018]. Because of the working U-tube, he could verify the data provided by the concentration meter. During this verification he discovered that the equipment's results are incorrect, probably due to wrong calibration of the apparatus.

De Vreede determined the deviation between U-loop and concentration meter data. He discovered that the measurement results of the latter are a factor 1.9 too high. This affected the scope of this research, because the targeted concentrations are not reached.

Electromagnetic flow meter
The set-up is equipped with a *Guanghua LDG-300S* electromagnetic flow meter (specifications are included in Table 3.4). At first instance it is installed in the up going limb of the U-loop, just in front of the concentration meter. During trial tests, a strange phenomena occurred. Starting at low flow rate, the results are as expected: a steady almost constant signal. Next the pump speed is increased and the signal started to show fluctuations. The magnitude of these fluctuations kept on increasing towards higher flow rates. Eventually the riser even started to vibrate.

To determine the cause, various possibilities have been taken into consideration. After elimination only one remains. It turns out to be that the flow meter's cable picked up the pump frequency. Therefore the equipment needed to be positioned elsewhere. It is relocated to the vertical tube downstream of the measuring section, as indicated in Figure 3.6. Since then no fluctuations occurred and the riser did not vibrate anymore.

Table 3.4: Specifications: Electromagnetic flow meter

Electromagnetic flow meter		
Company	**GUANGHUA**	
Type	**LDG-300S**	
Diameter	0.3	$[m]$
Weight	73.0	$[kg]$
Accuracy	0.5	[%]
Velocity range	0.5 - 10.0	$[m/s]$
Temperature range	-25 - 150.0	$[°C]$
Pressure range	0.6 - 4.0	$[MPa]$
Max. frequency	50.0	$[Hz]$

Centrifugal pump
The set-up is driven by a *Sanlian* centrifugal pump. The design specifications can be found in Table 3.5. The corresponding performance curve is included in appendix C. The pressure over the pump is measured with two total pressure meters. The pumps rotational speed is used to control the flow

velocity during experiments.

Table 3.5: Specifications: Centrifugal pump

Centrifugal pump		
Company	**Sanlian Pump**	
Type	**ASP1050-300-7000030W**	
Rated discharge	1600	$[m^3/h]$
Rated head	25.35	$[m]$
Rated speed	740	$[rpm]$
Rated power	151.60	$[kW]$

Thermometer

When the mixture temperature changes, so does the viscosity. This alteration in viscosity can influence the results of the experiments. The temperature change is caused by two mechanisms: the high ambient temperature [Linder, 2017] and the energy exchange between the slurry and the set-up when operating.

During the experiments, the temperature is monitored with two electronic thermometers. They are located between measurement locations 18-19 and just after location 34 (see Figure 3.6). The equipment has a range of 0-$100\ °C$, an accuracy of 0.2% and and inserted depth of $100\ mm$.

The sensors measured a maximum increase in temperature of circa six degrees Celsius, over a duration of two hours an a half. This change was negligible with regard to the change in viscosity. Therefore, the cooling section has never been put into service. An overview of the measured temperature increase during testing is given in Table 3.6. The representing graphs are added to appendix D.

Table 3.6: Temperature measurements

Temperature measurements								
$C[\%]$	$Date[-]$	$T_{min1}[°C]$	$T_{max1}[°C]$	$\Delta T_1[°C]$	$T_{min2}[°C]$	$T_{max2}[°C]$	$\Delta T_2[°C]$	$\Delta t[s]$
0.5	31 − 07	26.39	29.90	3.51	26.28	29.02	2.74	1864
0.7	04 − 08	26.04	30.17	4.13	26.46	28.38	1.92	2210
8.3	03 − 08	26.52	31.21	4.69	26.80	32.79	5.99	8799
12.3	04 − 08	27.42	31.90	4.48	27.55	32.68	5.13	10902
14.5	04 − 08	31.51	33.19	1.68	31.78	34.17	2.39	7927

Air vent

Operating an open loop brings the risk of air entering the system. The possibility that it occurs is the highest around the mixing tank. To avoid it, measures have been taken. Slurry needs to be released in the reservoir under the water surface. If air still gets trapped in the system, it can be removed in two ways. By the use of air removal tubes, installed at the pressure taps, or the use of vents. Of the latter, three have been installed. The first at the top of the U-loop. The second at the vehicle crossing, the connection between the cooling basin and the measurement section. The last one is located in the $180°$ turn between part 'A & B' of the measurement section. A visualisation of their locations and lay-out can be seen in Figure 3.6.

Perspex section

A Perspex pipe is installed between pressure taps 25-26 (see Figure 3.3). It has a length of $1.5\ m$ and is used to monitor the behaviour of the mixture. Therefore it is located 51 meter downstream of the $180°$ turn, where the flow structure is not disturbed by the bend. As can be seen in Figure 3.7, two rulers are attached to the sides.

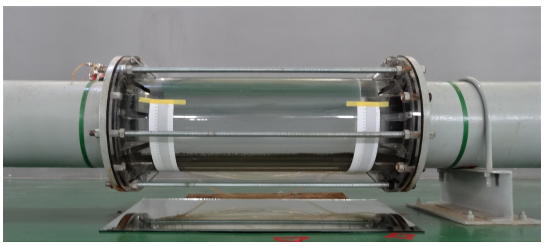

Figure 3.7: Perspex section

Data receiver
Equipment's output is collected by a *CTDAQS-5000* portable data receiving system. It contains three cards, providing 32 signal collecting channels. Adding up to a total of 96. The system can capture voltage and current signals. Limited by the maximum frequency of the differential pressure transmitter (Table 3.1), data is recorded at a frequency of $20\ Hz$.

3.3. Comparison of the configuration

The flow loop configuration and its apparatus are discussed. To answer the second sub-question:

Q_2: *Which test set-up is required to validate these models in a large diameter pipeline?*

The design is compared to five laboratory test set-ups, used for scientific experiments on slurry transport. Four of them are located in Europe, one in Asia. Regarding the technological advancement, it is necessary that the information is up-to-date. Therefore the consulted publications are not older than 20 years. For every comparable research facility, the source and design specifications are given (Table 3.7).

Matoušek (2002)

In 2002, at the Dredging laboratory of Delft University of Technology, Matoušek investigated the *'pressure drops and flow patterns in sand-mixture pipes'* [Matoušek, 2002]. Experiments are conducted on a 24 meter long closed flow-loop, with a pipeline diameter of 150 millimetre. The set-up is equipped with: two radiometric density meters, a magnetic flow meter, a Perspex observation section, an 18 meter high U-tube, temperature regulation and differential pressure transmitters. The latter is used to determine the head loss over a three meter interval. A sketch of the design, containing two measurement sections, is included in Figure 3.8.

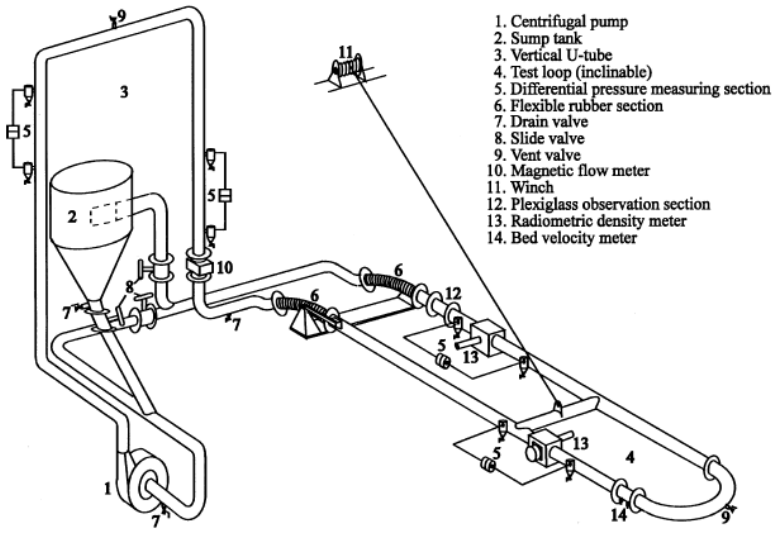

Fig. 1. Laboratory circuit with the 150-mm pipe.

Figure 3.8: Flow loop: Delft University of Technology (2002)

Talmon (2004/2007)
There are two publications on the research of *'self-excitation of concentration fluctuations in slurry pipelines'*, by Talmon [Talmon, 2004, Talmon et al., 2007]. He conducted experiments on a 52 meter long closed flow-loop of Delft Hydraulics. The pipeline, 100 millimetre in diameter, is equipped with: a radiometric density meter, an electro-magnetic flow meter, conductivity probes, an electronic thermometer, multiple Perspex observation sections and differential pressure transmitters. The pressure transducers measure over two intervals. The first over a 10 meter long pipeline section. The second determines the difference over the pump and thus the total hydrodynamic resistance. A drawing of the figure is included in Figure 3.9.

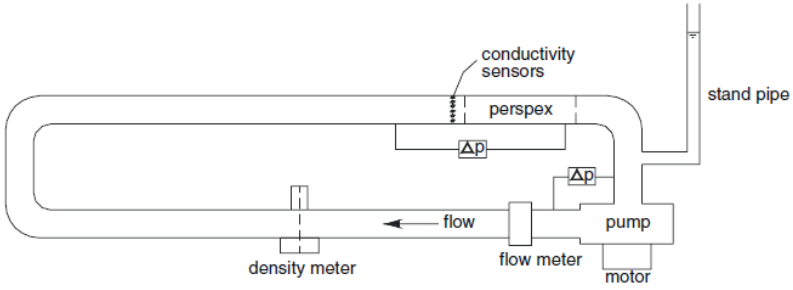

Figure 3.9: Flow loop: Delft Hydraulics (2004)

Ming (2007)
The laboratory of Hohai University in Nanjing houses a 200 millimetre closed-circuit. In 2007, Gu et al. used it in their research on the *'hydraulic transport of coarse gravel (investigation into flow resistance)'* [Gu et al., 2007]. The flow loop is equipped with: a radiometric density meter, a magnetic-inductive flow meter, a Perspex observation section, a U-tube and differential pressure transmitters. Dimensions of the design and the amount of measurement sections are not specified. Nor a sketch of the test set-up is available.

Matoušek & Krupička (2013)
In 2013, Matoušek and Krupička research *'different types of unsteady flow of solids'* at the Institute of Hydrodynamics in Prague. The laboratory facilitates a flow loop consisting of two parts. In the standard lay-out the pipeline has a length of 52 meter. It is equipped with an electromagnetic flow meter, a transparent observation section and three measuring sections containing differential pressure transmitters. Two of them are located in a horizontal pipe and have an interval of two meter. The other one, in a vertical tube, has a dimension of 1.5 meter. Data is recorded at a sampling rate of $2\ Hz$.

By opening the slide valves, the set-up is extended with an additional 41 meter. It opens up the possibility of using an inclinable U-loop. The design of the 100 millimetre circuit is visualised in Figure 3.10.

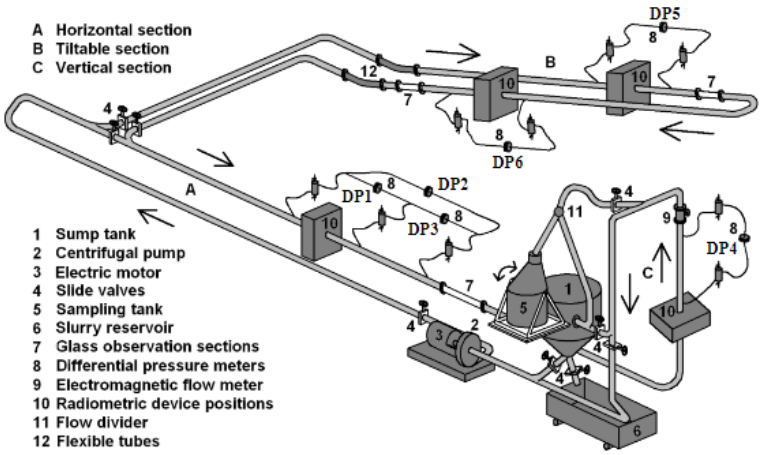

Figure 3.10: Flow loop: Institute of Hydrodynamics Prague (2013)

Talmon (2015)
For an investigation into *'stationary waves behind a bend in heterogeneous transport'*, Talmon used a flow loop manufactured out of Perspex. The internal diameter of the closed circuit is 40 millimetre. It is equipped with a U-tube and eight differential pressure transducers. At pressure tap locations, sand pots are installed to prevent sediment from entering the impulse tubes. The spacing between the taps is three meter and the experiments are conducted at a sampling frequency of $10\ Hz$. A sketch of the design is included in Figure 3.11.

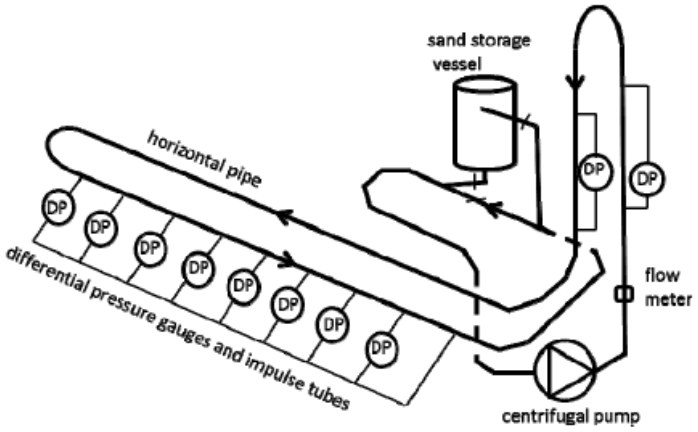

Figure 3.11: Flow loop: Delft University of Technology (2015)

Analysis
A summary of the flow loop specifications is given in Table 3.7. Main difference in the design is that in Shanghai there is operated on an open flow loop. Also the pipeline length and with it the amount of measurement locations, is significantly larger. Creating the possibility to measure under equilibrium conditions. Furthermore, the NERCD has the biggest internal pipe diameter.

Regarding the equipment, the Shanghai laboratory is the only one to use two techniques for the pressure measurement. It creates the possibility to check for malfunction in the devices and to validate the test results. Like all other test set-ups, a U-loop is available to determine the concentration and mixture density. Unfortunately it was not operational at the time.

There is one aspect of the NERCD's flow loop that is considered to be a disadvantage. They posses of an ultrasonic concentration meter. Therefore it is not possible to analyse the internal behaviour of

the mixture. This is a missed opportunity. With the information, research into more accurate hydraulic transport theories, two- or three-layer models, could be conducted. The other configurations feature a radiometric density meter. When the equipment is moved vertically along the pipeline wall, the internal structure of the mixture can be visualised.

Table 3.7: Flow loop comparison

Flow loop comparison			
	Matoušek	**Talmon**	**Gu et al.**
Location	Delft	Delft	Nanjing
Year	2002	2004 – 2007	2007
Loop	closed	closed	closed
Length [m]	24	52	–
Internal diameter [m]	0.15	0.2	0.2
Density meter	radiometric	radiometric	radiometric
Flow meter	electromagnetic	electromagnetic	electromagnetic
U-loop	V	–	V
Thermometer	V	V	–
Perspex section	V	V	V
Pressure meter	differential	differential	differential
Measurement sections	2	2	–
Interval [m]	3	10	–
Sampling frequency [Hz]	–	–	–

	Matoušek et al.	**Talmon**	**This experiment**
Location	Prague	Delft	Shanghai
Year	2013	2015	2017
Loop	closed	closed	open
Length [m]	52(93)	–	220
Internal diameter [m]	0.1	0.04	0.3
Density meter	–	X	ultrasonic
Flow meter	electromagnetic	V	electromagnetic
U-loop	V	V	X
Thermometer	–	–	V
Perspex section	V	V	V
Pressure meter	differential	differential	differential & total
Measurement sections	3	8	32/34
Interval [m]	2	3	3
Sampling frequency [Hz]	2	10	20

V: present , –: not specified, X: not present

3.4. Experimental protocol

The experiment starts with water flow tests, which serves multiple purposes. It gives opportunity to check whether the equipment works properly, ruling out the possibility of a factory error or malfunctioning due to wrong instalment. Second, it provides the hydraulic gradient for liquid flow.

The water experiment starts at high velocity. The pumps rotational speed is gradually decreased, until the lowest test velocity is reached. This process is repeated two more times. When the set-up is validated and the equipment found to work properly, there is proceeded to the mixture experiments.

Before every mixture test, one liquid test is carried out, for reference. For every concentration the slurry is transported at multiple velocities. This counts as one test run and is repeated two more times. Resulting in three different runs for every concentration.

The aim is to perform experiments for five different slurry concentrations: 5, 10, 15, 20 and 25 percent. Due to malfunction of the ultrasonic concentration meter (see section 3.2), the targeted values turned out to be lower. Respectively: 4.4, 8.1, 12.3 and 14.6 percent. Furthermore, one experiment could not be conducted due to a tight schedule. The test-matrix is included in appendix E. For every experiment it contains: the number of runs, transport velocities and measured delivered concentrations.

4

Preliminary calculations

The prediction methods are influenced by input parameters. Their definitions and how they are determined is discussed in this chapter. The topics in order of appearance are: sediment classification, elementary approach on the settling velocity and prediction methods for fitting losses. The chapter concludes with an overview of the parameters.

4.1. Sediment

The sediment is retrieved during dredging operations by the '*China Communications and Construction Company*'. It originates from Xiamen, a coastal city in Fujian province, located in the south of China. The material was send to the NERCD laboratory, to be analysed and used in scientific experiments.

To determine the particle size distribution, two techniques have been used: laser and sieving. The former is executed by and external company: '*Malvern Instruments Ltd.*'. They examined fifteen soil samples. The sieving analysis, conducted on three soil samples, is executed in house. Six sieves, with apertures of 0.075, 0.25, 0.5, 1, 2 and 5 mm, have been used in the process. The resulting cumulative grain size distribution is visualised in Figure 4.1. To keep it readable, the mean of fifteen laser tests is plotted and not the individual result.

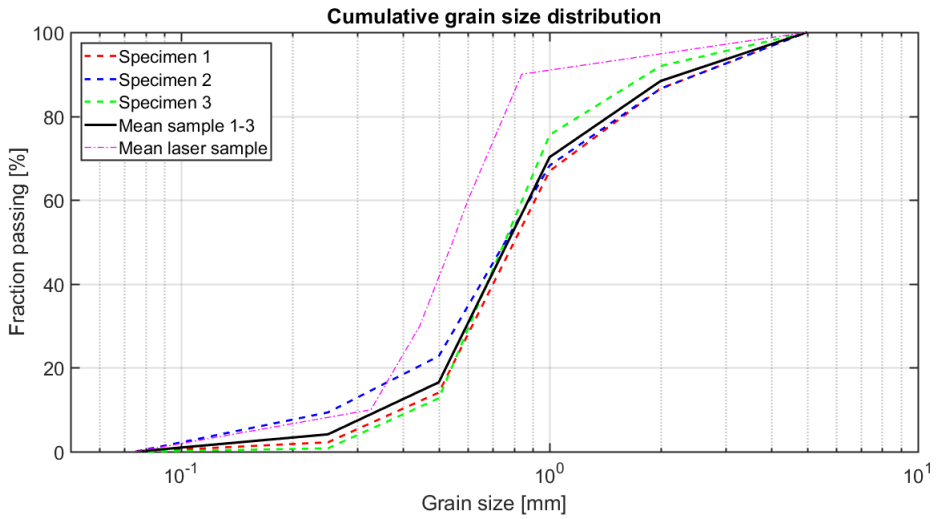

Figure 4.1: Grain size distribution

The result of the laser tests shows a significant lower d_{50}, compared to that of sieving. Considering that the sieving method is traditional in geotechnical engineering, further calculations are done with the outcome of the sieving tests. The values are presented in Table 4.1. According to soil classification

[Miedema, 2016b], the sediment is a mix of medium, coarse, very coarse sand and fine gravel. The decisive particle diameter, an input parameter for the Führböter head loss prediction, is calculated according to equation . The result is $0.866\ mm$. The density of the solids is found to be $2650\ \frac{kg}{m^3}$.

$$d_{mf} = \frac{d_{10} + d_{20} + ... + d_{80} + d_{90}}{9} \tag{4.1}$$

Table 4.1: Grain size distribution

Cumulative grain size distribution [mm]								
d_{10}	d_{20}	d_{30}	d_{40}	d_{50}	d_{60}	d_{70}	d_{80}	d_{90}
0.347	0.522	0.595	0.677	0.770	0.876	0.997	1.453	2.274

4.2. Settling velocity

The terminal settling velocity of a transported single particle, defined as the velocity at which it settles in a large volume of liquid, can be determined in multiple ways. Both Matousek [Matoušek, 2004b] and Durand [Durand, 1953] describe a technique depending on flow regime and grain size distribution. Applicable on the d_{50} of $0.77\ mm$, is the Budryck equation. Designed for particles between 0.1 and 1 millimetre and the transition zone between laminar and turbulent flow. The equation is written down in formula 4.2.

$$v_t = \frac{8.925}{d_{50}} * \left(\sqrt{1 + 95 * \frac{S_s - S_f}{S_f} * d_{50}^3} - 1 \right) \tag{4.2}$$

Where 'S_f' is the relative density of the liquid and 'S_s' the relative density of solids. Calculated according to formulas 4.3 and 4.4. The mass median particle diameter, 'd_{50}' is expressed in millimetre.

$$S_f = \frac{\rho_f}{\rho_w} \tag{4.3}$$

$$S_s = \frac{\rho_s}{\rho_w} \tag{4.4}$$

Because of the broad grain size distribution it is considered to use different calculation methods. One is the *Rittinger* equation (formula 4.5), developed for particles larger than $1\ mm$ in a turbulent flow regime. Again 'd_{50}' is expressed in millimetre.

$$v_t = 87 * \sqrt{\frac{S_s - S_f}{S_f} * d_{50}} \tag{4.5}$$

The other prediction method, applicable on mixtures with a broad grain size distribution, is developed by Ferguson and Church [Ferguson and Church, 2004]. The principle is written down in equation 4.6.

$$v_t = \frac{R_{sd} * g * d_{50}^2}{C_1 * v_f + \sqrt{0.75 * C_2 * R_{sd} * g * d_{50}^3}} \tag{4.6}$$

Where the coefficients C_1 and C_2, have values of 18 and 1. Equation 4.7 is used to determine the relative submerged density R_{sd}.

$$R_{sd} = \frac{\rho_s - \rho_w}{\rho_w * \frac{\rho}{1000}} \tag{4.7}$$

Nevertheless, this is a comparative study analysing frictional head loss prediction methods. Among them is the Durand principle, using the Budryck equation. Therefore formula 4.2 is used. The outcome is $0.087\ m/s$. The other techniques are only mentioned and not used during the research.

4.3. Minor losses

In the measurement section the pipeline makes a $180°$ turn. The bend can be considered as an obstruction, the flow contracts within. It changes the effective cross-sectional area and alters the flow direction, inducing an additional frictional loss. It is defined as a minor loss, because the energy dissipation is smaller in comparison with the loss in straight pipes. A drawing of the bend in Figure 4.2 displays the dimensions (mm) in green, pressure tap numbers in red and angles in black.

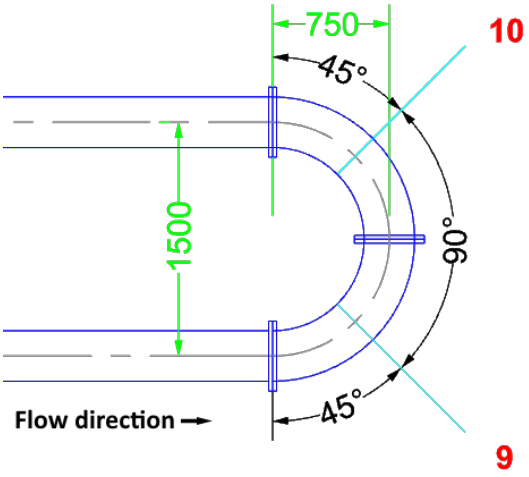

Figure 4.2: 180° turn

The pressure loss due to friction in a fitting can be predicted by two methods. One is described by Matoušek [Matoušek, 2004a], the other one proposed by the Hydraulic Institute [Karassik et al., 2000]. Both are discussed, one is used during the data processing.

Matoušek

The principle provided by Matoušek, uses friction coefficient 'ξ' to determine the minor loss. The coefficient depends on the angle of the bend and the r/D_p-ratio. Regarding the design of the test set-up, the ratio is 2.5. The related coefficients for different angles can be found in Table 4.2.

The theory does not provide a ξ-value for a 180° bend. Therefore the turn is divided in three intervals corresponding with the pressure tap locations. Respectively two fittings of 45° and one of 90°. A detailed view on the configuration is displayed in Figure 4.2.

Table 4.2: Fittings: friction coefficient

Fittings: ξ-value [-]		
r/D_p	45°	90°
1.5	0.130	0.20
2.0	0.090	0.13
2.5	0.085	0.13
3.0	0.080	0.13

Calculating the minor head loss, there is made a distinction between liquid and mixture flow. The former according to formula 4.8, the latter to 4.9. Transferring the result to a hydraulic gradient or pressure loss, formula 4.10 is used.

$$I_{bend,f} = \xi * \frac{V^2}{2 * g} \tag{4.8}$$

$$I_{bend,m} = \xi * \frac{V_m^2}{2 * g} * \frac{\rho_m}{\rho_f} \tag{4.9}$$

$$\Delta P_{bend} = I_{bend} * g \tag{4.10}$$

Hydraulic institute

In the '*Pump Handbook*', Messina describes the theory of the 'Hydraulic Institute' [Karassik et al., 2000]. Compared with the principle proposed by the Matoušek, no distinction between liquid and mixture flow is made. Resulting in only one formula for the minor head loss: 4.10. The friction coefficient 'ξ' is not pre-determined and needs to be read from a graph.

$$h_{bend} = \xi * \frac{V_m^2}{2 * g} \tag{4.11}$$

Analysis
The prediction methods are compared by means of a fictional situation. Having flow rates of respectively 700 and $1200\ m^3/h$. Because the approaches are almost identical, a similar outcome is expected. The result is visualised in Figure 4.3. Where the bend is located around the 25 meter pipeline position. The difference in prediction for the low flow rate is less than $0.5\ kPa$. Regarding the other transport velocity, the difference is never higher than $1.5\ kPa$. The black line added to the figure, is to represent how the initial pressure profile compares to the linear profile after the fitting loss.

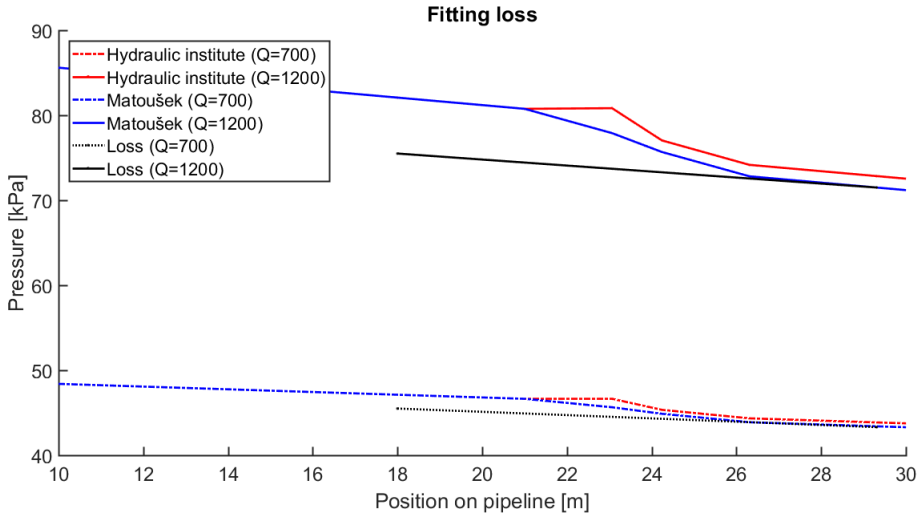

Figure 4.3: Fitting loss

However, the figure is not representative of reality. This is due to the division in intervals. The comparison is showing the summation of minor losses over the three intervals. While the actual loss manifests in the third interval. This can be seen in figures in chapter 5.4, where results of the water flow experiments are discussed. The physical explanation goes as follows: when the cross-sectional area changes in the first interval, the pressure increases. In the second interval there is a combination of two working principles. First the pressure is further accumulated. Next it is released and the pressure starts to drop. Now the fitting causes an additional frictional head loss. This loss continues in interval three.

The principles are compared and an analysis is made. The disadvantages and advantages are itemised and a prediction method is chosen:

- In the theory described by Matoušek, a distinction is made between liquid and mixture flow. Messina considers the loss to be equal for both situations.
- Matoušek's friction coefficients are pre-determined and ready to use. According the the Hydraulic Institute, the factor needs to be read from a graph. The graphs contain a logarithmic scale, creating the possibility of reading errors.
- For a flow rate higher than 1000 m^3/h, the difference in outcome is less than 1.5 kPa.

Considering the arguments, it is opted to predict the additional friction loss according to the principle of Matoušek.

4.4. General parameters

An overview of parameters defined in advance of the experimental research, is to be found in Table 4.3.

Table 4.3: General parameters

General parameters			
Symbol	Definition	Value	Dimension
d_{50}	Mass-median particle diameter	0.770	$[mm]$
d_{mf}	Decisive particle diameter	0.866	$[mm]$
D_p	Pipe diameter	0.30	$[m]$
f_s	Sampling frequency	20	$[Hz]$
g	Gravitational acceleration	9.81	$[m/s^2]$
S_f	Relative density of fluid	1	$[-]$
S_s	Relative density of solids	2.65	$[-]$
v_t	Terminal settling velocity of a single particle	0.087	$[m/s]$
μ_s	Mechanical friction coefficient	0.4	$[-]$
v_f	Kinematic viscosity of liquid	$1 * 10^{-6}$	$[m^2/s]$
ρ_f	Density of fluid	1000	$[kg/m^3]$
ρ_s	Density of solids	2650	$[kg/m^3]$

5

Analysis water flow experiment

The data acquired in the water-flow experiment is compared with three theories: Swamee & Jain [Swamee and Jain, 1976b], RangaRaju & Garde [Swamee and Jain, 1976a] and Darcy-Weisbach [Churchill, 1977]. All of them are derived from the Colebrook-White equation [Colebrook, 1939]. The comparison serves multiple purposes:

- The flow loop and equipment are brand new. To check for malfunctions, there is examined if the result matches the expectation.
- The absolute pipe wall roughness 'k', is not provided by the pipeline manufacturer. To determine the value, assumptions are made. In an iterative process, theory is fitted to the data until an accurate result is achieved. The prediction method showing the most similarity is used in calculations for the mixture flow experiments.

This chapter started with the plan of approach on the water flow experiment. Next the three major theories are explained, a flow loop correction equation is developed and the absolute pipe wall roughness is determined. At last, the results are discussed and visualised.

5.1. Applicable theories

Darcy-Weisbach
The frictional pressure loss over desired pipeline length ΔL, is predicted by Darcy-Weisbach according to equation 5.1.

$$\Delta P = \frac{I_f * \rho_f * g}{1000} * \Delta L \tag{5.1}$$

The formula contains the dimensionless hydraulic gradient for liquid flow I_f. Which is determined by equation 5.2.

$$I_f = \frac{\lambda_f}{D_p} * \frac{V^2}{2 * g} \tag{5.2}$$

It holds the unknown parameter λ_f. Multiple options to determine the Darcy-Weisbach friction coefficient are available. It is opted to use the computational method proposed by Churchill [Churchill, 1977] in formula 5.3. This way of calculating leaves less room for errors in contrast with the Moody method [Moody, 1944], where the value has to be read from a graph. There are two input arguments that need to be defined. The Reynolds number 'R_e' is calculated according to equation 5.4. The determination of absolute pipe wall roughness 'k' is explained in section 5.3.

$$\lambda_f = 8\left[\left(\frac{8}{R_e}\right)^{12} + \left\{\left(-2.457 * ln\left[\left(\frac{7}{R_e}\right)^{0.9} + \frac{0.27k}{D_p}\right]\right)^{16} + \left(\frac{37530}{R_e}\right)^{16}\right\}^{-1.5}\right]^{\frac{1}{12}} \tag{5.3}$$

$$R_e = \frac{V * D_p}{\upsilon_f} \tag{5.4}$$

RangaRaju & Garde
RangaRaju and Garde provide two equations for the head loss prediction, expressed in a hydraulic gradient. Which formula to apply depends on a dimensionless parameter that is subjected to the flow rate. If the terms of formula 5.5 are met, equation 5.6 is used.

$$\frac{Q}{\upsilon_f * k} * \left(\frac{k}{D_p}\right)^{2.633} < 0.282 \tag{5.5}$$

$$I_f = \left[\frac{Q}{\upsilon_f * k} * \left(\frac{k}{D_p}\right)^{2.633} * \frac{1}{3.39}\right]^{\frac{1}{0.54}} * \frac{\upsilon_f^2}{k^3 * g} \tag{5.6}$$

Meeting the requirements of formula 5.7, equation 5.8 is used.

$$\frac{Q}{\upsilon_f * k} * \left(\frac{k}{D_p}\right)^{2.633} > 0.282 \tag{5.7}$$

$$I_f = \left[\frac{Q}{\upsilon_f * k} * \left(\frac{k}{D_p}\right)^{2.633} * \frac{1}{2.85}\right]^{\frac{1}{0.502}} * \frac{\upsilon_f^2}{k^3 * g} \tag{5.8}$$

Equation 5.9 provides the calculation method for the friction factor.

$$\lambda_f = \frac{\pi^2 * g * D_p^5 * I_f}{8 * Q^2} \tag{5.9}$$

Swamee & Jain
The Swamee and Jain theory is derived from the Colebrook-White equation. In their research a distinction between two flow types is made: smooth-turbulent and rough-turbulent. In their conclusion they came to equations suitable for both situations. For the friction factor this is equation 5.10 and the frictional head loss is described in formula 5.11.

$$\lambda_f = \frac{0.25}{\left[log\left(\frac{k}{3.7D_p} + \frac{574}{R_e^{0.9}}\right)\right]^2} \tag{5.10}$$

$$I_f = \frac{\frac{0.203Q^2}{g*D_p^5}}{\left[log\left(\frac{k}{3.7D_p} + \frac{574}{R_e^{0.9}}\right)\right]^2} \tag{5.11}$$

5.2. Flow loop correction equation

Thirty-seven water flow experiments have been carried out. An overview of the measured velocities and concentrations is included in Table 5.1.

Table 5.1: Test matrix: liquid flow

Test matrix										
CONCENTRATION: 0%										
RUN 1	V_m $[m/s]$	5.66	5.34	5.27	4.64	4.48	3.89	3.18	–	–
	C [%]	0.78	0.63	0.59	0.44	0.40	0.38	0.33	–	–
RUN 2	V_m $[m/s]$	2.40	2.99	3.81	4.56	5.27	5.93	6.60	–	–
	C [%]	0.97	0.99	0.93	0.83	0.73	0.63	0.54	–	–
RUN 3	V_m $[m/s]$	2.44	3.10	3.77	4.44	5.27	6.05	6.56	–	–
	C [%]	0.97	0.97	0.95	0.84	0.72	0.60	0.50	–	–
RUN 4	V_m $[m/s]$	2.40	3.07	3.77	4.56	5.19	6.01	6.60	–	–
	C [%]	0.97	0.95	0.94	0.85	0.78	0.58	0.48	–	–
RUN 5	V_m $[m/s]$	5.93	6.01	6.01	5.31	4.60	4.24	3.89	4.64	4.64
	C [%]	1.28	1.26	1.26	0.85	0.66	0.61	0.57	0.60	0.62

The total pressure profile measurements for water are visualised in Figure 5.1. The color of a line represents a velocity as defined in the colorbar at the right. Observations show variations over the total pipeline length in every experiment. The magnitude of these variations grow when the velocity increases. The similarity between the deviations at a pressure tap give reason to believe that they are caused by differences in the equipment installation. When drill holes aren't completely equal or pipes at flanges are misaligned and the sensors aren't located exactly at the pipe wall, the measured water pressure can differ a little. It are these inaccuracies that give way to deviations at specific measurement locations. To get rid of these anomalies, a correction equation for every total pressure meter is developed, with exemption of those located in the bend.

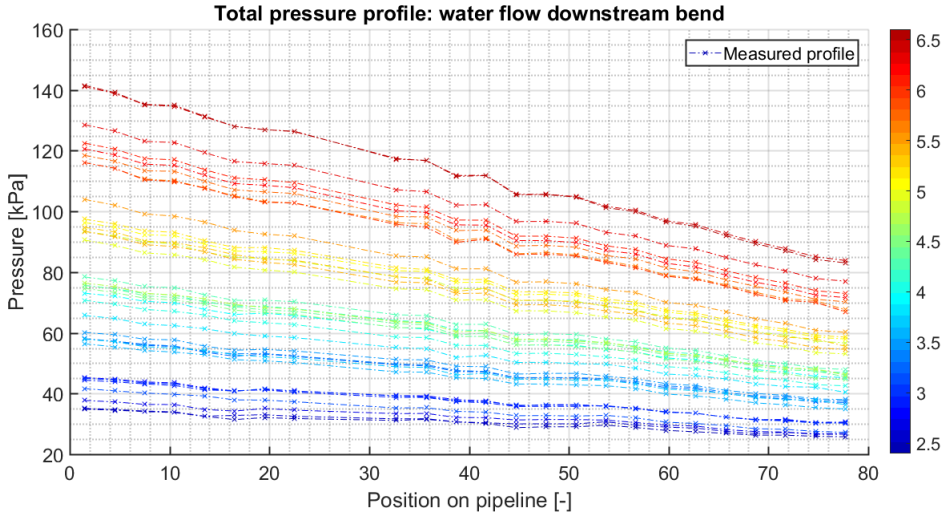

Figure 5.1: Total pressure profile: water flow downstream bend

To develop a correction equation, the experiment is categorised in two parts: what takes place downstream of the vehicle crossing, in measuring section 'A' (Figure 3.3), is found in Appendix G. What takes place downstream of the 180° turn, is discussed in this section. The distinction is necessary, because the fitting disturbs the linearity of the pressure profile. In both situations the theoretical approach is similar, the figures differ.

The flow loop correction equation is constructed according to the principle of Maciej and Talmon, described in '*Stationary waves in pipeline flow*' [van Es and Boone, 2015]. It is developed for an experiment using differential pressure transducers. Nevertheless, it is also applicable on data of the total

pressure meters.

The procedure goes as follows: for every experiment a linear fit is made through the related data points. The difference between points on the curve and fitting are determined. Next the pressure taps are analysed. Regarding a tap, 37 deviations are know with their corresponding velocity. To correlate the deviation with velocity, the outcome is plotted against $0.5 * \rho * V^2$. A linear fit is made through the points. The result is a second degree equation in the form of $a + b * V^2$. The values of coefficients a and b are tap dependent and used in equation 5.12 to correct the measured pressure.

$$P_{corrected} = P_{measured} + a + b * \frac{\rho_f * V^2}{2} \tag{5.12}$$

The values for coefficients a and b, with the corresponding tap number, can be found in Table 5.2. Using the correction equation results in a more linear pressure profile, this is visualised in Figure 5.2. It is concluded that the correction method is suitable. Therefore it is applied on all the acquired data, for both mixture and liquid experiments.

Table 5.2: Flow loop correction coefficients

Flow loop correction coefficients					
Tap number	**a [kPa]**	**b**	**Tap number [-]**	**a [kPa]**	**a [-]**
1	-0.3846	-0.0108	18	0.4433	-0.072
2	0.1687	-0.0460	19	-0.1232	0.0055
3	0.2919	0.0777	20	-0.3218	-0.0565
4	0.0902	0.0095	21	-0.0059	0.0701
5	-0.0606	-0.0083	22	0.2246	-0.0664
6	-0.1597	-0.0043	23	0.0885	0.1192
7	0.3432	-0.0391	24	-0.1190	0.0214
8	-0.2941	0.0220	25	-0.3320	-0.0344
9	-	-	26	-1.3496	0.0485
10	-	-	27	-0.6765	-0.0172
11	-0.2323	-0.0178	28	-0.1389	0.0131
12	-0.1958	-0.0168	29	-0.0622	-0.0327
13	-0.2557	0.063	30	0.3770	-0.0278
14	0.0244	-0.028	31	0.7039	-0.0161
15	0.6036	-0.0177	32	0.2220	0.0102
16	0.7334	0.0276	33	0.3212	0.0056
17	-0.0405	0.0258	34	0.1051	-0.0055

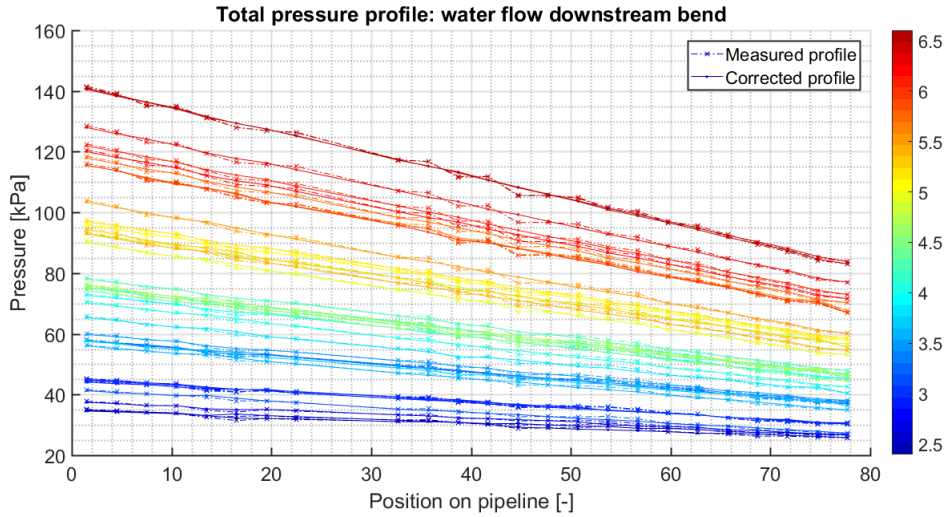

Figure 5.2: Corrected total pressure profile: water flow downstream bend

To clarify the correction principle, an example is given by means of the $5.9\ m/s$ velocity experiment. The result of the laboratory test is included in Figure 5.3. The blue curve represents the original measurement, recorded by the total pressure meters. The black line indicates the linear fit through the data points. The pressure is corrected according to equation 5.12, by use of coefficients a and b. The result, the corrected pressure profile, is plotted in green and almost similar to the linear fit. Furthermore, the figure includes the measured and corrected hydraulic gradients over the pipeline.

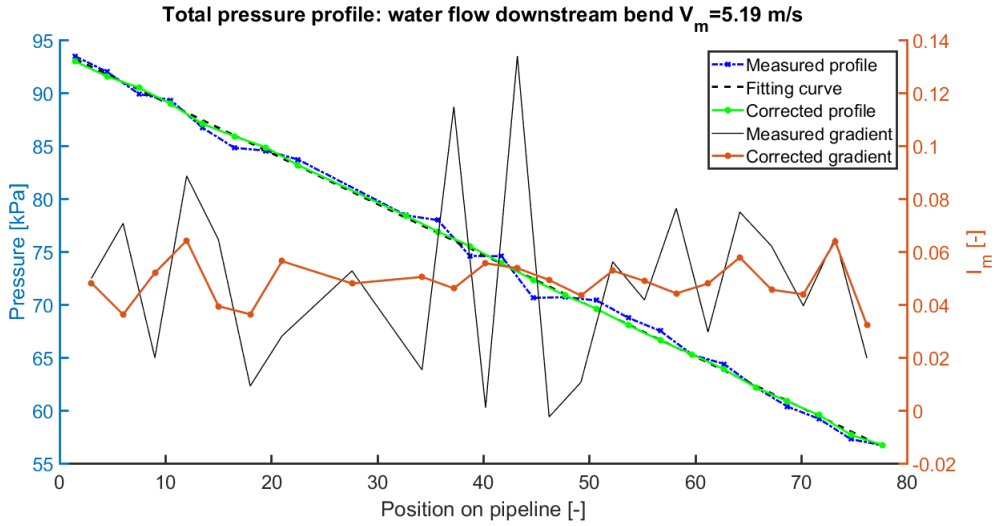

Figure 5.3: Corrected total pressure profile: water flow downstream bend

5.3. Pipe wall roughness

An estimation of the hydraulic roughness is made by a process of trial and error. According to the prediction methods considered in section 5.1, theoretical waterlines are plotted with the acquired data for different values of 'k'. The best fit results in a 'smooth' pipe wall. Therefore 'k' is assumed to be zero in both Darcy-Weisbach and Swamee and Jain. Assigning the same value to the RangaRaju and Garde theory will make the denominator negative. To avoid this, the roughness is assumed to be 10^{-8} meter. The resulting resistance curve, for data collected with the local pressure meters, can be found in Figure 5.4. The graph representing the differential pressure measurement is included in appendix F.

Results are so similar that differences between them are almost negligible. This lead to the possi-

bility of using all of them for calculations with the mixture experiments. For simplicity only one is used: the Darcy-Weisbach method.

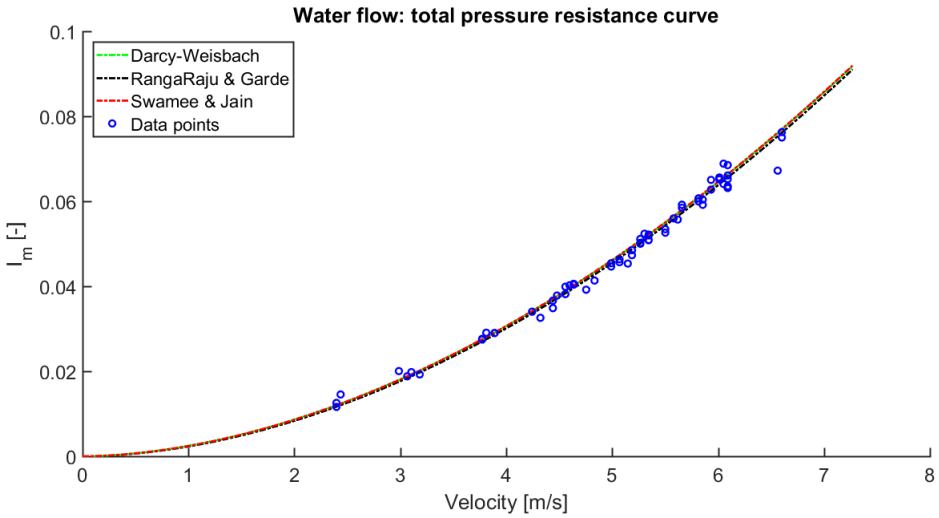

Figure 5.4: Resistance curve: total pressure

5.4. Analysis

The overall result of the water flow experiment, the resistance curve, is included in the previous section (Figure 5.4). There is a good correlation between hydraulic gradients and the theoretical curve for a smooth pipeline. On one occasion the result showed a large divergence with regard to the prediction. This is at a flow speed of $6.56\ m/s$. Because it occurred only once out of thirty-seven, it is considered to be a measurement error.

The individual experiments are analysed and the figures containing the pressure profiles and hydraulic gradients are included in Appendix H. The result is explained on the basis of three flow rates. The lowest examined velocity of $2.4\ m/s$, an intermediate of $4.6\ m/s$ and the highest of $6.6\ m/s$. Their pressure profiles can be found in Figure 5.5. The related hydraulic gradients in Figure 5.6. The results of this specific experiments can be found in Figures: H.1a, H.10a and H.18b.

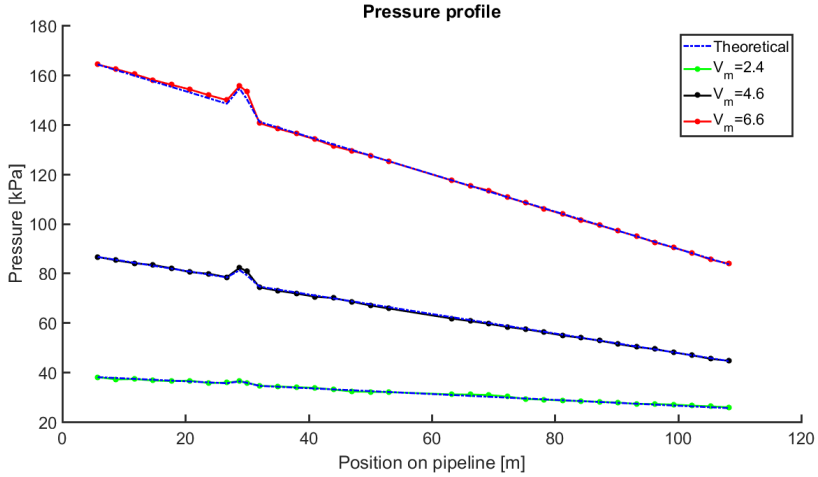

Figure 5.5: Pressure profile: water flow

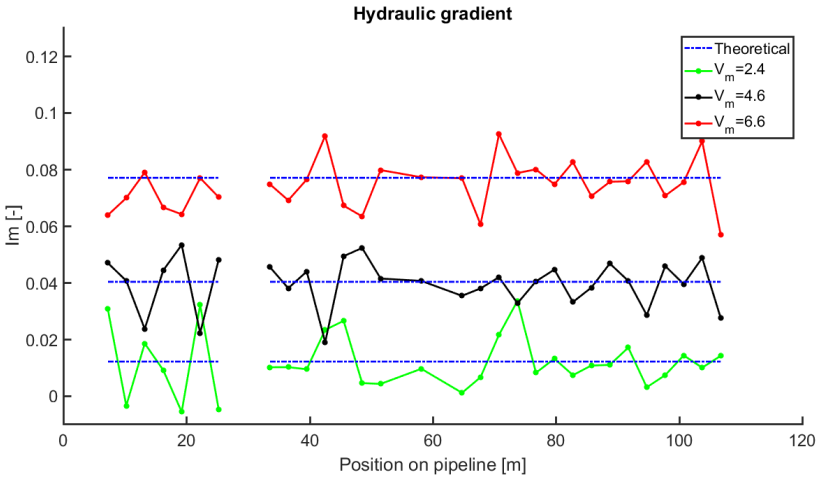

Figure 5.6: Hydraulic gradient: water flow

A first observation is that for velocities larger than $4\ m/s$, the value recorded by *total pressure meter* 34 deviates (located at 108 meter). This is clearly visible in Figure 5.6, containing the hydraulic gradients. Seventeen times a sudden decrease is monitored and in nine occasion the gradient increases. There are two possible explanations. The first is malfunction of the equipment. The second has to do with the location. The pressure tap is the last one in the measuring section (see Figure 3.3). Downstream at a distance of two and a half meter a $180°$ turn is located. This is less than nine times the pipeline diameter. In comparable research [Matoušek, 2002] the distance from a bend is $44xD_p$, in order to avoid flow disturbance due to the fitting. Therefore the data acquired on pressure tap 34 is left out of consideration.

Furthermore, the pressure profiles give a good fit to the Darcy-Weisbach theoretical prediction. The peak at the 30 meter position corresponds to the location of the $180°$ turn. There the expected head loss, according to the calculation method in section 4.3, did not correspond to the experimental data. Therefore the theoretical profile is modified to match the result. In the first interval (Figure 4.2) the pressure increases, to drop in the second and third section. In total, the additional friction loss due to the fitting is equal to that of a $90°$ bend. The same calculation method for fitting losses is not applied in the mixture experiment. With the additional density term, see equation 4.9.

Considering the hydraulic gradients, a gap is found where the bend is located (Figure 5.6). It is not taken in to account because there the result definitely deviates from the prediction. Regarding the other intervals a good result is achieved. The gradients vary around the expected values and there is a clear distinction between the data of different velocities.

6

Analysis mixture flow experiment

In the mixture-flow experiment the acquired data is compared with four theories: Durand [Durand, 1953], Führböter [Führböter, 1961], Jufin-Lopatin [Jufin and Lopatin, 1966] and Wilson [Wilson et al., 2006b]. The chapter starts with an introduction of the prediction models. Discussing their applicability to different flow regimes. What follows is a discussion on how they relate to each other and the experiments conducted in this research. Then the acquired data is compared to the predictions, an analysis is made.

6.1. Applicable theories

In this section the background of the prediction models is examined and their theoretical principles are explained. The calculation methods hold the information to answer research question three:

Q_3: *What do the mathematical models predict for a pipeline of 300 millimetre diameter?*

Durand

It is in 1952, at the *Laboratoire Dauphinois d'Hydraulique* in Grenoble, that Durand developed an empirical prediction model for the frictional pressure loss during slurry transport in pipelines. He conducted experiments at multiple locations. In Grenoble he possessed of pipelines with diameters of 40, 104, 150 and $120\ mm$. In Nantes and Donzère larger scale test, using diameters of 330, 580 and $700\ mm$, took place. Experiments were carried out with uniform solids, categorised as sand and gravel. The particle size varying between $20\ \mu m$ and $100\ mm$. Concentrations ranged between 2% to 22%.

In the report Durand distinguishes three transportation types in the heterogeneous flow regime, that depend on the particle size. In the conclusion he links the velocity to the head loss and describes how to predict it. The result is formula 6.1, used to determine the hydraulic gradient.

$$I_m = 180 * \left(\frac{V_m^2 * \sqrt{g * d_{50}}}{g * D_p * v_t} \right)^{-1.5} * I_f * C_{vd} + I_f \tag{6.1}$$

Using various pipeline diameters and grain sizes, the research has a broad scope. That only the heterogeneous flow regime is studied, is considered as a limitation. When head loss predictions are made at transition zones to stratified or pseudo-homogeneous flow, inaccuracies are shown. This difference between reality and theory diminishes the applicability of the model.

Führböter

In 1961 Alfred Führböter presented his dissertation at the *Technische Hochschule Hannover*. The research on frictional head loss has been carried out on a $300\ mm$ diameter flow loop. It considered grain sizes between 0.15 and $4.6\ mm$. But a detailed analysis of the experiments was limited to the range of 0.26 to $0.83\ mm$. The resulting prediction method is expressed in equation 6.2.

$$I_m = S_{kt} * \frac{C_{vd}}{V_m} + I_f \tag{6.2}$$

The formula is simplistic and therefore easy to use. It contains a single input parameter, the empirically determined transport factor S_{kt}. The value, for a decisive particle diameter of $0.866\ mm$, is calculated according to equation 6.3.

$$S_{kt} = 2.59 * d_{mf} - 0.037 \tag{6.3}$$

Instead of d_{mf}, the mass-median particle diameter can figure as an input parameter. Both possibilities are analysed, the results using d_{50} show a better correlation with the experimental data. Therefore all Führboter predictions are made using the mass-median particle diameter. The result using the decisive diameter is included in appendix I.

The transport factor depends on the spatial volumetric concentration C_{vi} and the assumption of a constant slip ratio. That the approach is simplistic, is a limiting factor for the applicability of the model. First, the settling velocity is not taken into account. Second, a constant value of the slip ratio does not stroke with the principles of mixture flow: containing a broad range of transport velocities, concentrations, applicable pipeline diameters and grain sizes. The possibility of a broad particle size distribution, investigated in this experiment, is not even considered.

Jufin & Lopatin

In 1966, the Soviet Union developed a technical norm regarding slurry transport through pipelines. The authors, Jufin and Lopatin, analysed four models proposed by research facilities. The prediction methods were tested with collected experimental data and records of dredge installations. Covering particle sizes of 0.25 to $11\ mm$, categorised as sand and gravel, and tube diameters of 24 to $900\ mm$. The final result is the equation presented in formula 6.4. Unlike other models, this principle appears to describe the lower limit of the head loss [Talmon, 2017].

$$I_m = \left[1 + 2\left(\frac{V_{min}}{V_m}\right)\right]^3 * I_f \tag{6.4}$$

Where V_{min} is the minimum velocity. The value is determined according to the empirical correlation given in equation 6.5.

$$V_{min} = 5.3 * \left(C_{vd} * D_p * \Psi^*\right)^{\frac{1}{6}} \tag{6.5}$$

It contains the particle settling parameter Ψ^*, equation 6.6. Which depends on the particle Froude number Fr_{vt}.

$$\Psi^* = Fr_{vt}^{1.5} = \left(\frac{v_t}{\sqrt{g * d_{50}}}\right)^{1.5} \tag{6.6}$$

The outcome assigns a value 0.716 to Ψ^*. Nevertheless, a broad grain size distribution affects the parameter. Therefore an addition is made in formula 6.7.

$$\Psi^* = \frac{\sum_i Fr_{vt,i}^{1.5} * p_i}{100} \tag{6.7}$$

The equation depends on the soil fraction pi, expressed as a percentage of the total weight. The result is 0.978, the input for the calculation is included in Table 6.1. A comparison is made between the use of formulas 6.6 and 6.7. The result is included in section 6.3.6.

Table 6.1: Particle settling parameter

Particle settling parameter				
d_{sieve} [mm]	P_i [%]	d_i [m]	$Fr_{vt,i}^{1.5}$	$Fr_{vt,i}^{1.5} * P_i$
5	0.00			
2	13.40	0.0035	0.32	4.31
1	19.69	0.0015	0.61	11.96
0.5	52.82	0.00075	1.02	53.96
0.25	11.86	0.00038	1.72	20.37
0.075	2.23	0.00016	1.32	7.16
SUM	–	100	–	–	97.76

Wilson
The Wilson - Georgia Iron Works model, the last of four analysed prediction methods, is the most recent. It dates back to 1979 and is developed for the heterogeneous flow regime. According to the authors, the regime is a transition zone between two flow types: the fully stratified and fully-suspended. Each having a clearly distinctive transport mechanism. The former by contact loads, the latter by suspension. This model formed the base for the 4-component model [Sellgren et al., 2016].

The research consisted of experiments on two flow loops with different cross-sectional area. The first has a pipeline diameter of $200\ mm$, the second of $440\ mm$. The mixture contained particles that are categorised as medium to coarse sand. The delivered volumetric concentration did not exceed a value of 16%.

$$I_m = 0.5 * \mu_s * \left(\frac{V_m}{V_{50}}\right)^{-M} * C_{vd} * (S_s - 1) + I_f \tag{6.8}$$

Where $\frac{V_m}{V_{50}}$ is the stratification ratio.

$$V_{50} = 3.93 * d_{50}^{0.35} * \left(\frac{S_s - 1}{1.65}\right)^{0.45} \tag{6.9}$$

The empirically determined exponent M, relates the stratification ratio with the particle size distribution. It is calculated according to formula 6.10.

$$M = ln\left(\frac{d_{85}}{d_{50}}\right)^{-1} \tag{6.10}$$

The value of d_{85}, read in Figure 4.1, is 1.759. Resulting in M to be 1.21. However, recent developments give reason to believe that the calculation method should be altered. The data set, used to empirically determine the exponent, contained measurements under deposition limit velocity. Removing data of experiments with a stationary bed, should alter the exponent. Therefore the value should become closer to one [Matoušek, 2018]. Because this research has an investigative character, the principle of Wilson is used as first proposed.

6.2. Comparison of the prediction models

The four prediction methods analysed in the previous section are developed for a heterogeneous flow regime. This suits the scope of this project. Due to the flow loops length and the limited pump capacity, it is not possible to achieve a transport velocity high enough to reach pseudo-homogeneous flow. Furthermore, there is no possibility to conduct experiments in fully stratified flow. The design of the set-up contains various turns and height differences. With it comes the risk of blockage. To avoid it, experiments can only be carried out at the limit of deposition velocity.

To compare the principles, a summary of the underlying experimental parameters is given in Table

6.2. In general the NERCD fits the range of the prediction methods, for both concentration and pipeline diameter. One significant difference is found in the mass-median particle diameter. Where most of the theories are developed using uniform solids, this experiment is carried out with a broad grain size distribution.

Table 6.2: Comparison of prediction models

Prediction models for mixture flow				
Model	Year	D_p $[mm]$	d_{50} [mm]	C_{vd} [%]
Durand	1953	$40, 104, 105, 120, 580, 700, 330$	$20 * 10^{-3}$ - 100	≤ 22
Führböter	1961	300	0.15 - 1.8	–
Jufin & Lopatin	1966	103 - 800	0.25 - 11	–
Wilson	1992	$200, 440$	–	≤ 16
Scope of this experiment				
–	2017	300	0.770	≤ 15

–: not specified

6.3. Result

To commence, the slurry transport experiment is analysed per mixture concentration. In order of appearance: 4, 8, 12 and 15 percent. First a general description of the test result is given. The measured hydraulic gradients are plotted against their theoretical prediction. The figures contain a blue line representing an ideal situation: where a test result matches the prediction of an examined principle. When a data point falls left of the line, the frictional head loss is higher than expected. If it is located at the right side, the pressure drop is underestimated by the prediction method.

After separately analysing the concentration measurements, all data is brought together in a resistance curve. Containing the hydraulic gradients and the theoretical predicted curves. The results are discussed and a conclusion is drawn. To conclude the section, the hydraulic gradients over the pipeline length are analysed, in order to answer the additional research question.

The analysing procedure equal to that of liquid flow, is included in appendix J. For three different transport velocities: the pressure profiles over the pipeline length are given. The flow velocities used are the lowest recorded, an intermediate one and the highest transport velocity. The results are compared with the four theoretical prediction models.

Table 6.3 contains an overview of measured velocities and concentrations for the conducted mixture experiments.

Test matrix								
CONCENTRATION: 4.41%								
RUN 1	V_m $[m/s]$	4.01	4.64	4.91	4.99	5.38	6.01	–
	C [%]	8.88	8.08	8.13	8.40	9.07	8.90	–
RUN 2	V_m $[m/s]$	5.97	5.78	5.27	5.19	4.91	4.20	3.73
	C [%]	8.96	8.90	8.26	7.88	7.68	7.40	7.48

Test matrix									
CONCENTRATION: 8.12%									
RUN 1	V_m $[m/s]$	5.15	5.03	4.64	4.60	3.81	3.34		
	C [%]	14.84	14.98	15.83	16.35	16.73	12.74		
RUN 2	V_m $[m/s]$	5.62	5.11	4.79	4.52	3.73	–		
	C [%]	14.41	14.63	15.80	16.23	15.18	–		
RUN 3	V_m $[m/s]$	5.07	4.68	4.52	3.93	3.34	–		
	C [%]	14.37	15.59	15.98	16.09	11.64	–		
CONCENTRATION: 12.31%									
RUN 1	V_m $[m/s]$	5.38	5.31	4.91	4.56	4.24	4.09	3.89	3.65
	C [%]	22.95	22.68	24.99	25.58	24.61	23.82	23.40	20.66
RUN 2	V_m $[m/s]$	5.38	4.91	4.76	4.24	4.09	3.65	–	–
	C [%]	21.13	23.26	24.52	23.63	23.71	21.39	–	–
RUN 3	V_m $[m/s]$	5.54	5.19	4.79	4.40	4.09	3.73	–	–
	C [%]	20.34	22.80	24.33	24.04	21.52	21.88	–	–
CONCENTRATION: 14.55%									
RUN 1	V_m $[m/s]$	5.34	4.83	4.64	4.28	4.01	3.38		
	C [%]	26.93	28.76	29.15	28.52	27.81	23.18		
RUN 2	V_m $[m/s]$	5.23	5.03	4.60	4.20	3.89	3.50		
	C [%]	26.66	28.96	28.91	28.64	27.84	24.66		
RUN 3	V_m $[m/s]$	4.95	4.60	4.44	4.09	3.50	–		
	C [%]	28.42	28.85	28.32	27.83	23.94	–		

Table 6.3: Test matrix: mixture flow

6.3.1. 4% concentration

Two test runs are carried out with a four percent concentration slurry. The amount of examined velocities is thirteen. The lowest flow velocity is $3.7\ m/s$, the intermediate is $4.9\ m/s$ and the highest is $6.0\ m/s$. The gradients in this experiment, determined by distraction the measured total pressures over an interval, are plotted against the theoretical prediction in Figure 6.1.

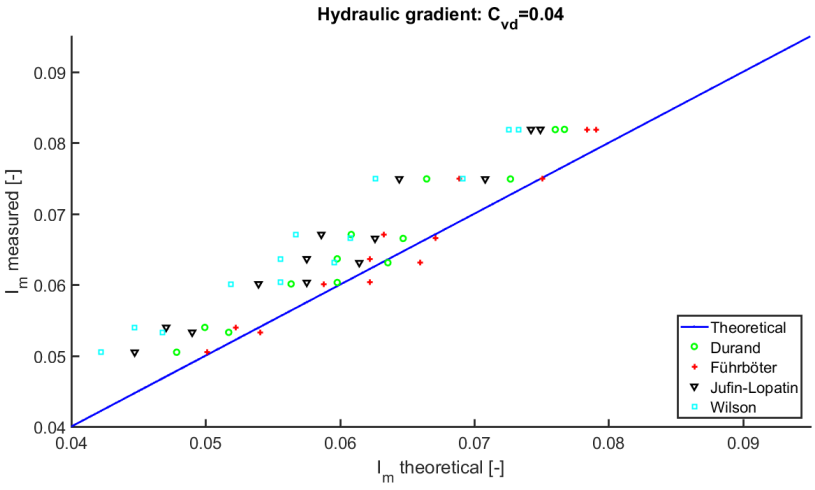

Figure 6.1: Result mixture experiment: (C=4%)

For the lowest examined concentration, the Führboter model gives the best result. There the acquired data corresponds to the theoretical prediction. The other models underestimate the pressure drop in the pipeline. Considering the Wilson model, the difference between theory and experimental data is small. Therefore these two principles are considered to be suitable for frictional head loss predictions

at this concentration.

Data points of the Jufin & Lopatin and Wilson model fall left of the theoretical line. Both methods predicted the pressure loss to be lower with regard to the experimental results. The divergence between theory and the measured data is largest for the Wilson principle.

6.3.2. 8% concentration

Three test runs are carried out with an eight percent concentration slurry. The amount of examined velocities is sixteen. The lowest flow velocity is $3.3\ m/s$, the intermediate is $4.5\ m/s$ and the highest is $5.6\ m/s$. The comparison between theory and experimental data is visualised in Figure 6.2.

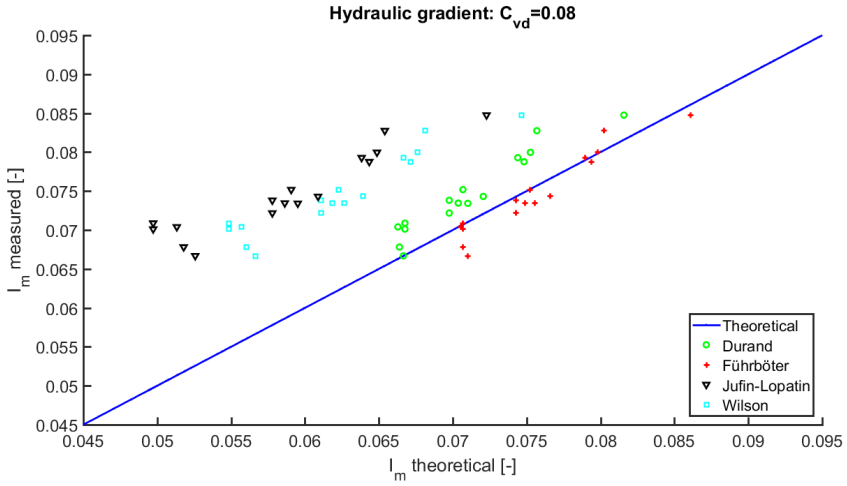

Figure 6.2: Result mixture experiment: (C=8%)

With increase in concentration, the principles start to distinguish themselves. The underestimation of the frictional pressure loss by the Jufin-Lopatin and Wilson models sets through. The divergence between expectation and test results, is largest for the first mentioned.

The blue line representing the theoretical prediction, separates the Durand and Fûhrböter data points. The former slightly underestimates the head loss in the pipeline, while the later over-predicts. Nevertheless the differences are small. Both principles are considered to be suitable for estimating the pressure drop at this concentration.

6.3.3. 12% concentration

Three test runs are carried out with a twelve percent concentration slurry. The amount of examined velocities is twenty. The lowest flow velocity is $3.7\ m/s$, the intermediate is $4.6\ m/s$ and the highest is $5.5\ m/s$. The gradients measured in this experiment, are plotted against the theoretical prediction in Figure 6.3.

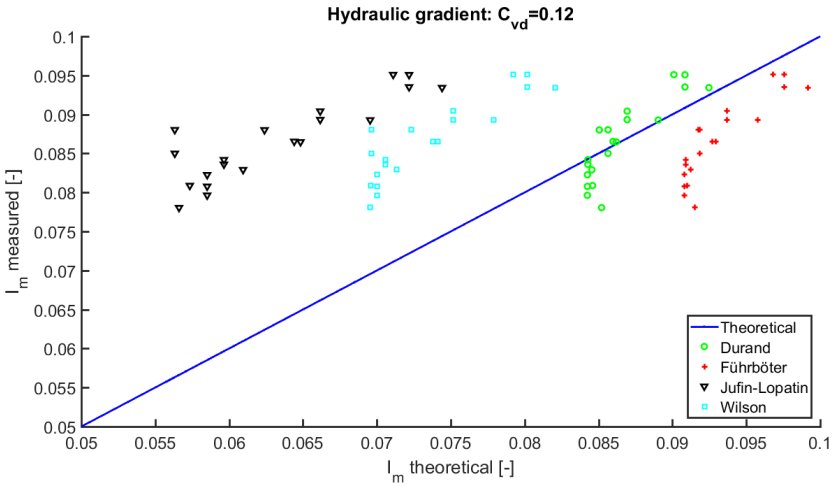

Figure 6.3: Result mixture experiment: (C=12%)

For the twelve percent concentration mixture, the measured data shows good correspondence with the Durand principle. The Führböter method overestimates the frictional pressure loss in the pipe. Again, the two other theories predict the hydraulic gradient lower than measured. With increase in concentration, they show a larger divergence between expectation and experimental result.

6.3.4. 15% concentration

Three test runs are carried out with a four percent concentration slurry. The amount of examined velocities is seventeen. The lowest flow velocity is $3.4\ m/s$, the intermediate is $4.4\ m/s$ and the highest is $5.3\ m/s$.

General analysis

The gradients measured in this experiment, are plotted against the theoretical prediction in Figure 6.4.

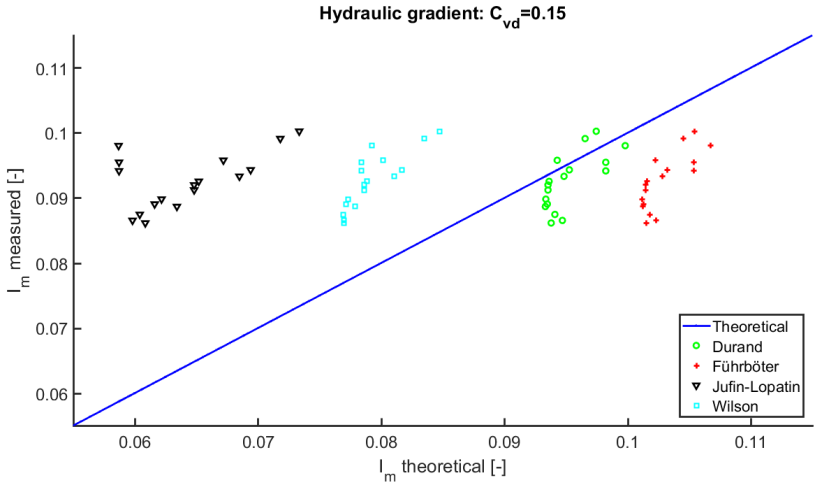

Figure 6.4: Result mixture experiment: (C=15%)

The result is similar to that of the twelve percent concentration experiment. The acquired test data matches best with the Durand method. The other theories diverge more from the theoretical line. The Führböter model overestimates and the two other principles underestimate the frictional head loss. The difference is significantly larger for the Jufin and Lopatin model.

Durand

The pressure profiles are compared to Durand's theoretical prediction in Figure 6.5. Upstream of the $180°$ turn, the experimental result matches the expectations. Downstream of the bend this progresses

for the utmost velocities. This does not apply to the profile of the intermediate flow velocity. For the first time there is a clear distinction between what is calculated with the Durand principle and the outcome of the laboratory test. Around the 50 meter pipeline position the curves start to separate. Due to an over prediction of the frictional pressure loss.

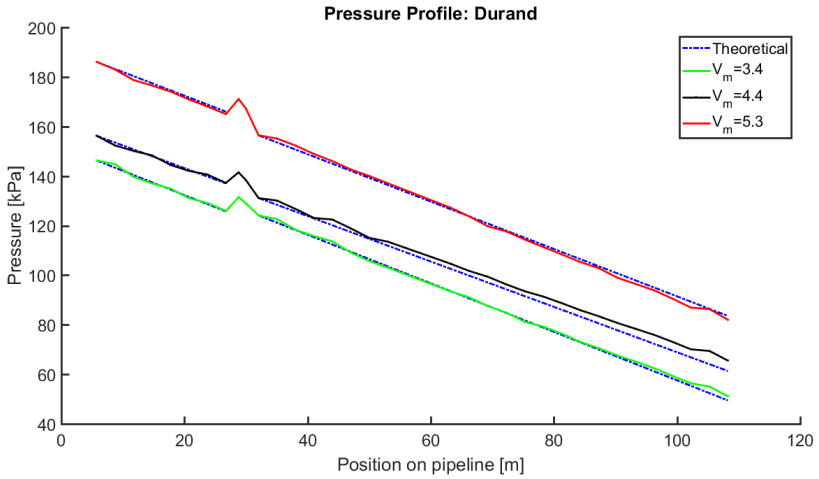

Figure 6.5: Pressure profile: Durand (C=15%)

Führböter

The pressure profiles are compared to Führböter's theoretical prediction in Figure 6.6. The trend started at the 12 percent concentration continues. Downstream of the bend the curves separate. This time the divergence is larger in comparison with the result at the lower concentration. Now it clearly shows that the measured hydraulic gradient is smaller than predicted.

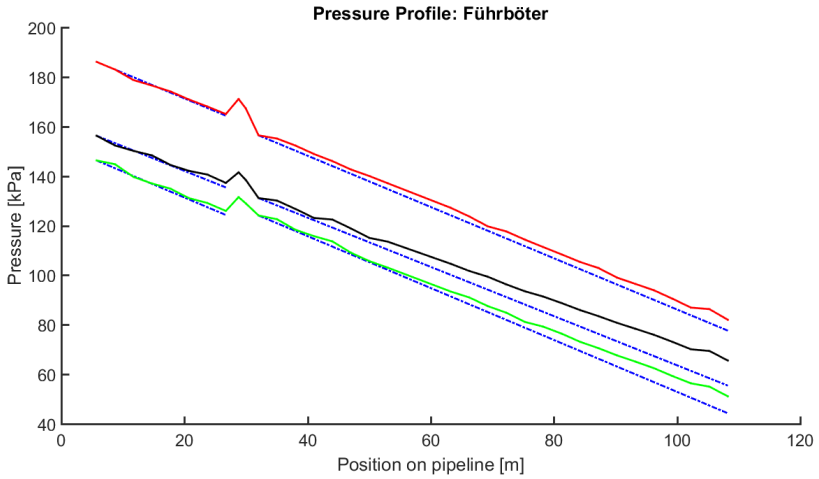

Figure 6.6: Pressure profile: Führböter (C=15%)

Jufin & Lopatin

The pressure profiles are compared to the theoretical prediction method of Jufin and Lopatin in Figure 6.7. It is observed that the divergence grows larger with increase in concentration. At the highest analysed concentration the distinction between result and expectation continues. The difference between theory and the data acquired in the experiment is large. At the end of the pipeline, the pressure curve of the highest flow velocity nearly touches the expected value of the lowest flow velocity.

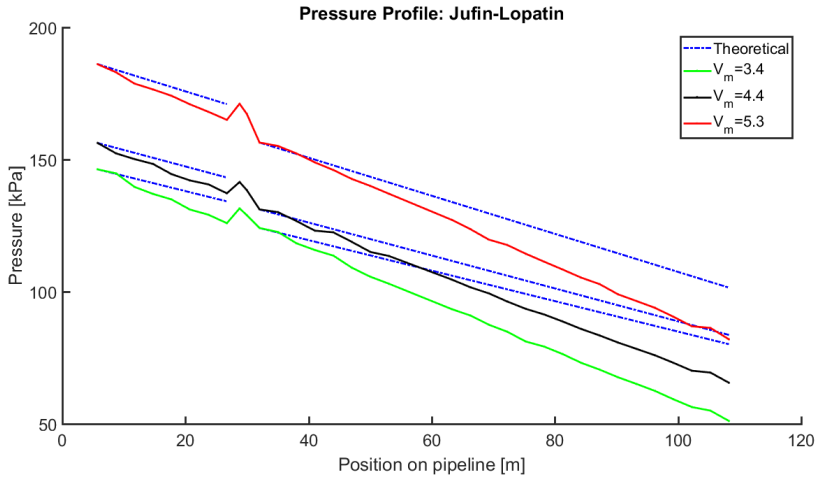

Figure 6.7: Pressure profile: Jufin-Lopatin (C=15%)

Wilson

The pressure profiles are compared to the theoretical prediction method of Wilson in Figure 6.8. The result can be compared with the Jufin and Lopatin model. Every time the concentration increases the divergences between expectation and measurement increases with it. Nevertheless the differences are smaller.

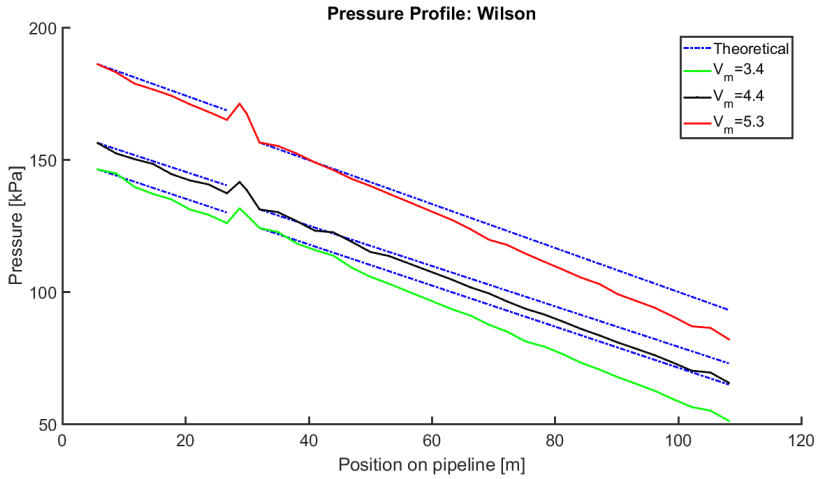

Figure 6.8: Pressure profile: Wilson (C=15%)

6.3.5. Resistance curves

The data collected for mixture experiments with various concentrations, is combined to construct a resistance curve. The hydraulic gradients are plotted against velocity, together with the theoretical head loss profiles of the considered prediction methods. Now every principle is analysed individually and not the specific concentration experiments. The results are similar.

Durand

The resistance curve containing the Durand prediction is found in Figure 6.9. Overall, the data shows close resemblance with the theoretical profiles. There is a slight under-prediction of the hydraulic gradient for the lowest concentrations. Considering the two higher concentrations, there is an accurate result for velocities above $4.5\ m/s$. At lower flow velocities the pressure losses are predicted too high.

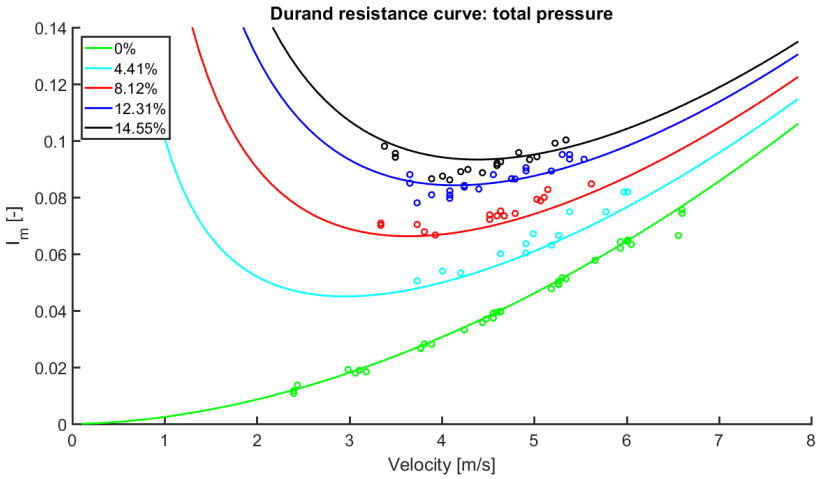

Figure 6.9: Resistance curve: Durand

Führböter

The resistance curve in Figure 6.10, has the Führböter prediction included. There is a good correlation between the experimental data and theory for the two lowest concentrations. When the concentration increase to values above 10 percent, the frictional head loss is overestimated.

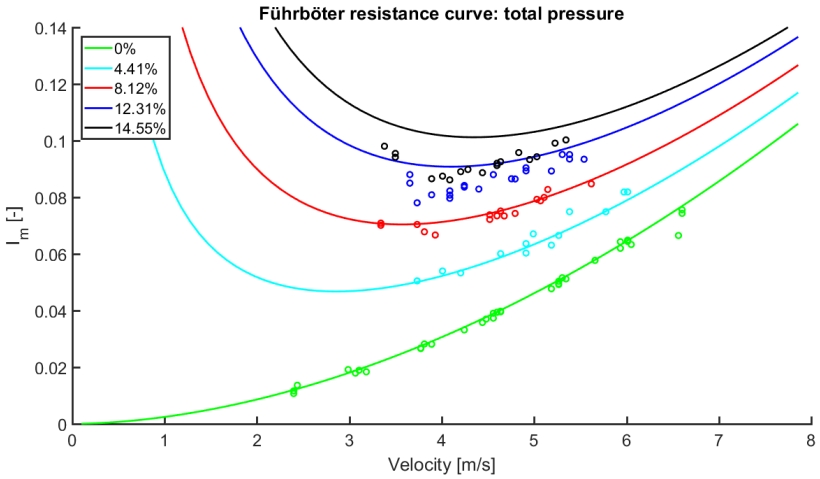

Figure 6.10: Resistance curve: Führböter

Jufin & Lopatin

Figure 6.11 contains the resistance curves predicted by Jufin and Lopatin. It clearly shows the underestimations of the frictional head loss that is observed in the pressure profiles of the previous section. The divergence between expectation and experimental result increases significantly, with increase in velocity.

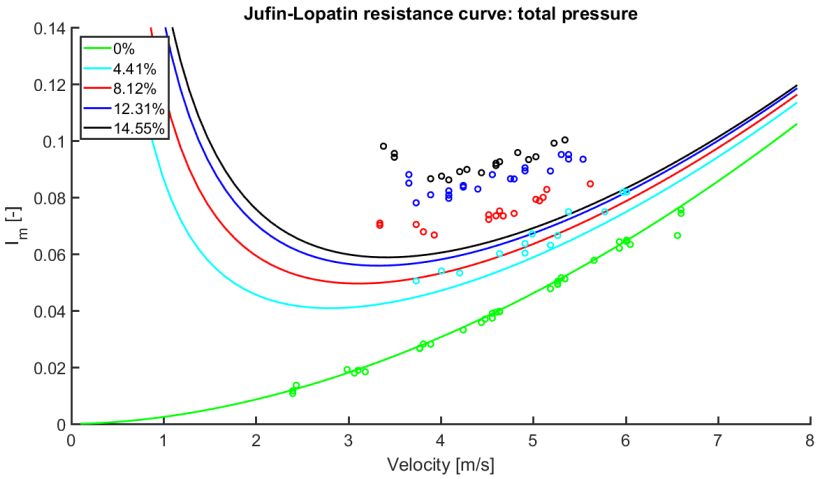

Figure 6.11: Resistance curve: Jufin & Lopatin

Wilson

Figure 6.12 contains the resistance curves predicted by Wilson. The result can be compared to the Jufin and Lopatin principle. The pressure losses over the pipeline are underestimated. Nevertheless the difference between theory and experimental data is smaller with regard to the former method.

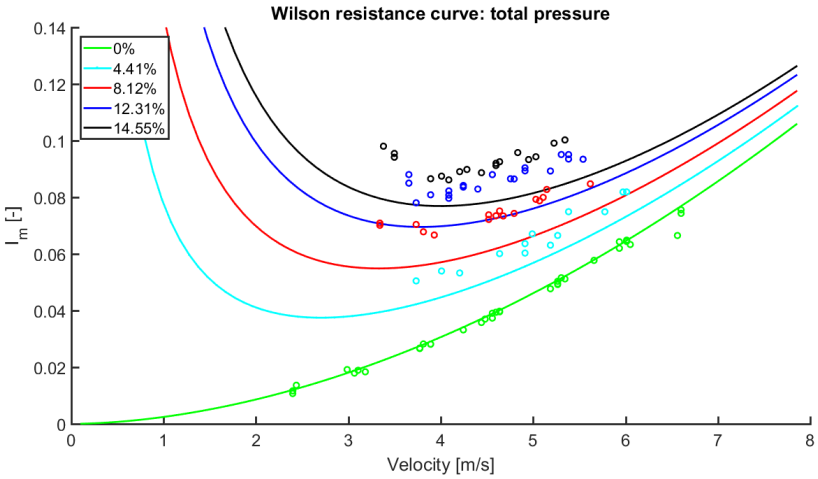

Figure 6.12: Resistance curve: Wilson

6.3.6. Analysis

The experimental data is compared to the predictions of the four theoretical principles. In this section the results are analysed and the applicability of the models is examined. Each method is discussed individually. Thereby an answer is given to the fourth research question:

Q_4: *To what extent are the test results from the laboratory in agreement with expectations from the mathematical models?*

Durand

Compared to the other theoretical prediction methods, the Durand principle showed to be the most suitable. Considering all transport velocities and concentrations, it gives the best correlation between theory and the experimental data. Therefore all test results are compared with the Durand principle. Pressure profiles and hydraulic gradients for the 4, 8, 12 and 15 percent concentration can be found in appendices K, L, M and N.

Führböter

In the analysis of the Führböter model, the mass-median particle diameter is used instead of the decisive particle diameter. With regard to the two lowest mixture densities, the principle produced the best fit between prediction and measurements. Considering the highest two, the frictional head loss is overestimated. This is due to the pipeline length. Within the first 40 meter the theoretical pressure profile fits the test results. Downstream of that position, the curves starts to diverge. This deviation increases with increase in concentration. It is expected that this phenomena set through at higher, not analysed mixture densities.

It is concluded that the Führböter prediction methods gives a good indication of the hydraulic gradient for slurries with a concentration below ten percent and small distances.

Jufin-Lopatin

The principle makes a distinction between two types of mixture. The sediment can contain either uniform solids or have a broad grain size distribution. The effect on the frictional pressure loss of both conditions, is analysed for the concentrations of twelve and fifteen percent. The predicted hydraulic gradients for both sediment types are compared in Figures 6.13 and 6.14. It shows that the effect of a broad grain size distribution on the particle settling parameter, is almost nil. That no significant difference is shown in the hydraulic gradient, is due to the power term of $1/6$ in the calculation of V_{min}.

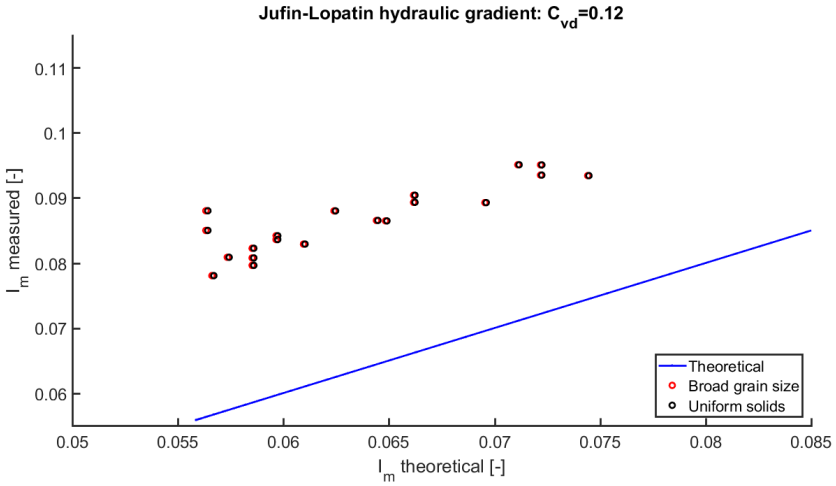

Figure 6.13: Jufin-Lopatin Hydraulic gradient: C=4%

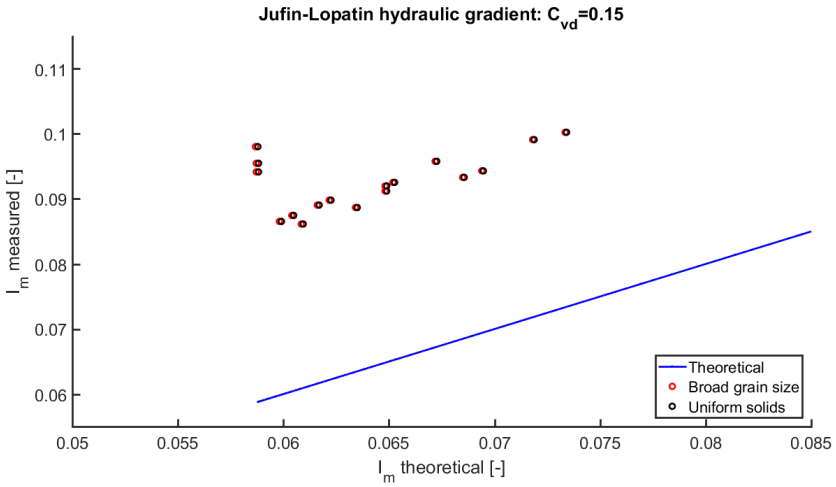

Figure 6.14: Jufin-Lopatin Hydraulic gradient: C=12%

Jufin & Lopatin developed a model to predict the lower limit of their collected experimental data. For the four percent concentration test in this research, the principle performs as expected. In the resistance curve in Figure 6.11, the lowest measured hydraulic gradient corresponds to the theoretical curve. But when concentration increases, the pressure loss is underestimated for every experiment.

The model is based on the simplistic assumption that the hydraulic gradient at the minimum velocity equals three times the gradient for liquid flow. Within the calculation method, the influence of the concentration seems to have a minimal effect. Therefore it is concluded that the Jufin & Lopatin principle is not suitable for a broad range of concentrations.

Wilson
The experimental results do not match the theory of Wilson for the analysed concentrations. There is an under-prediction of the frictional head loss, that increases when the mixture density increases.

6.3.7. Stationary waves

The $180°$ turn in the measurement section disturbs the flow. For high concentrations and low flow rates, the effect of the bend manifests itself in the form of stationary waves. It originates from the varying momentum exchange between the sliding bed and suspension layer, the mass exchange due to erosion and sedimentation. The waves are expected to damp out downstream of the fitting. The long pipeline length creates the opportunity to clearly visualise the transition to equilibrium flow. Therefore the three lowest transport velocities of the twelve and fifteen percent concentration experiments are examined. Then an answer is given to the additional research question:

Q_A: *To which extent do stationary waves develop in a test set-up of greater length and greater pipe diameter?*

Twelve percent concentration
In the twelve percent concentration experiment, three test runs are carried out. In all series the lowest recorded transport velocity is $3.7\ m/s$. During these experiments a sliding bed with fluctuating layer thickness is observed. In Figures 6.15, 6.16 and 6.17, the mean of the measured hydraulic gradients at a pressure tap, are visualised. The profile that results from it is plotted in green.

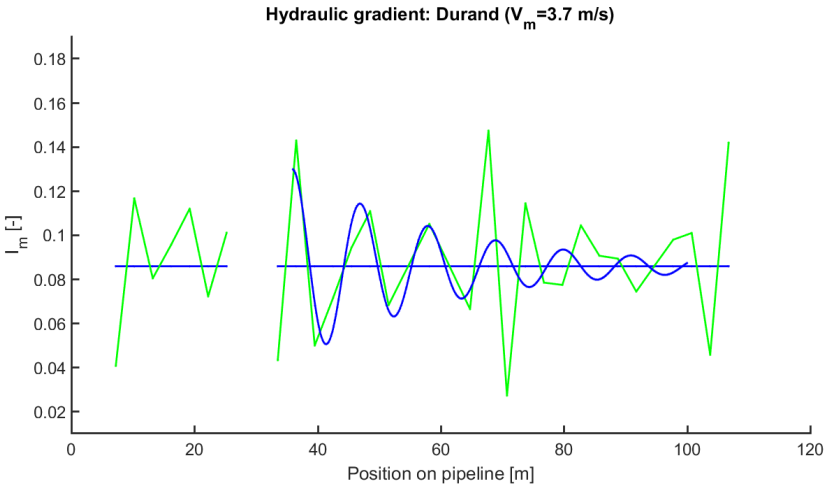

Figure 6.15: Stationary wave: C=12%, V_m=3.7)

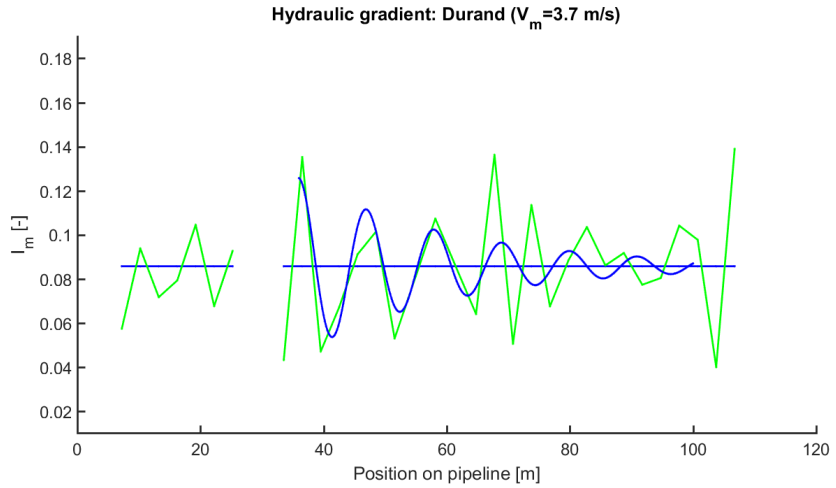

Figure 6.16: Stationary wave: C=12%, V_m=3.7)

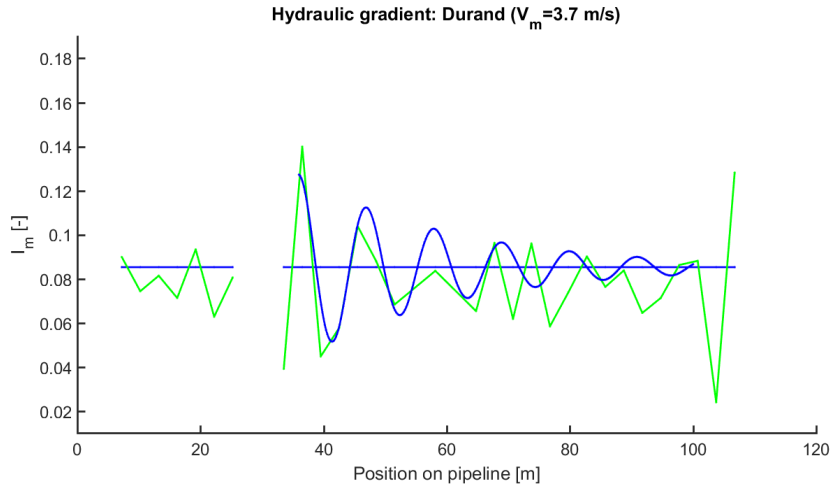

Figure 6.17: Stationary wave: C=12%, V_m=3.7)

The blue curve added to the figures, indicates a stationary wave that damps out downstream in the pipeline. The examined flow velocities give a similar result. Behind the $180°$ turn, at a position of 30 meter, the measured and theoretical profiles correlate over a distance of 30 meter. In the interval, three waves can be clearly indicated.

Furthermore, the re-stratification effect is visible. With exception of the peaks measured around a 70 meter position, in Figures 6.15 and 6.16. The amplitude of the sinusoidal curve damps out near the end of the measurement section. The peak and trough in the hydraulic gradient at the far end of the pipeline are not taken into account. There the flow is disturbed by the presence of a bend, downstream of the pressure tap locations.

That it concerns stationary waves, is proven with results of experiments at higher flow rates. For example the hydraulic gradient profile of the $5.5\ m/s$ test run, included in Figure 6.18. There no sinusoidal curve, damping out over the pipeline length, is shown.

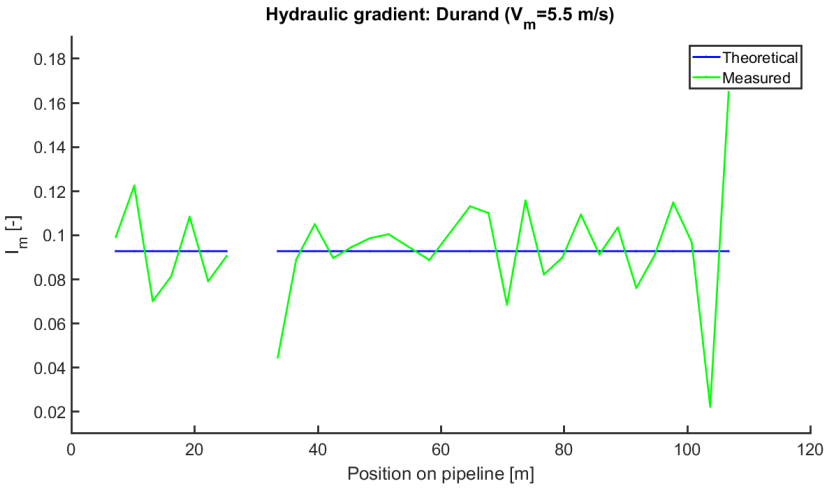

Figure 6.18: Hydraulic gradient profile: C=12%, V_m=5.5)

Fifteen percent concentration

In the fifteen percent concentration experiment, three test runs are carried out. The lowest recorded transport velocities are respectively: 3.4 and twice $3.5\ m/s$. The approach is equal to the method described under the previous heading. The hydraulic gradient profile over the pipeline length is plotted in green, a theoretical sinusoidal curve in blue. In the low flow rate experiments a sliding bed with fluctuating layer thickness is observed.

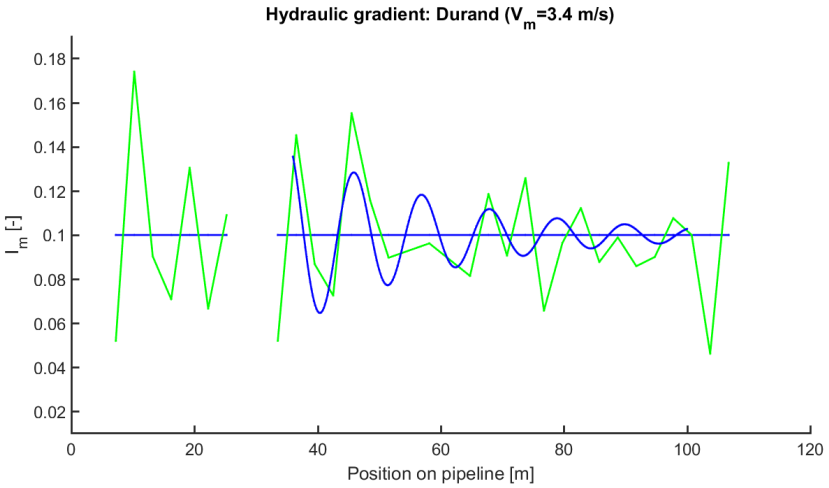

Figure 6.19: Stationary wave: C=15%, V_m=3.4)

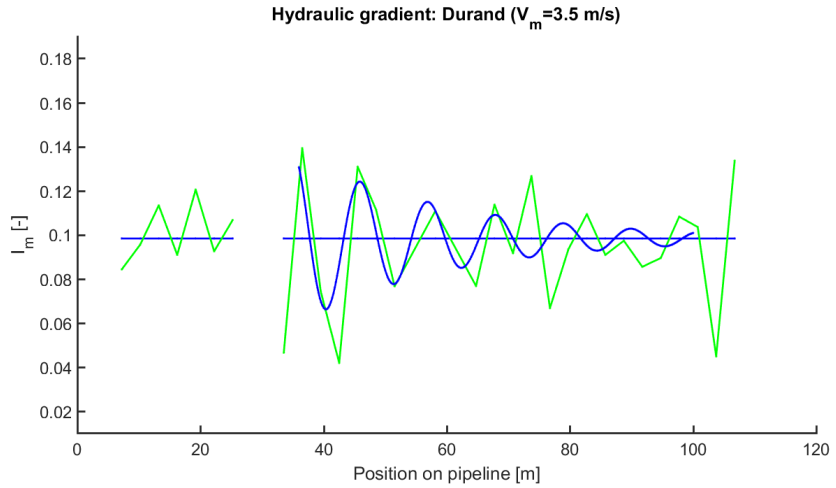

Figure 6.20: Stationary wave: C=15%, V_m=4.4)

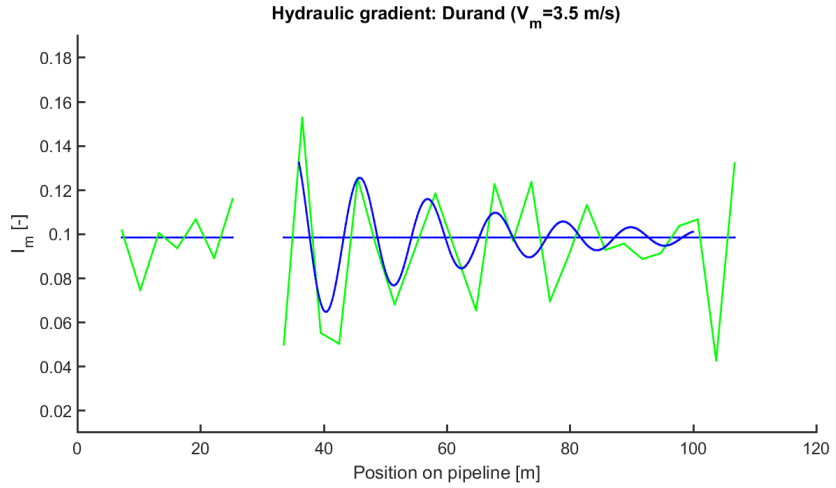

Figure 6.21: Stationary wave: C=15%, V_m=5.3)

For the higher concentration, no peak in the hydraulic gradient is observed at a 70 meter position. Therefore the re-stratification effect becomes clearly visible. The effect correlates with the blue line, representing the fitted stationary wave, over a distance of 35-40 meter downstream of the 180° turn. In the interval three waves can be indicated for the examined velocities.

That it concerns stationary waves, is proven with results of experiments at higher flow rates. When the flow rate increased to 4.2 m/s, the initial position shifts one meter to the right. Furhermore, the wavelength increased from 11 to 12.5 meter. This is visualised in Figure 6.22.

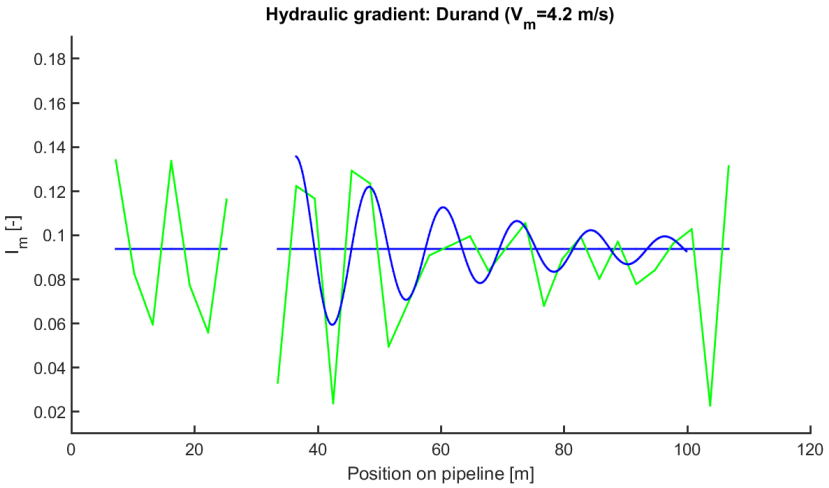

Figure 6.22: Hydraulic gradient profile: C=15%, V_m=4.2)

Studying the hydraulic gradient profile of the $5.2\ m/s$ test run, included in Figure 6.23. It shows that the variation of the hydraulic gradient is almost constant over the pipeline length and visibly lower compared to the results at the lowest transport velocities.

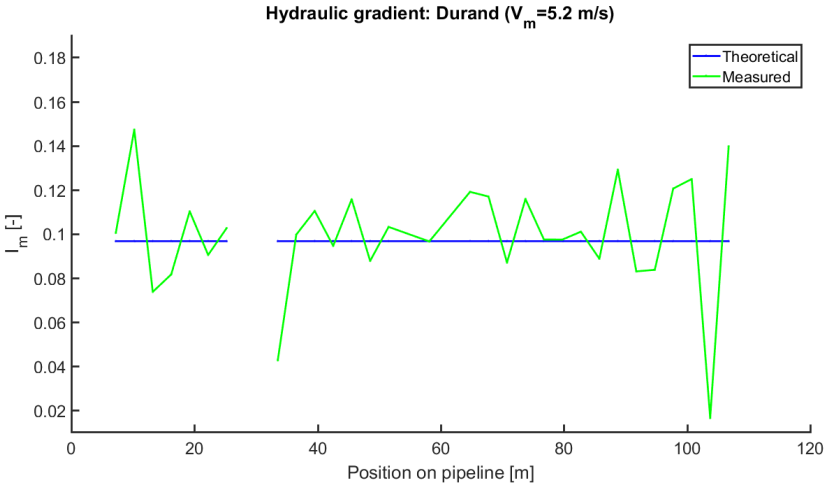

Figure 6.23: Hydraulic gradient profile: C=15%, V_m=5.2)

Double peaked hydraulic gradient curves, as observed by Tamlon [Talmon, 2015], are not shown in the experimental result. Visualising the restratifictaion effect, the thickening of the bed layer with increase in velocity behind a disturbance, is only possible when measuring close to the bend. Around a position of $x < 50 * D_p$ and a distance between pressure taps of $\approx 10 * D_p$. In this research the measurements are carried out over large intervals and great distance from the $180°$ turn. Therefore it represents equilibrium conditions. Furthermore, there is no information on the bed layer thickness available.

Dynamic travelling waves

The presence of stationary waves is demonstrated and it is expected that in the same experiments, dynamic travelling waves occur. The assumption is substantiated by fluctuations in the ultrasonic concentration measurement, included in appendix O. The acquired data is analysed, but the phenomena could not be clearly observed. There are two explanations. One is due to the amount of pressure taps. Over the test duration, sudden peaks and troughs occur in the hydraulic gradients. They influence the result and diminish the visibility. Furthermore, the dynamic waves result of mass exchange between the bed and suspension layer. That experiments are carried out at the limit of deposition limit velocity, also diminishes the visibility. In order to observe travelling waves, further research should focus on lower flow rates.

7

Conclusion

The conclusion of this research is divided in two parts. First the water flow experiments are discussed. Subsequently, the results of the slurry transport experiments. The later is subdivided in the analysed concentrations.

Water experiment
In the water experiment three head loss prediction methods are analysed: Darcy-Weisbach, RangaRadju & Garde and Swamee & Jain. The difference in outcome, regarding a smooth pipeline, is almost nil. Therefore only one principle, the first mentioned, is compared with the experimental data. In the believe that if one theory's applicability is confirmed, it is also proven for the other two. Observation showed that result and expectation are in good correlation.

Mixture experiment
In the mixture experiment four head loss prediction methods are analysed for concentrations of : 4.4, 8.1, 12.3 and 14.6 percent. The tests are conducted in the heterogeneous flow regime. With a velocity ranging from three to six meters per second. The result obtained at at large laboratory test set-up:

- **Durand:** considering all transport velocities and concentrations, this principle showed the best correlation between theory and experimental data. It is concluded that the Durand principle is a suitable prediction method.
- **Führböter:** with regard to the two lowest mixture densities, this principle produced the best fit between prediction and measurements. Considering the highest two, the frictional head loss is overestimated. This is due to the pipeline length. Within the first 40 meter the theoretical pressure profile fits the test results. Downstream of that position, the curves starts to diverge. This deviation increases with increase in concentration. It is expected that this phenomena set through at higher, not analysed mixture densities. It is concluded that the Führböter prediction methods gives a good indication of the hydraulic gradient: for slurries with a concentration below ten percent and small distances.
- **Jufin & Lopatin:** with this principle the pressure loss is underestimated for every experiment. The model is based on the simplistic assumption that the hydraulic gradient at the minimum velocity equals three times the gradient for liquid flow. Therefore it is concluded that the Jufin & Lopatin principle is not suitable for a broad range of concentrations. Furthermore, the model describes two methods to determine particle settling parameter ψ. One is for uniform solids, the other for sediments with a broad grain size distribution. Results show no significant difference between the them. Therefore a broad grain size distribution can not be taken into account.
- **Wilson:** the experimental results do not match the theory of Wilson for the analysed concentrations. There is an under-prediction of the frictional head loss, that increases when the mixture density increases.

Furthermore, as a novelty for large diameter pipe size, a conclusion can be made outside of the research objective. For the lowest velocities of the twelve and fifteen percent slurry experiments, stationary waves over the pipeline length are observed. In previous research they appeared stronger:

broader particle size distribution and lower sand concentrations could be the reason. It demonstrates that longer flow loops give opportunity to conduct further research into the extent of waves, being more prominent at higher sand concentrations and possibly more prominent with steeper particle size distribution.

Given the measured stationary waves, double peaked curves would occur when measuring close to the bend, around a position of $x < 50 * D_p$ and a distance between pressure taps of $\approx 10 * D_p$. In this research the measurements are carried out over large intervals and great distance from the bend. Therefore it represents equilibrium conditions.

8

Recommendations

In the first phase of the project, the experimental research encountered some start-up problems. Considering the brand-new facility and equipment, that was expected. Over the course of a few months, the set-up was optimized and improved. After the optimization, valid and reliable results are obtained. For further research on this test set-up, various improvements are suggested:

- Adding an Electrical Resistance Tomography (ERT) or a radiometric density meter to the set-up, can be beneficial. Both options create the possibility to analyse the behaviour and structure of the slurry inside the pipeline. Which is especially interesting when transporting at around deposition limit velocity. The equipment provides accurate information about the cross-sectional area of the bed-layer. With this information, research into more accurate theories on hydraulic transport, like the two - or three-layer models, can be conducted.
- In this experiment, the lower velocity regimes at concentrations below 15% were investigated. It would be useful to gather more data with regard to higher flow rates and concentrations in a homogeneous flow regime. This, however, would require a pump with a greater capacity.
- The characteristics of the sediment, originating from an actual dredging project in Xiamen, show a broad particle size distribution. Considering the theoretical study purpose, it is recommended to have a more uniform distribution. Increasing the reproducibility of the experiments.
- It is observed that the use of a long flow loop creates the opportunity to conduct research into the extent of stationary waves. To do this, further research should focus on higher mixture concentrations and transport velocities around deposition limit. It is expected that then, the phenomena will become clearly visible.

9

Acknowledgement

First of all I want to express my gratitude to director Zhang Qingbo and professor Cees van Rhee. Who enabled the collaboration between the NERCD and DUT. I feel blessed with the opportunity they gave me and I hope, for them, it was the the start of a long lasting prosperous cooperation.

The list of people who joined in on this international research project is long. Of the NERCD I would like to thank everyone who contributed. In particular my supervisor doctor Feixin Wang, Mr Hong Guojun, Ms Zhang Lu and especially Mr Shu Wei, who's hospitality I will never forget. Also worth to mention, the ones that did not take part in the research but gave me a warm welcome at your company.

I also want to mention Xiuhan Chen, who has been a real asset to the team. The amount of time he invested in this project is tremendous; the communication with the NERCD, all of the translating, the meetings he attended and his guidance into the Chinese culture. It would almost make you forget he has a PhD-project to work on.

They did not contributed to the project but supported my throughout my complete education. My parents: Jan and Inge, Laura, Hanne and Lena. Thank you for all the opportunities you have given me. Maarten de Vreede, looking back at this incredible experience, I have always had an amazing friend at my side. Anouk and Dineke, your doors have always been open to me. When the opportunity comes along, I will pass by again.

Last, so the reader will definitely remember, my TU Delft daily supervisor Arno Talmon. In the corridors of the 3ME faculty, it was mentioned that he also has a professional career outside the university. I found this hard to believe. The man, who I value because of his tranquillity and patience, who provided me with his knowledge and insight on the topic, who guided me throughout the project from start till end, has always made time for me. Instant e-mail replies, long Skype conversations and corrections made to the paper from a seat at Schiphol airport. Thank you.

I wish all of you a fortunate future,
Jelte de Ridder

Appendices

A

Flow loop design

The purpose of the figures included in this appendix, is to clarify the test set-up design. First, line drawings of the top, side and front view are presented. Second the ground plan of the laboratory and next some additional images. Including a drawing of the pipeline's cross-section at a pressure tap location. The dimensions are in millimetre.

A.1. Line drawings

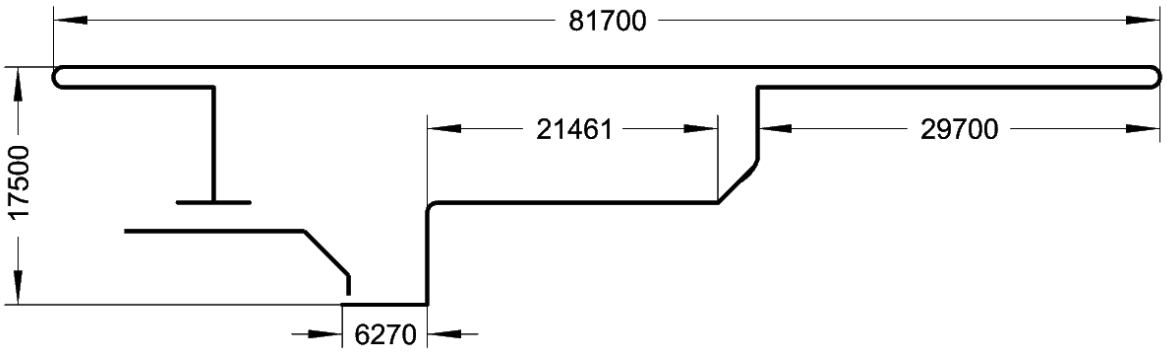

Figure A.1: Flow loop: top view

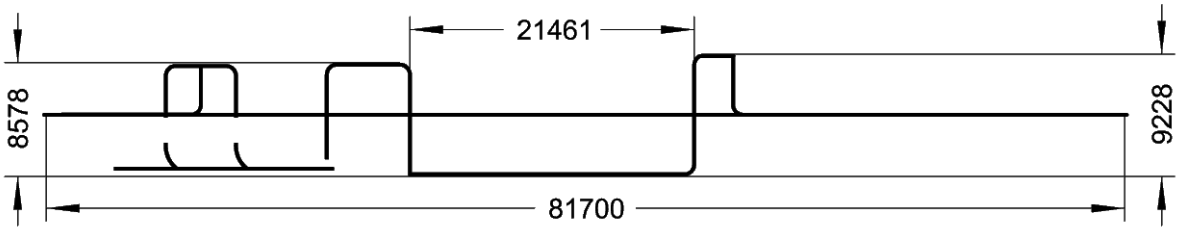

Figure A.2: Flow loop: side view

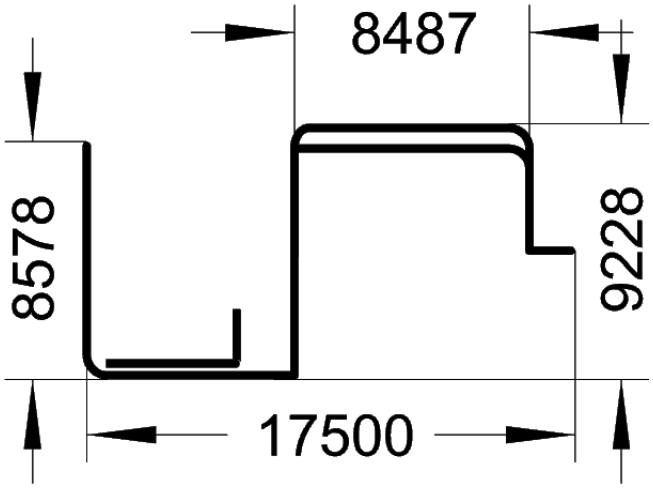

Figure A.3: Flow loop: front view

A.2. Ground plan

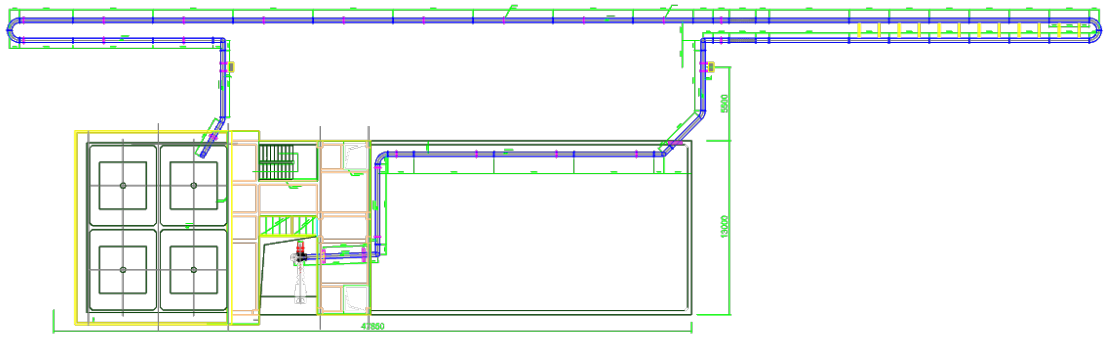

Figure A.4: Laboratory: top view

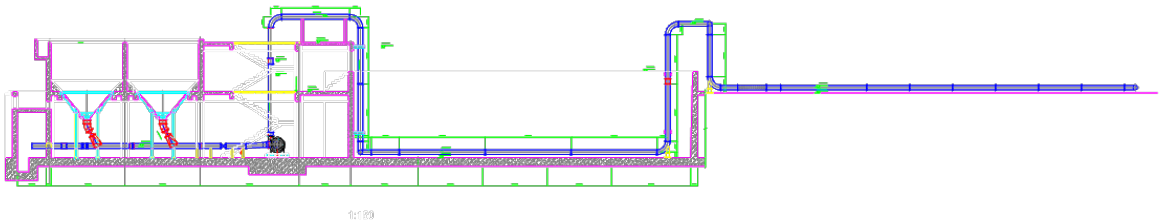

Figure A.5: Laboratory: side view

A.3. Various

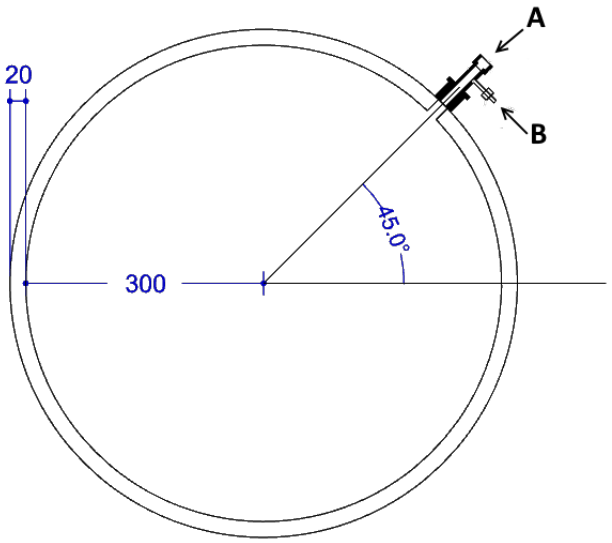

A: total pressure meter, B: impulse tube

Figure A.6: Pipeline: cross-section

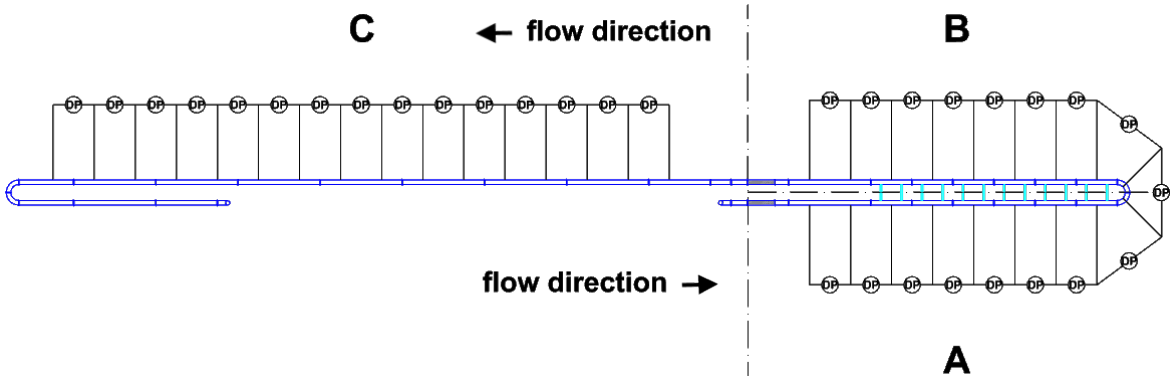

Figure A.7: Connection of differential pressure transmitters

B

Position of pressure taps

Figure B.1 shows the pressure tap locations in the measurement section. The beginning of the horizontal pipe is considered to be the starting point. The distance between this point and a specific tap is given in table B.1.

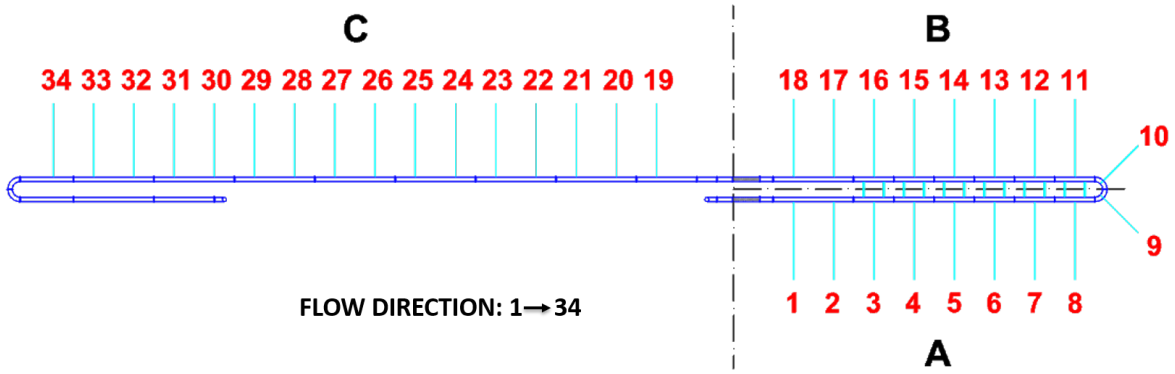

Figure B.1: Position: pressure taps

Figure B.2 shows the numbering of pressure tap intervals. The distances from starting point till interval are specified in table B.2.

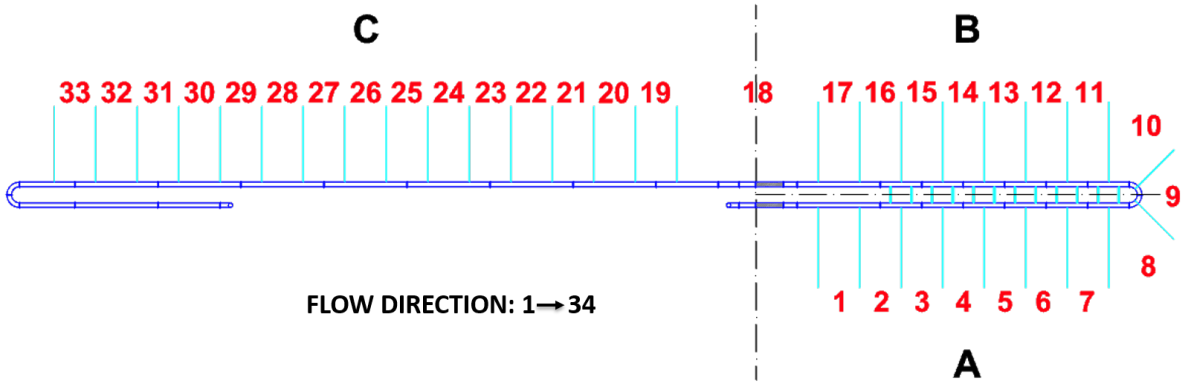

Figure B.2: Position: pressure tap interval

Table B.1: Position of pressure taps

Position of pressure taps			
Tap number	**Position** $[m]$	**Tap number**	**Position** $[m]$
Start	0		
1	5.725	18	53.031
2	8.725	19	63.256
3	11.725	20	66.256
4	14.725	21	69.256
5	17.725	22	72.256
6	20.725	23	75.256
7	23.725	24	78.256
8	26.725	25	81.256
9	28.789	26	84.256
10	29.967	27	87.256
11	32.031	28	90.256
12	35.031	29	93.256
13	38.031	30	96.256
14	41.031	31	99.256
15	44.031	32	102.256
16	47.031	33	105.256
17	50.031	34	108.256

Table B.2: Position of pressure tap interval

Position of pressure tap interval			
Tap interval	**Position** $[m]$	**Tap interval**	**Position** $[m]$
Start	0		
1	7.225	18	58.1441
2	10.225	19	64.756
3	13.225	20	67.756
4	16.225	21	70.756
5	19.225	22	73.756
6	22.225	23	76.756
7	25.225	24	79.756
8	27.757	25	82.756
9	29.378	26	85.756
10	30.999	27	88.756
11	33.531	28	91.756
12	36.531	29	94.756
13	39.531	30	97.756
14	42.531	31	100.756
15	45.531	32	103.756
16	48.531	33	106.756
17	51.531		

C

Pump characteristics

检 测 报 告

（ 性能曲线 ）

试验编号：	ASP1050-300-7000030W	合同号：		试验日期：	2015.10.12
泵名称：	离心泵	泵型号：	ASP1050-300-700	出厂编号：	15102058

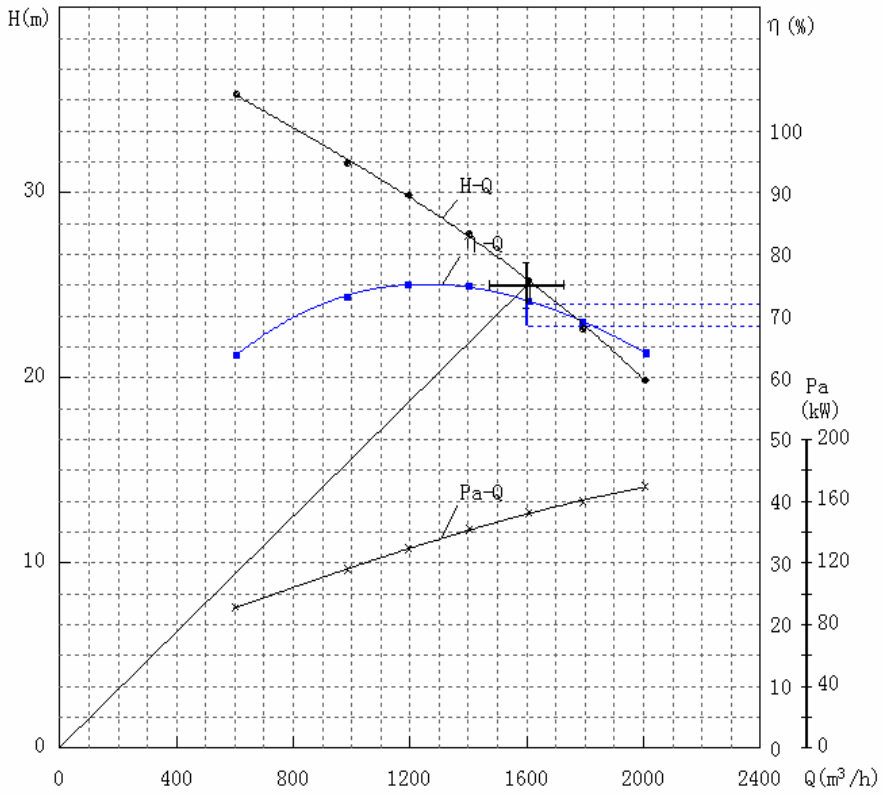

保证点性能参数测试结果

参数名称	流量(m^3/h)	扬程(m)	转速(r/min)	输入功率(kW)	泵效率(%)	
测量数据	1600	25.35	740	151.6	72.5	

检测：	校核：	试验主管：

安徽三联泵业股份有限公司

Figure C.1: Pump curve

D

Temperature measurements

The figures in this appendix contains thermometer data of experiments conducted with different concentrations.

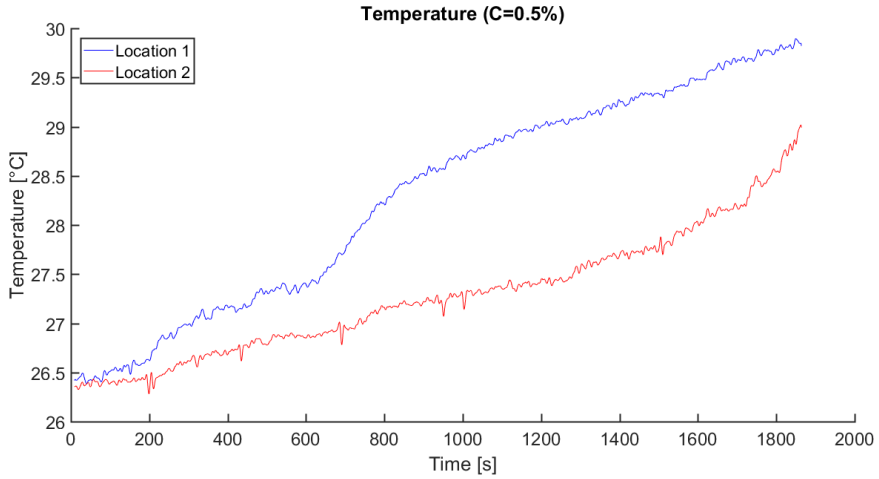

Figure D.1: Temperature 07/31

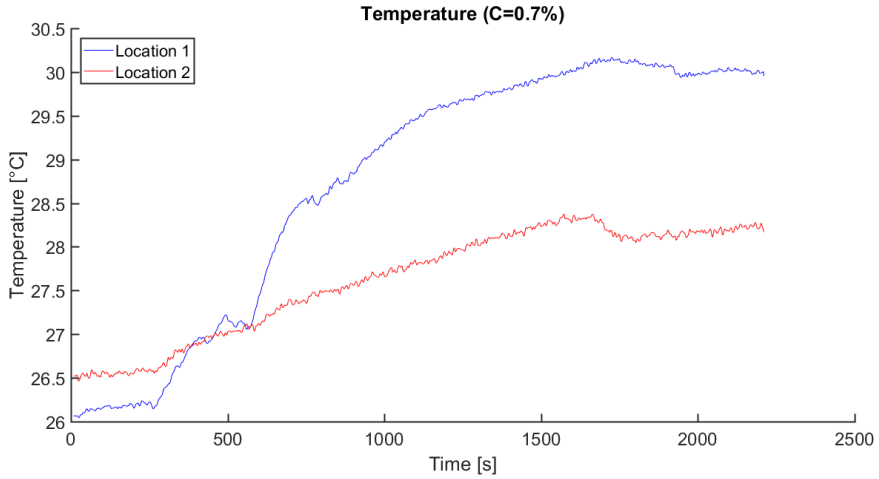

Figure D.2: Temperature 08/04

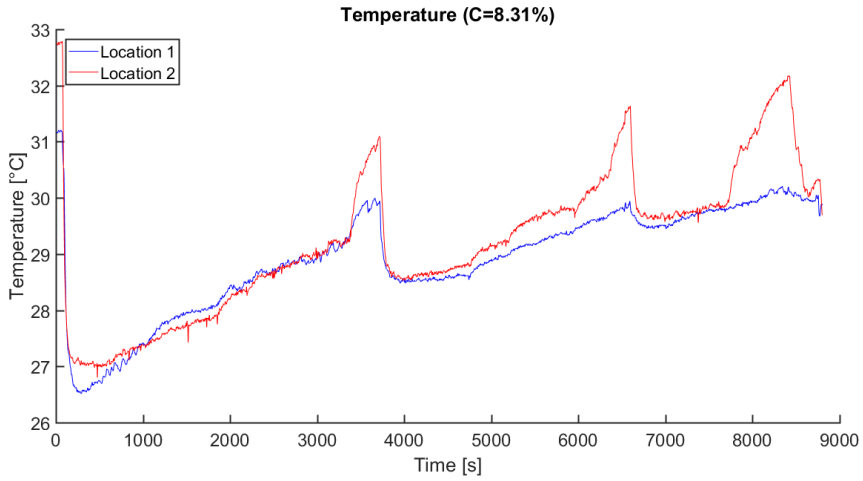

Figure D.3: Temperature 08/03

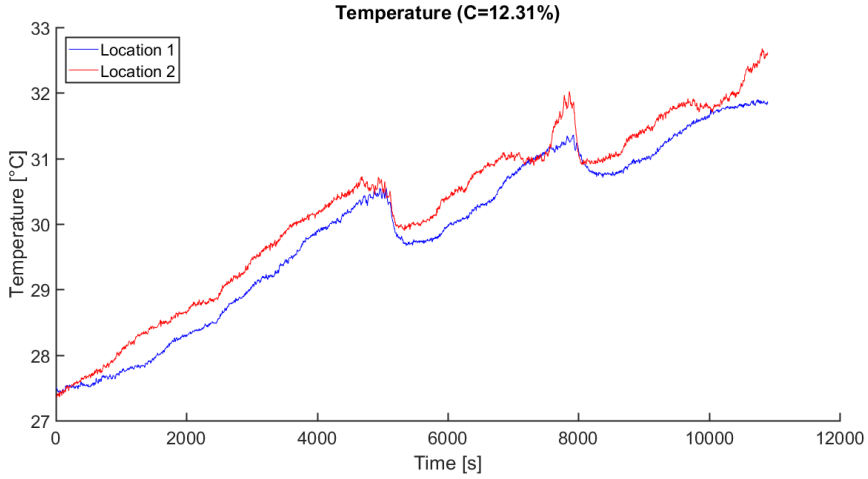

Figure D.4: Temperature 08/04

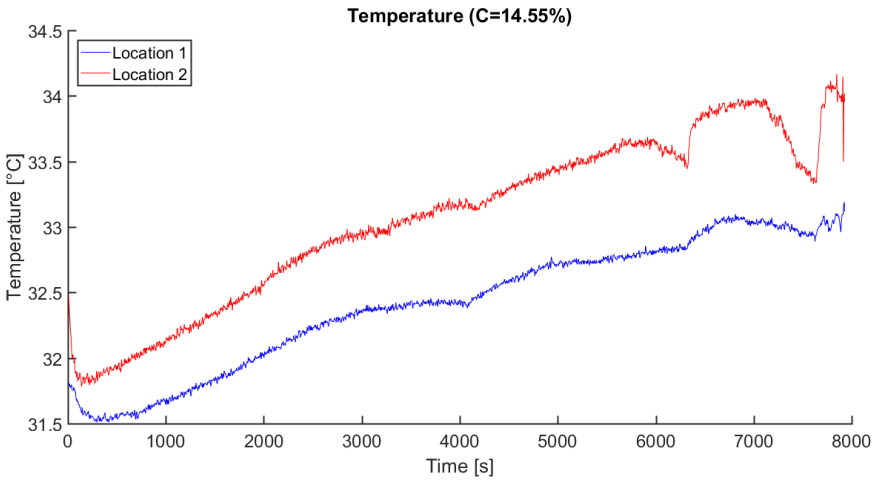

Figure D.5: Temperature 08/04

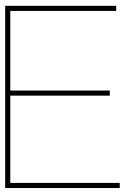

Test matrix

Test matrix									
CONCENTRATION: 0%									
RUN 1	V_m $[m/s]$	5.66	5.34	5.27	4.64	4.48	3.89	3.18	–	–
	C [%]	0.78	0.63	0.59	0.44	0.40	0.38	0.33	–	–
RUN 2	V_m $[m/s]$	2.40	2.99	3.81	4.56	5.27	5.93	6.60	–	–
	C [%]	0.97	0.99	0.93	0.83	0.73	0.63	0.54	–	–
RUN 3	V_m $[m/s]$	2.44	3.10	3.77	4.44	5.27	6.05	6.56	–	–
	C [%]	0.97	0.97	0.95	0.84	0.72	0.60	0.50	–	–
RUN 4	V_m $[m/s]$	2.40	3.07	3.77	4.56	5.19	6.01	6.60	–	–
	C [%]	0.97	0.95	0.94	0.85	0.78	0.58	0.48	–	–
RUN 5	V_m $[m/s]$	5.93	6.01	6.01	5.31	4.60	4.24	3.89	4.64	4.64
	C [%]	1.28	1.26	1.26	0.85	0.66	0.61	0.57	0.60	0.62
CONCENTRATION: 4.41%									
RUN 1	V_m $[m/s]$	4.01	4.64	4.91	4.99	5.38	6.01	–		
	C [%]	8.88	8.08	8.13	8.40	9.07	8.90	–		
RUN 2	V_m $[m/s]$	5.97	5.78	5.27	5.19	4.91	4.20	3.73		
	C [%]	8.96	8.90	8.26	7.88	7.68	7.40	7.48		
CONCENTRATION: 8.12%									
RUN 1	V_m $[m/s]$	5.15	5.03	4.64	4.60	3.81	3.34			
	C [%]	14.84	14.98	15.83	16.35	16.73	12.74			
RUN 2	V_m $[m/s]$	5.62	5.11	4.79	4.52	3.73	–			
	C [%]	14.41	14.63	15.80	16.23	15.18	–			
RUN 3	V_m $[m/s]$	5.07	4.68	4.52	3.93	3.34	–			
	C [%]	14.37	15.59	15.98	16.09	11.64	–			
CONCENTRATION: 12.31%									
RUN 1	V_m $[m/s]$	5.38	5.31	4.91	4.56	4.24	4.09	3.89	3.65	
	C [%]	22.95	22.68	24.99	25.58	24.61	23.82	23.40	20.66	
RUN 2	V_m $[m/s]$	5.38	4.91	4.76	4.24	4.09	3.65	–	–	
	C [%]	21.13	23.26	24.52	23.63	23.71	21.39	–	–	
RUN 3	V_m $[m/s]$	5.54	5.19	4.79	4.40	4.09	3.73	–	–	
	C [%]	20.34	22.80	24.33	24.04	21.52	21.88	–	–	
CONCENTRATION: 14.55%									
RUN 1	V_m $[m/s]$	5.34	4.83	4.64	4.28	4.01	3.38			
	C [%]	26.93	28.76	29.15	28.52	27.81	23.18			
RUN 2	V_m $[m/s]$	5.23	5.03	4.60	4.20	3.89	3.50			
	C [%]	26.66	28.96	28.91	28.64	27.84	24.66			
RUN 3	V_m $[m/s]$	4.95	4.60	4.44	4.09	3.50	–			
	C [%]	28.42	28.85	28.32	27.83	23.94	–			

Table E.1: Test matrix

F

Water flow: resistance curve

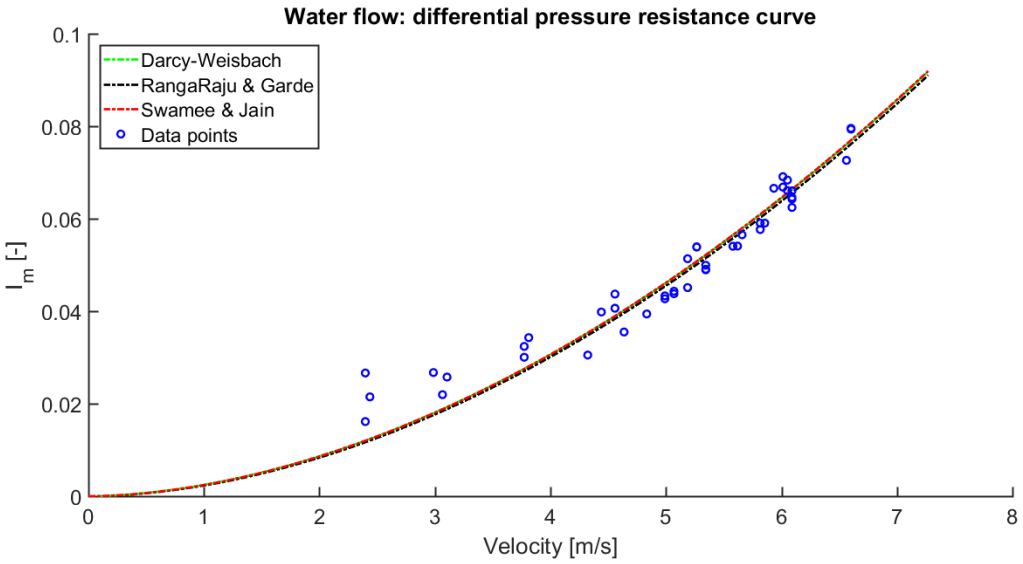

Figure F.1: Resistance curve: differential pressure

G

Water flow: pressure profile downstream vehicle lane

Figure G.1 shows the 37 absolute pressure profiles for water flow in the pipeline downstream of the vehicle line (pipeline section 'A' in figure 3.3). The color of a line represents a velocity as defined in the colorbar at the right.

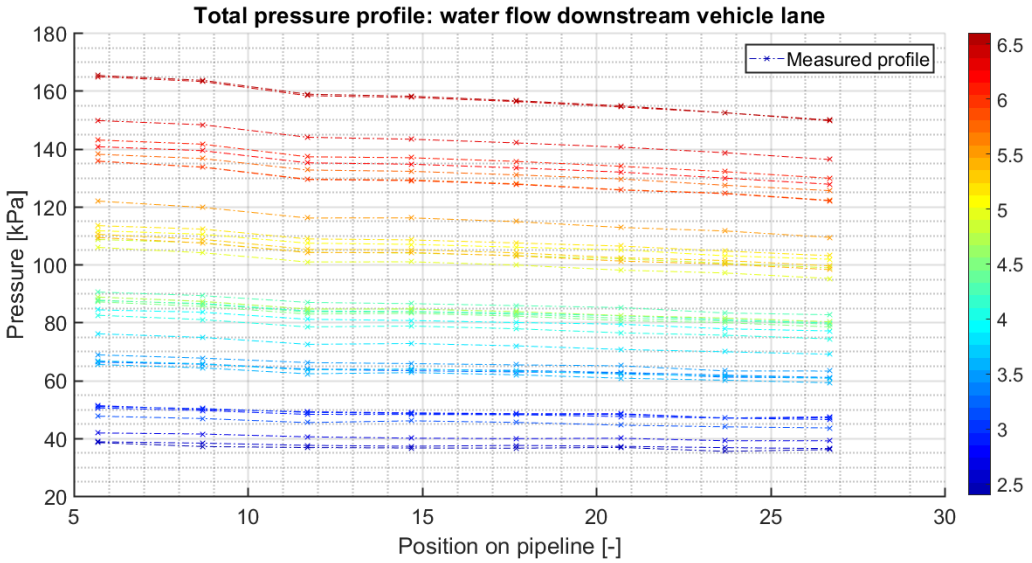

Figure G.1: Total pressure profile: water flow downstream vehicle lane

Figure G.2 contains the pressure profiles after the flow loop correction equation is applied.

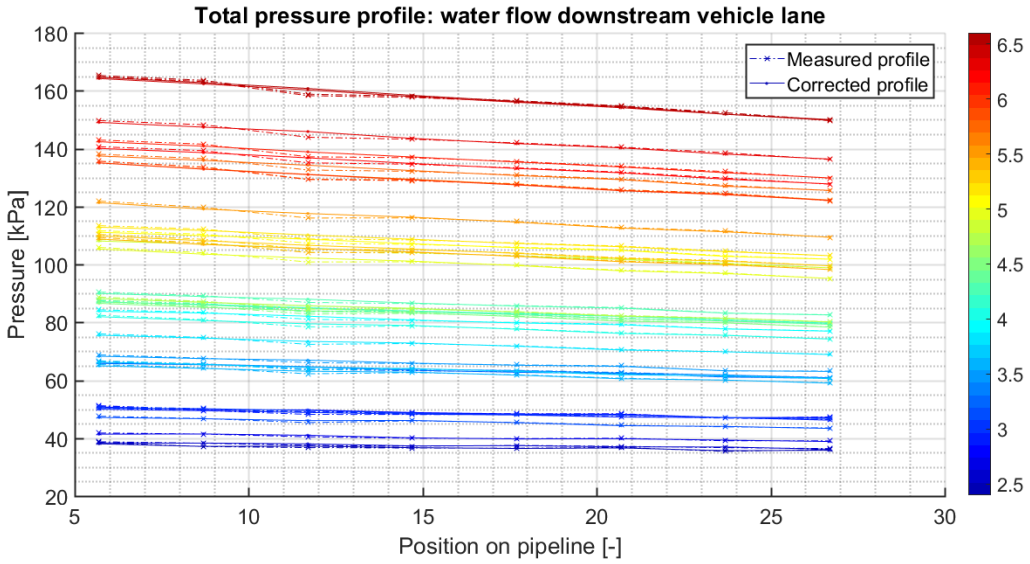

Figure G.2: Corrected total pressure profile: water flow downstream vehicle lane

Water flow: pressure profile & hydraulic gradient

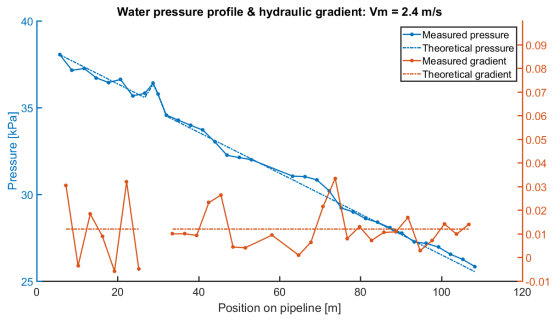

(a) Water experiment #1

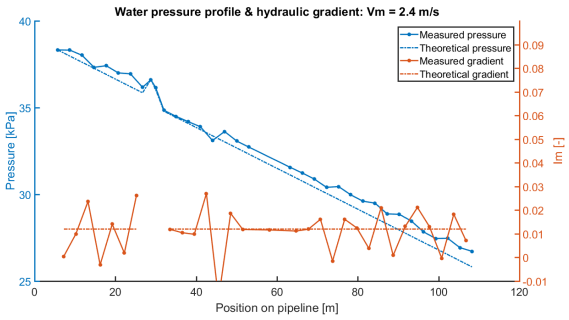

(b) Water experiment #2

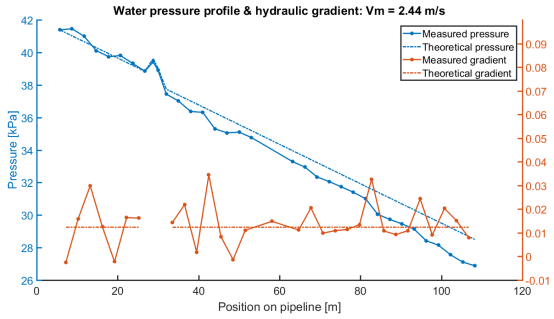

(a) Water experiment #3

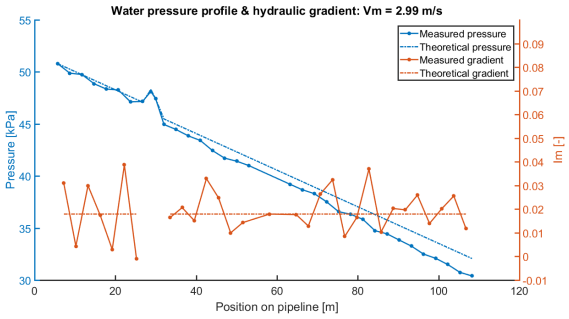

(b) Water experiment #4

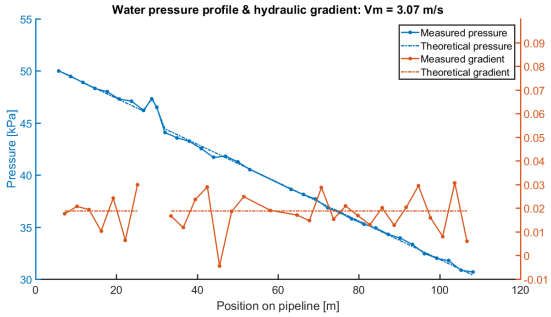

(a) Water experiment #5

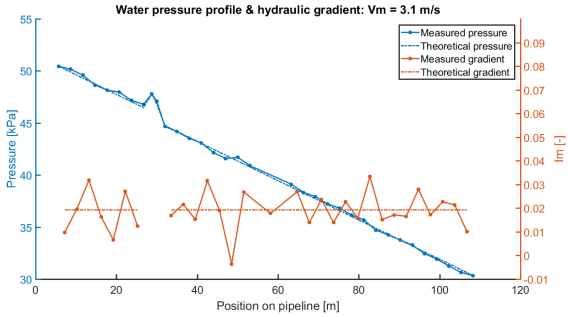

(b) Water experiment #6

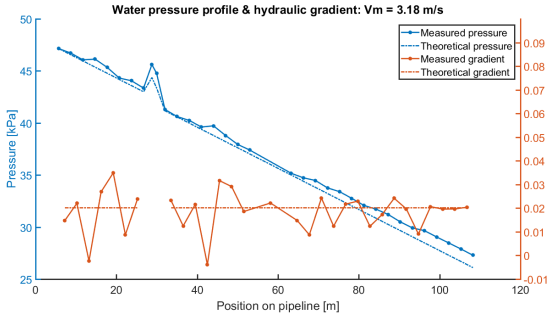

(a) Water experiment #7

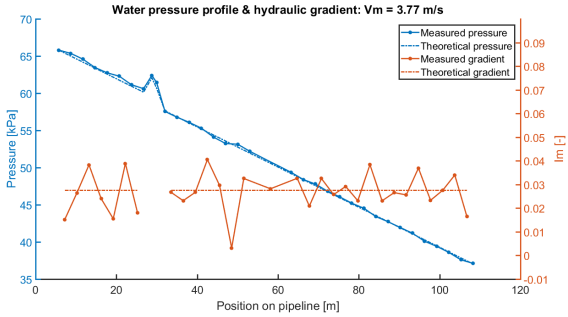

(b) Water experiment #8

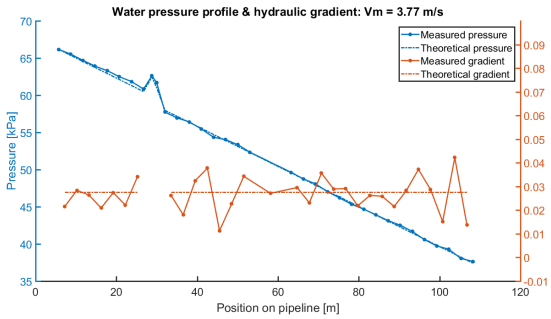

(a) Water experiment #9

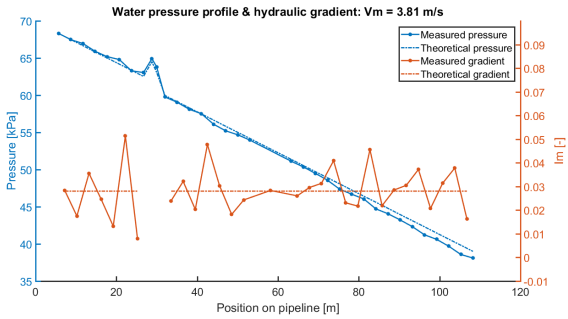

(b) Water experiment #10

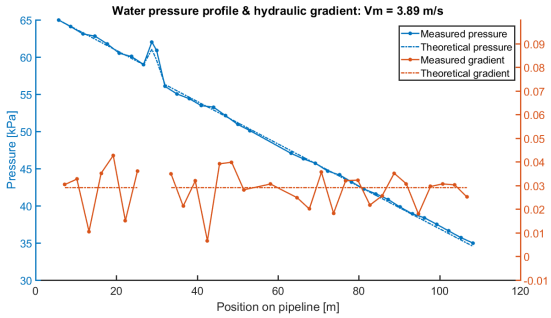

(a) Water experiment #11

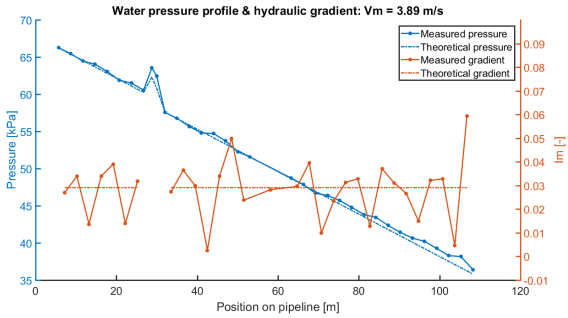

(b) Water experiment #12

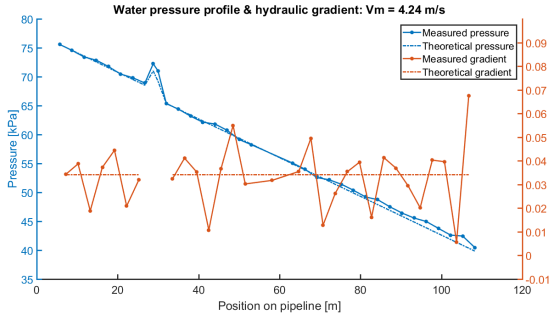

(a) Water experiment #13

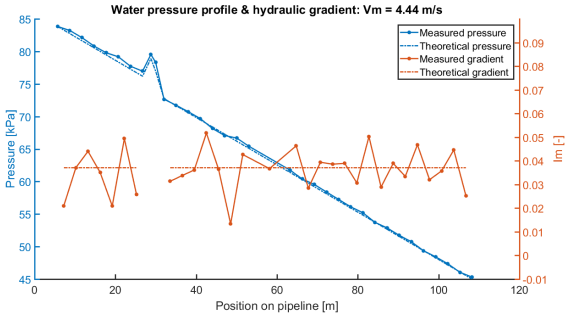

(b) Water experiment #14

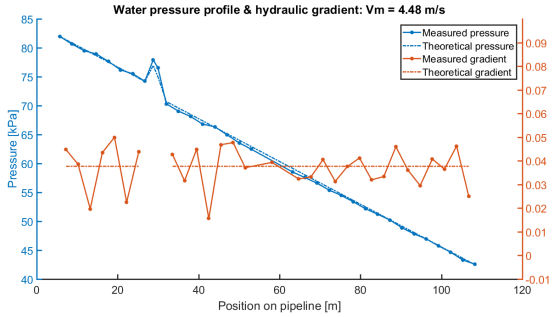

(a) Water experiment #15

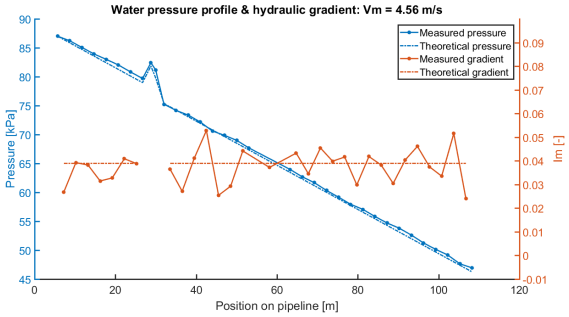

(b) Water experiment #16

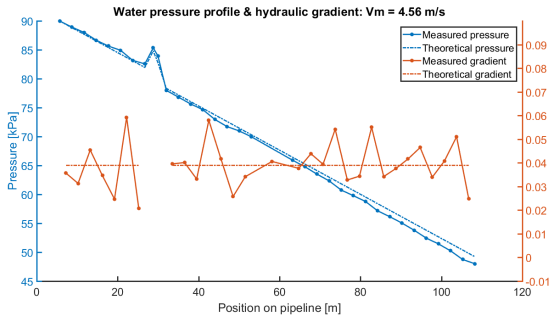

(a) Water experiment #17

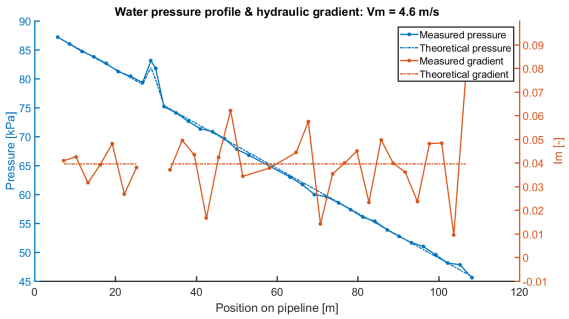

(b) Water experiment #18

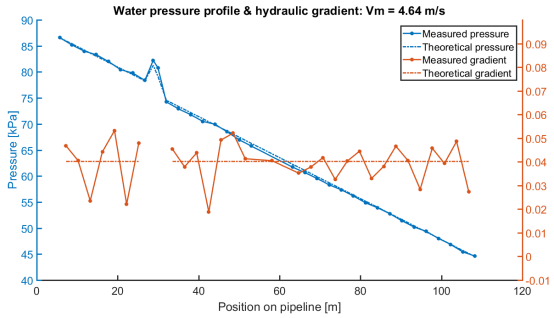

(a) Water experiment #19

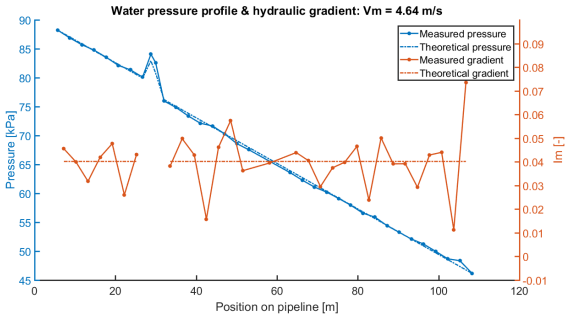

(b) Water experiment #20

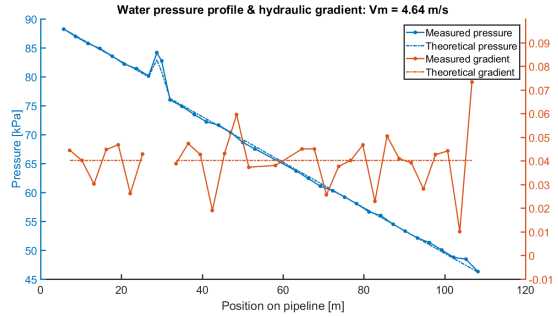

(a) Water experiment #21

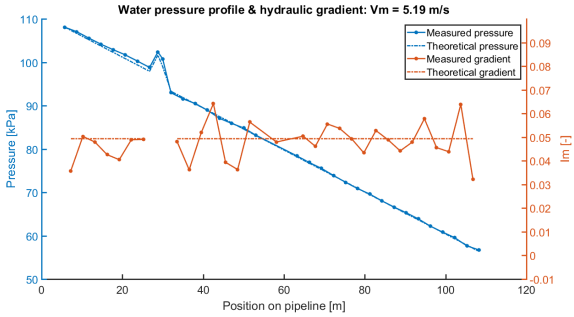

(b) Water experiment #22

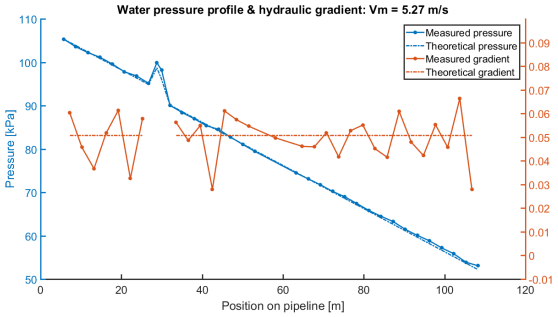

(a) Water experiment #23

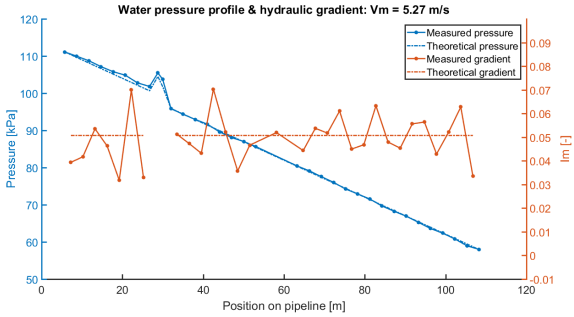

(b) Water experiment #24

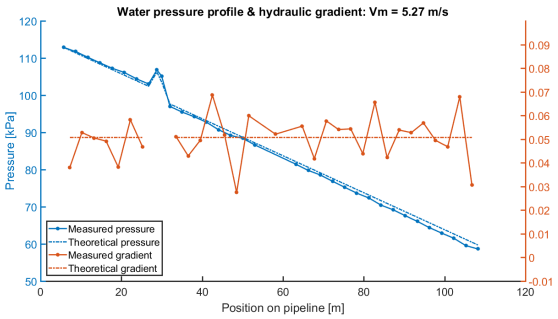

(a) Water experiment #25

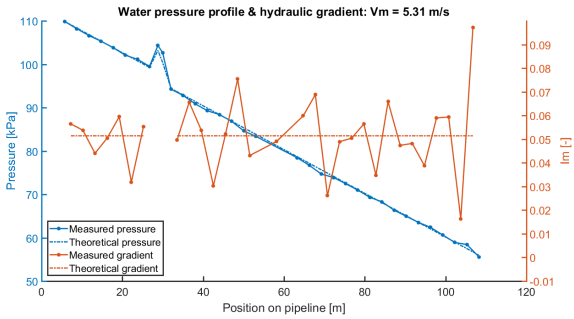

(b) Water experiment #26

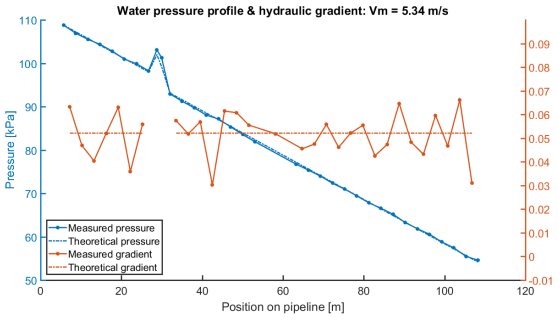

(a) Water experiment #27

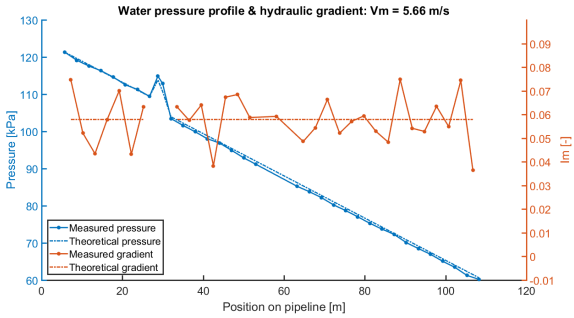

(b) Water experiment #28

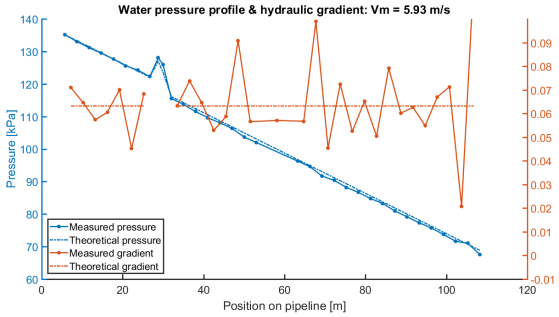

(a) Water experiment #29

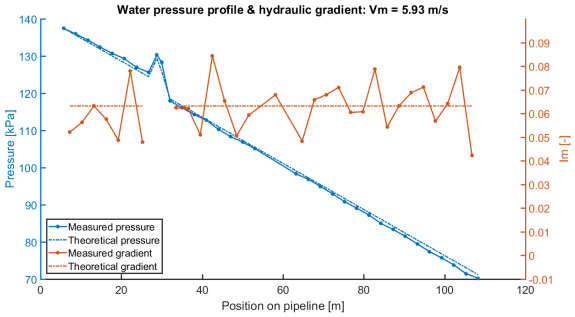

(b) Water experiment #30

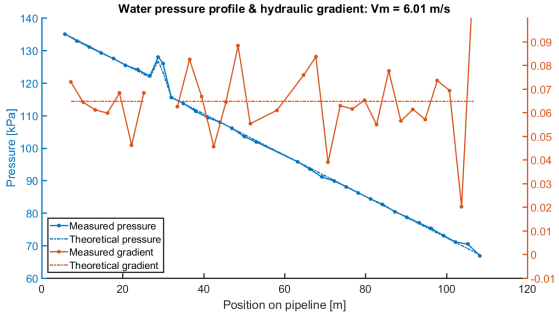

(a) Water experiment #31

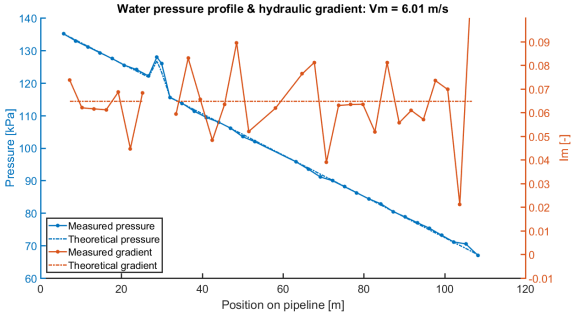

(b) Water experiment #32

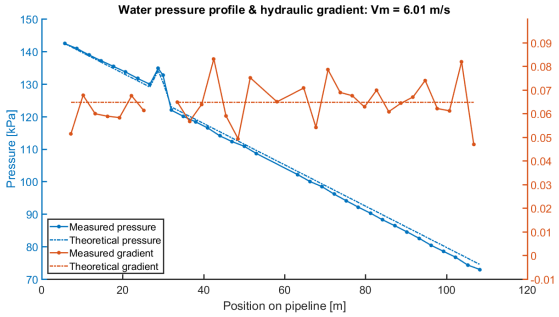

(a) Water experiment #33

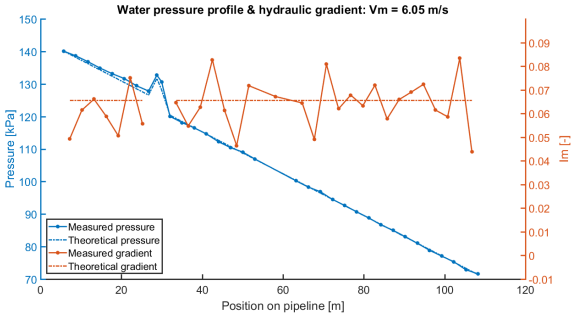

(b) Water experiment #34

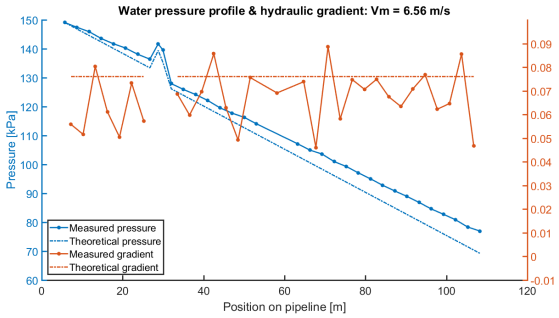

(a) Water experiment #35

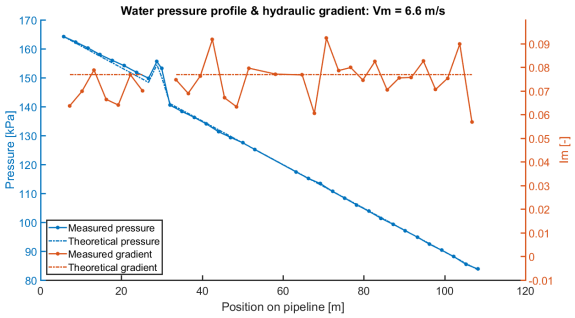

(b) Water experiment #36

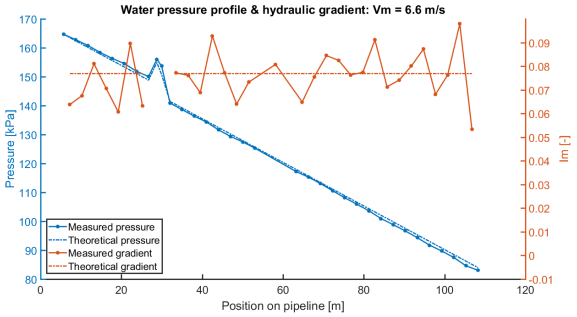

(a) Water experiment #37

Result mixture experiment: Führböter

The result of the slurry experiment when the decisive particle diameter is used in the Führböter model, instead of the mass-median particle diameter.

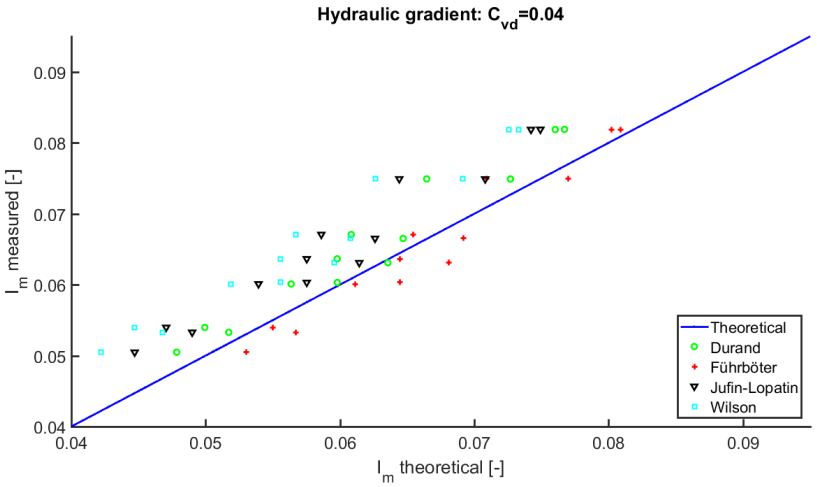

Figure I.1: Result mixture experiment: (C=4%)

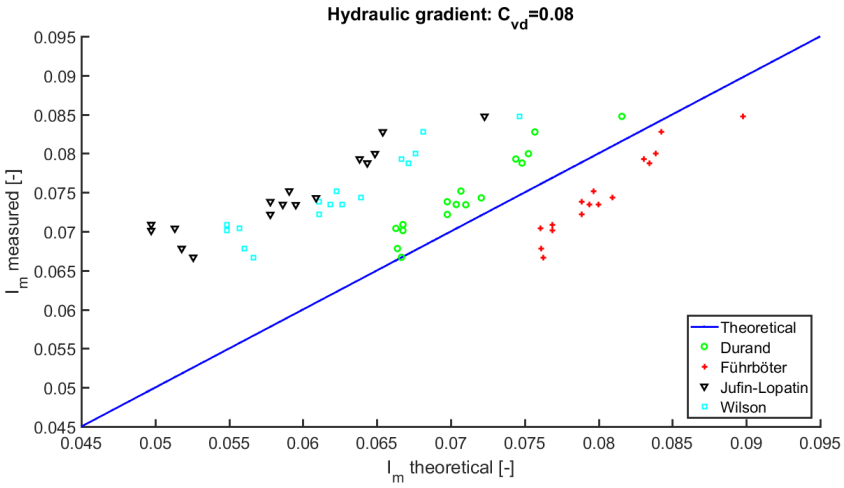

Figure I.2: Result mixture experiment: (C=8%)

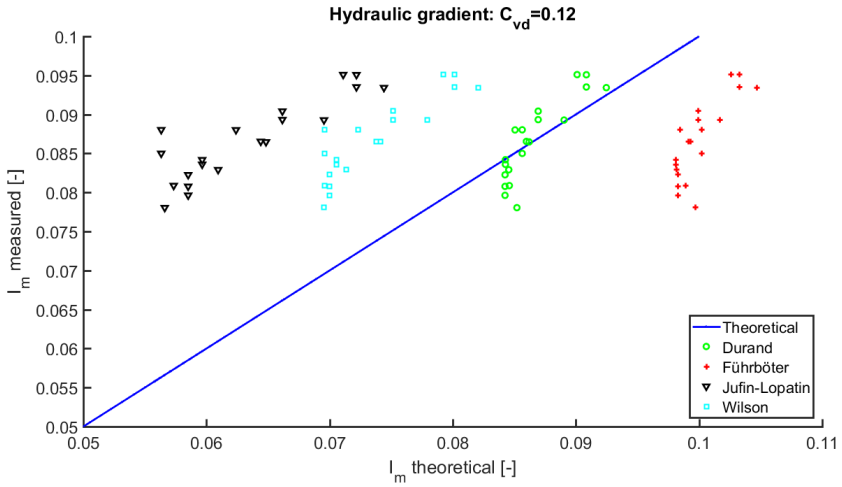

Figure I.3: Result mixture experiment: (C=12%)

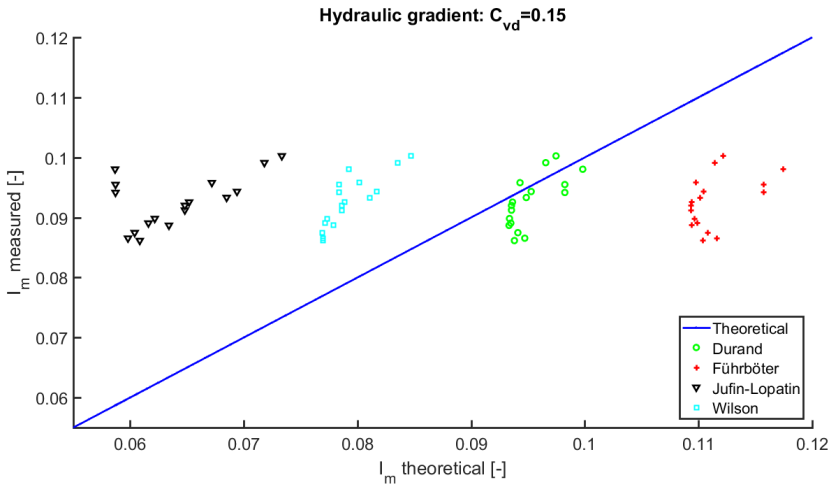

Figure I.4: Result mixture experiment: (C=15%)

J

Mixture flow: pressure profiles

In this appendix the pressure profiles of the mixture experiment are compared to the four theoretical prediction methods. The analysis is divided into the tested concentrations. In order of appearance: 4, 8, 12 and 15 percent.

J.1. 4% concentration

Two test runs are carried out with a four percent concentration slurry. The amount of examined velocities is thirteen. The lowest flow rate is $3.7\ m/s$, the intermediate is $4.9\ m/s$ and the highest is $6.0\ m/s$.

Durand

The pressure profiles are compared to Durand's theoretical prediction in Figure J.1. Regarding the lowest and highest velocities, the profile fits to the expectation until the end of the pipeline is reached. There a small distinction is observed, this is considered as an underestimation of the frictional head loss. The pressure loss at the intermediate flow rate falls precisely on the theoretical curve. In general the Durand principle is observed to be suitable for the prediction of low concentration mixtures.

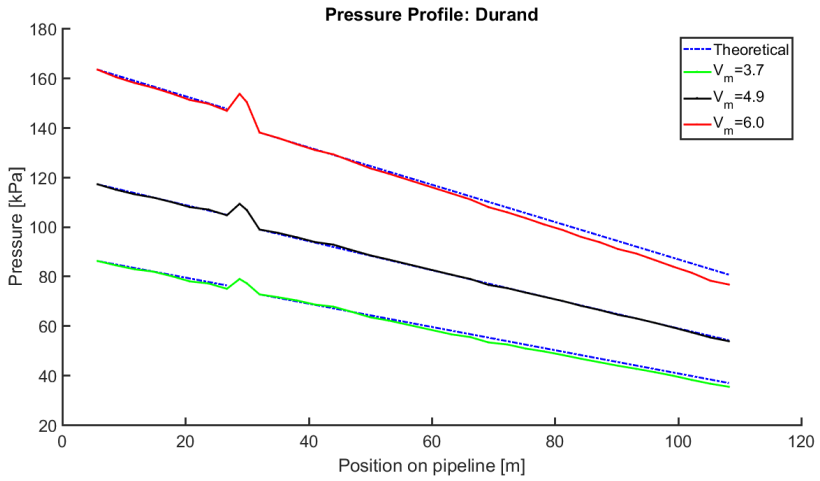

Figure J.1: Pressure profile: Durand (C=4%)

Führböter

The pressure profiles are compared to Fûhrböter's theoretical prediction in Figure J.2. Both up- and downstream of the bend, there is an excellent correspondence between them for all the considered velocities. The examined principle shows to be suitable for frictional head loss predictions at this concentration.

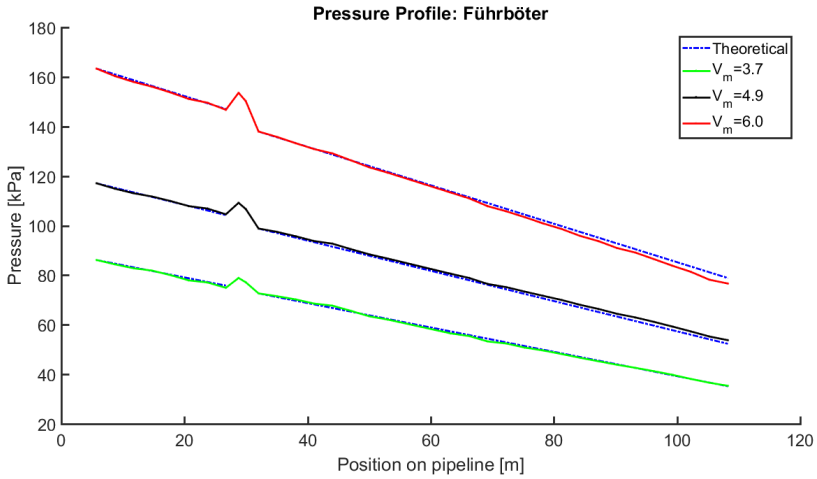

Figure J.2: Pressure profile: Führböter (C=4%)

Jufin & Lopatin

The pressure profiles are compared to the theoretical prediction method of Jufin and Lopatin in Figure J.3. In the first part of the measurement section the profiles fit to the expectation. Around the 50 meter pipeline position, the curves of the utmost velocities start the separate. At the 70 meter distance, this is also the case for the intermediate velocity. There is a underestimation corresponding to the lower limit of the data acquired by Jufin and Lopatin.

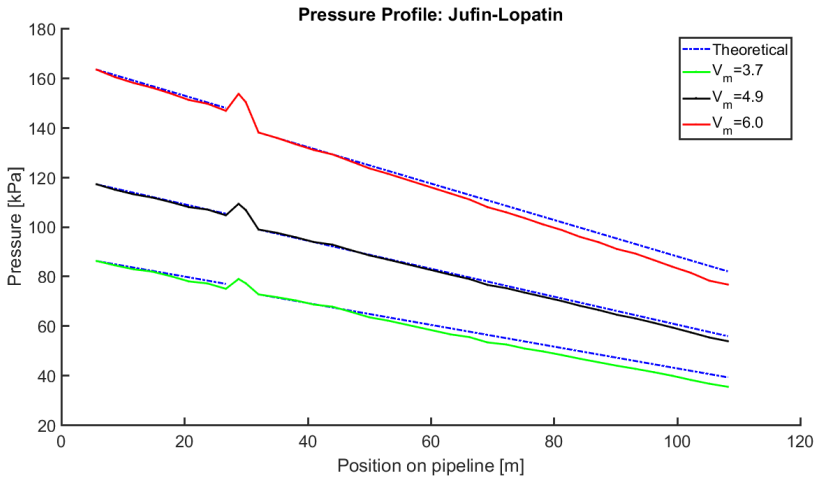

Figure J.3: Pressure profile: Jufin-Lopatin (C=4%)

Wilson

The pressure profiles are compared to the theoretical prediction method of Wilson in Figure J.4. The same phenomenon occurs as observed in the Jufin and Lopatin comparison for this concentration. At the start of the pipeline theory and measurement show good correspondence. Downstream the curves start to diverge as the prediction is lower with regard to the experimental data.

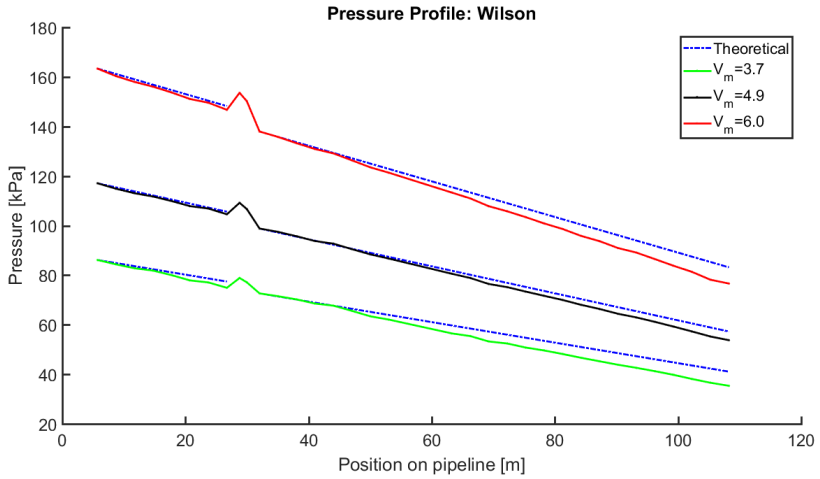

Figure J.4: Pressure profile: Wilson (C=4%)

J.2. 8% concentration

Three test runs are carried out with an eight percent concentration slurry. The amount of examined velocities is thirteen. The lowest flow rate is $3.3\ m/s$, the intermediate is $4.5\ m/s$ and the highest is $5.6\ m/s$.

Durand

The measured pressure profiles are compared to Durand's theoretical prediction in Figure J.5. There is good resemblance between expectation and the acquired data at all velocities. The slope of the lowest velocity curve is a bit steeper compared to theory. But the difference is almost nil. In general the Durand principle seems suitable to determine the pressure drop for mixture transport at a slurry concentration of eight percent.

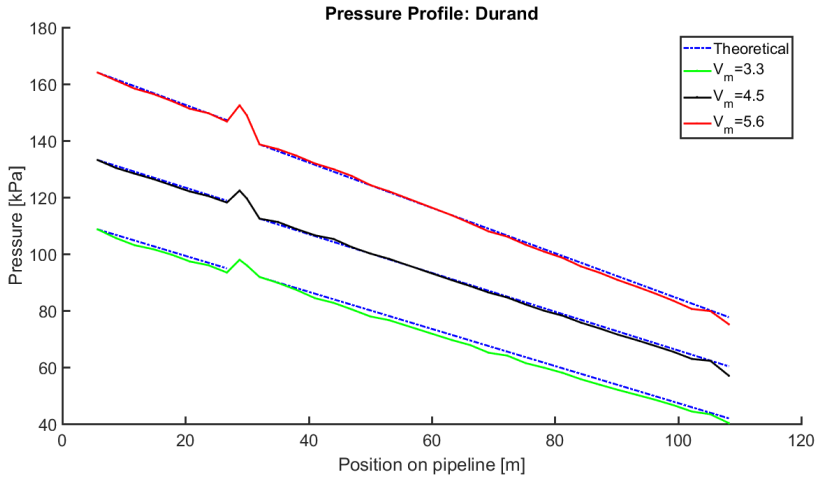

Figure J.5: Pressure profile: Durand (C=8%)

Führböter

The pressure profiles are compared to Führböter's theoretical prediction in Figure J.6. Again this principles shows good correspondence between measurement and expectations. For the highest velocities there are small deviations towards the end of the pipeline. Indicating the pressure drop is slightly lower than what the theory describes.

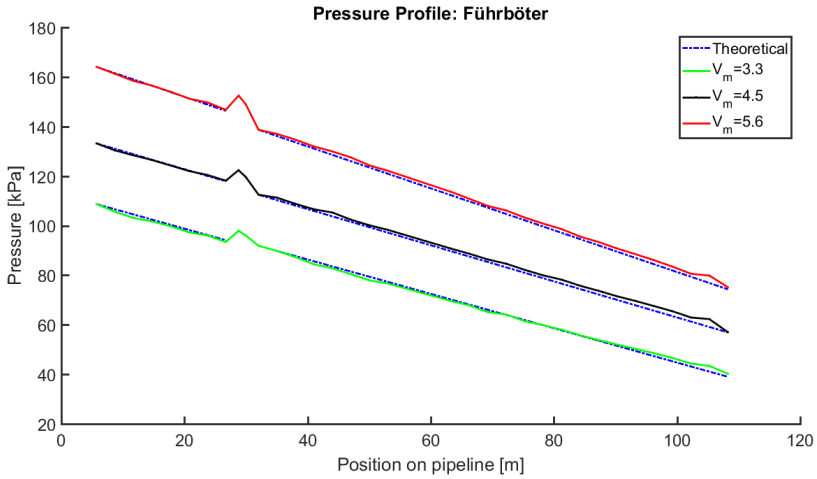

Figure J.6: Pressure profile: Führböter (C=8%)

Jufin & Lopatin

The pressure profiles are compared to the theoretical prediction method of Jufin and Lopatin in Figure J.7. The phenomenon observed at the lower concentration sets through. Now the separation is even more distinct. At the end of the pipeline the difference between the measured result and the expectation is, almost $14\ kPa$ for the lowest velocity, $12\ kPa$ for the intermediate and $10\ kPa$ for the highest.

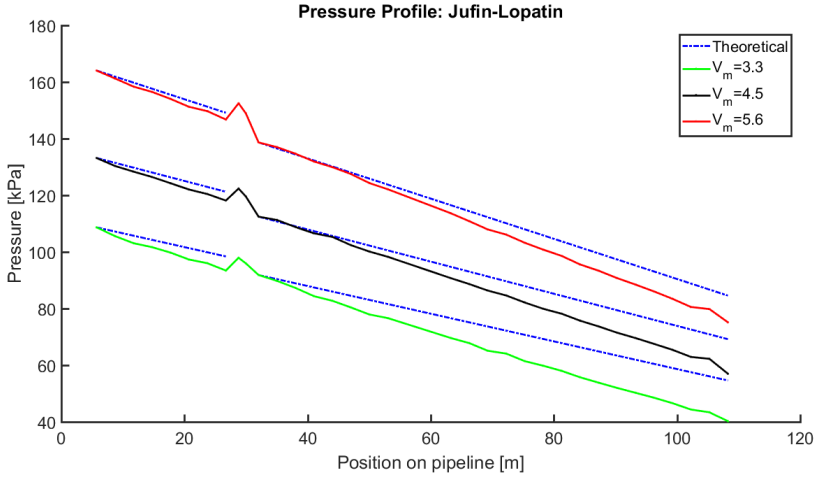

Figure J.7: Pressure profile: Jufin-Lopatin (C=8%)

Wilson

The pressure profiles are compared to the theoretical prediction method of Wilson in Figure J.8. Again the result is similar to the Jufin-lopatin model. There is a clear divergence visible between the experimental data and the estimated pressure drop. Nevertheless the difference at the end of the pipeline is smaller compared to the other model. The curves separate respectively: 11 for the lowest, 10 for the intermediate and $8\ kPa$ for the highest flow rate.

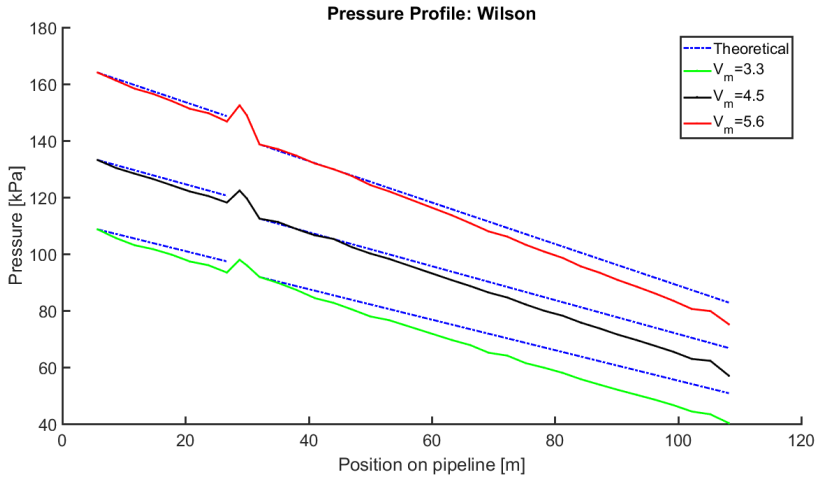

Figure J.8: Pressure profile: Wilson (C=8%)

J.3. 12% concentration

Three test runs are carried out with a twelve percent concentration slurry. The amount of examined velocities is twenty. The lowest flow rate is $3.7\ m/s$, the intermediate is $4.6\ m/s$ and the highest is $5.5\ m/s$.

Durand

The pressure profiles are compared to Durand's theoretical prediction in Figure J.9. The result is similar to the outcome of the 4 and 8 percent concentration experiments. Overall there is a good correspondence between what is expected and what is measured. The pressure profile of lowest velocity shows a small deviation towards the end of the pipeline.

Regarding the utmost velocities, the profile fits to the expectation until the end of the pipeline is reached. There a small distinction is observed, this is considered as an underestimation of the frictional head loss. The pressure loss at the intermediate flow rate falls precisely on the theoretical curve. In general the Durand principle is observed to be suitable for the prediction of low concentration mixtures.

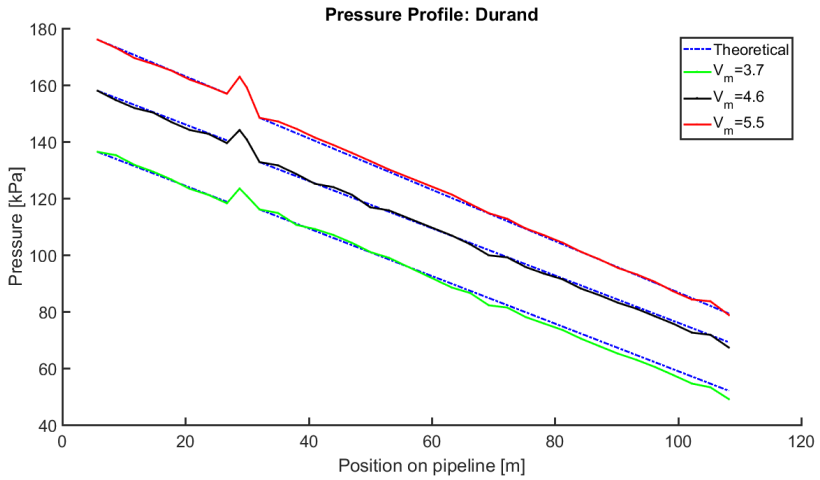

Figure J.9: Pressure profile: Durand (C=12%)

Führböter

The pressure profiles are compared to Führböter's theoretical prediction in Figure J.10. A distinction needs to be made between section 'A' and section 'B+C' of the pipeline (Figure 3.3). In the former part of the flow loop a good resemblance is observed. For all examined velocities the measured profile fits

the expectations.

Downstream of the 180° turn, the curves start to separate. The observed deviation grows larger with increase in velocity. It indicates that the predicted pressure drop is larger than measured. Nevertheless the divergence is small and seems to be in a tolerable margin.

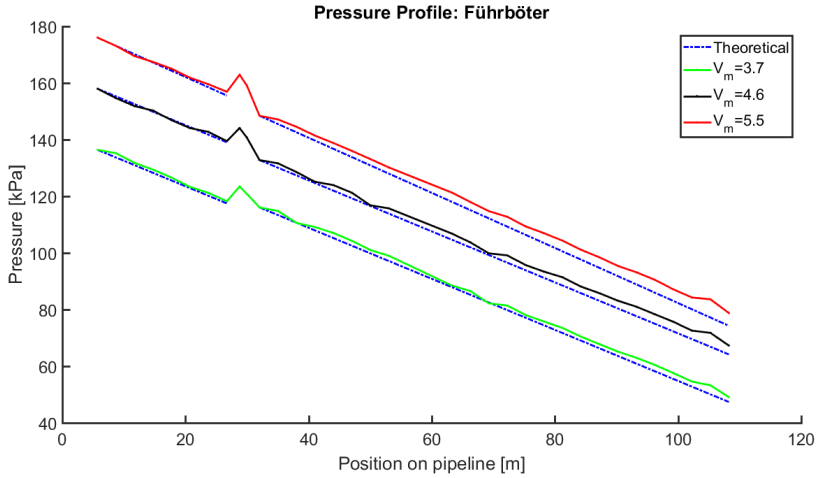

Figure J.10: Pressure profile: Führböter (C=12%)

Jufin & Lopatin

The pressure profiles are compared to the theoretical prediction method of Jufin and Lopatin in Figure J.11. Compared to the lower concentrations, the difference between theoretical and measurement curves increases. The lines representing the test results even cross the expected profiles of the lower velocities. To this principle applies: the higher the concentration, the larger the divergence.

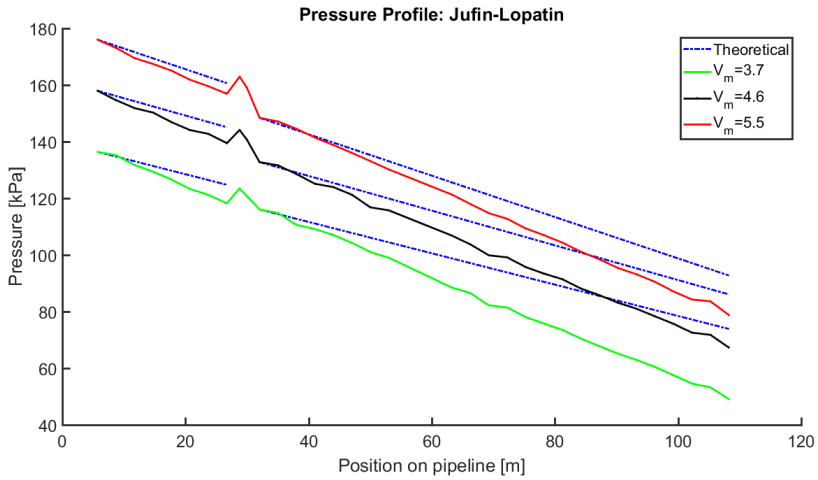

Figure J.11: Pressure profile: Jufin-Lopatin (C=12%)

Wilson

The pressure profiles are compared to the theoretical prediction method of Wilson in Figure J.12. What occurred at the lower concentrations sets through. At the end of the pipeline the differences are now: 14 kPa for the lowest transport velocity and 12 for the intermediate. For the highest flow rate the difference is almost equal compared to the 8 percent concentration experiment: 8 kPa.

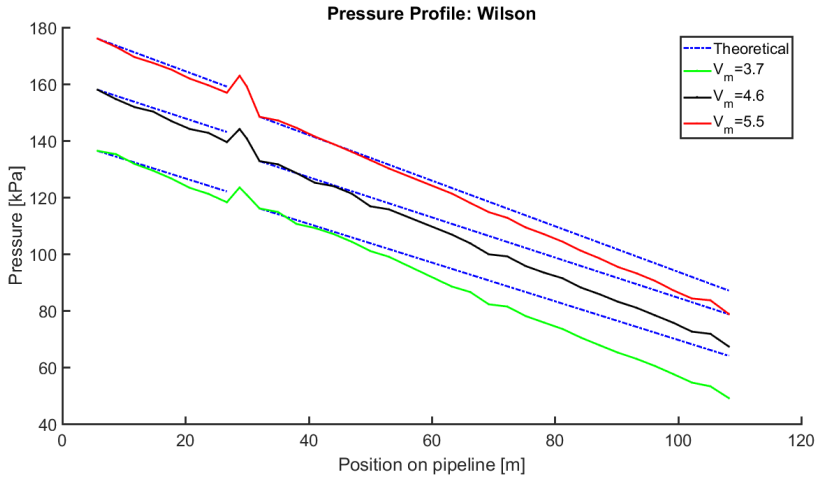

Figure J.12: Pressure profile: Wilson (C=12%)

J.4. 15% concentration

Three test runs are carried out with a four percent concentration slurry. The amount of examined velocities is seventeen. The lowest flow rate is $3.4\ m/s$, the intermediate is $4.4\ m/s$ and the highest is $5.3\ m/s$.

Durand

The pressure profiles are compared to Durand's theoretical prediction in Figure J.13. Upstream of the 180° turn, the experimental result matches the expectations. Downstream of the bend this progresses for the utmost velocities. This does not apply to the profile of the intermediate flow rate. For the first time there is a clear distinction between what is calculated with the Durand principle and the outcome of the laboratory test. Around the 50 meter pipeline position the curves start to separate. Due to an over prediction of the frictional pressure loss.

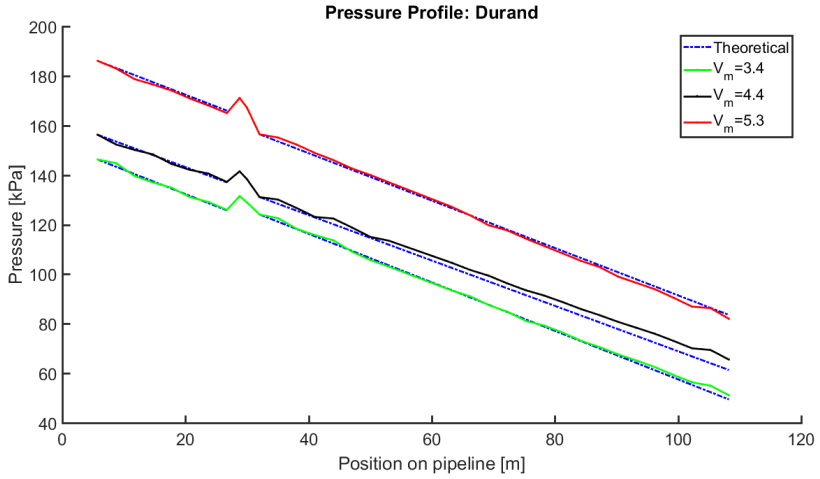

Figure J.13: Pressure profile: Durand (C=15%)

Führböter

The pressure profiles are compared to Führböter's theoretical prediction in Figure J.14. The trend started at the 12 percent concentration continues. Downstream of the bend the curves separate. This time the divergence is larger in comparison with the result at the lower concentration. Now it clearly shows that the measured hydraulic gradient is smaller than predicted.

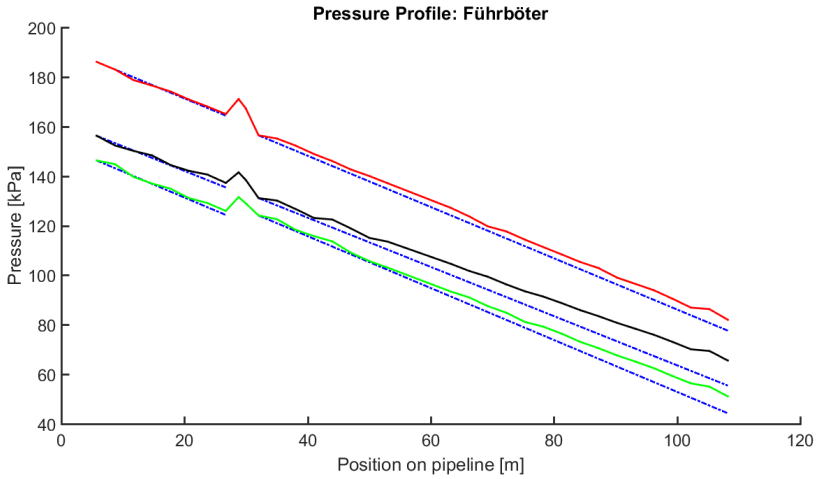

Figure J.14: Pressure profile: Führböter (C=15%)

Jufin & Lopatin

The pressure profiles are compared to the theoretical prediction method of Jufin and Lopatin in Figure J.15. It is observed that the divergence grows larger with increase in concentration. At the highest analysed concentration the distinction between result and expectation continues. The difference between theory and the data acquired in the experiment is large. At the end of the pipeline, the pressure curve of the highest flow velocity nearly touches the expected value of the lowest flow rate.

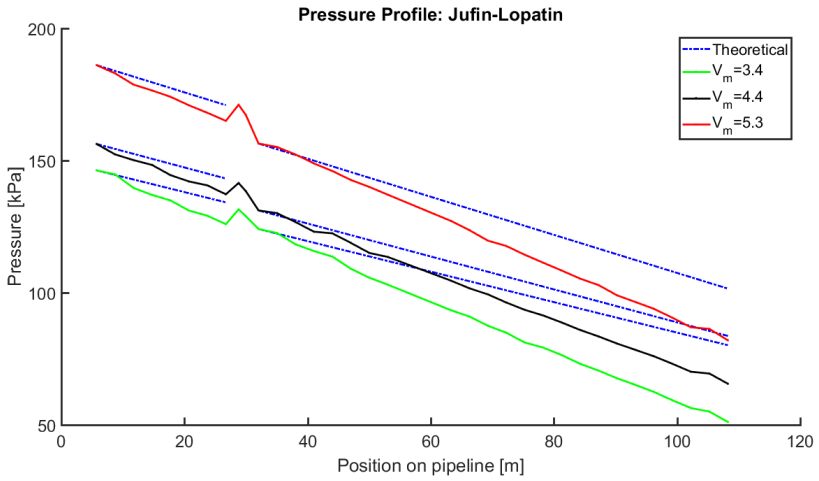

Figure J.15: Pressure profile: Jufin-Lopatin (C=15%)

Wilson

The pressure profiles are compared to the theoretical prediction method of Wilson in Figure J.16. The result can be compared with the Jufin and Lopatin model. Every time the concentration increases the divergences between expectation and measurement increases with it. Nevertheless the differences are smaller.

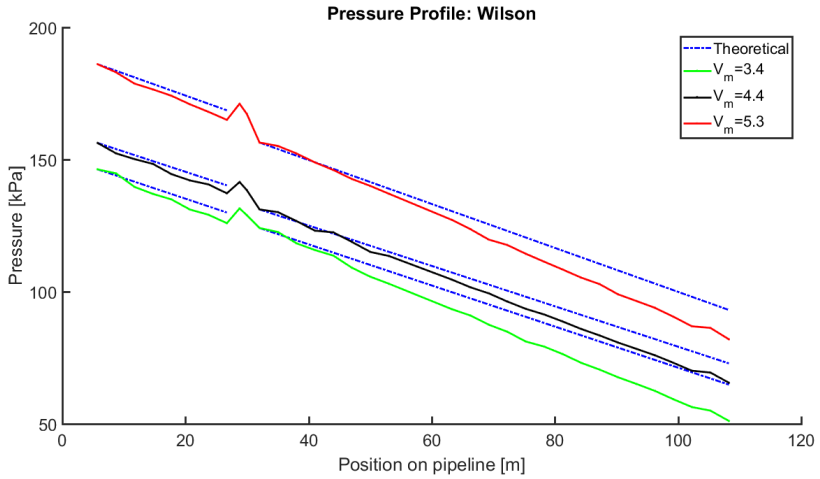

Figure J.16: Pressure profile: Wilson (C=15%)

K

Result: 4% concentration

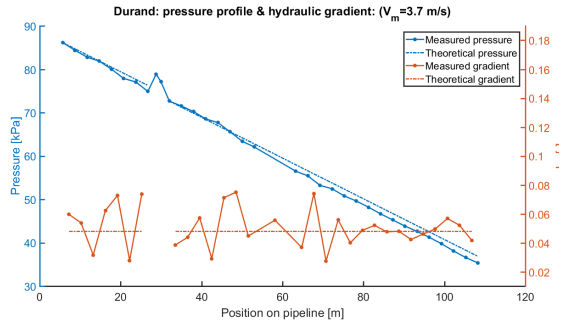

(a) Experiment #1

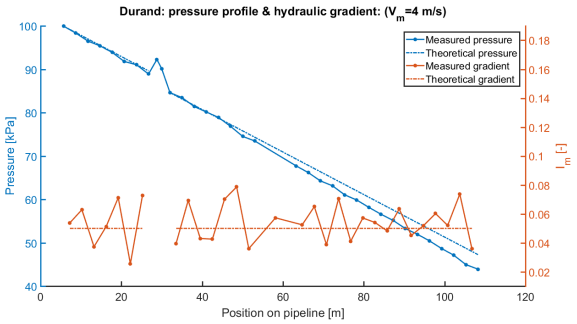

(b) Experiment #2

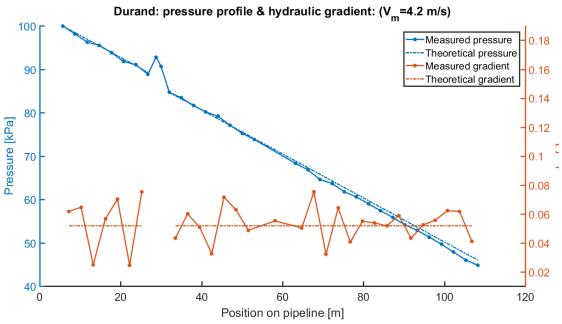

(a) Experiment #3

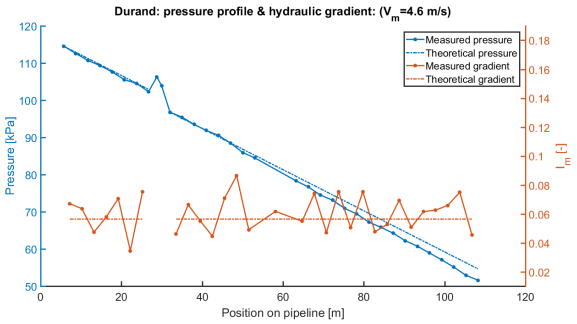

(b) Experiment #4

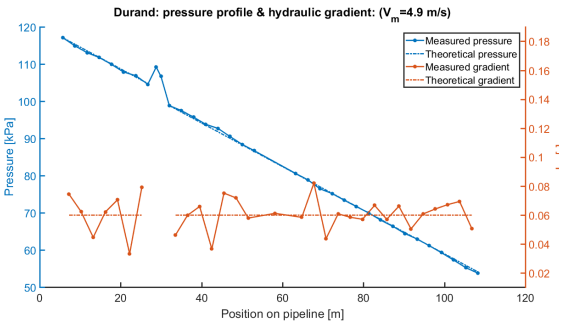

(a) Experiment #5

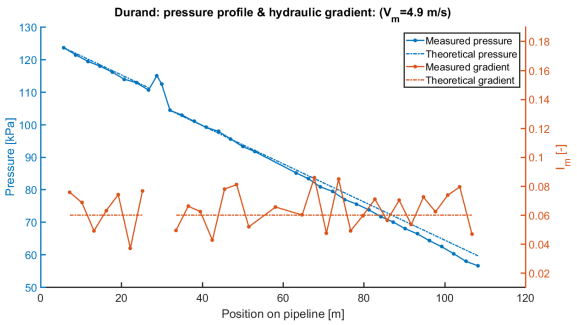

(b) Experiment #6

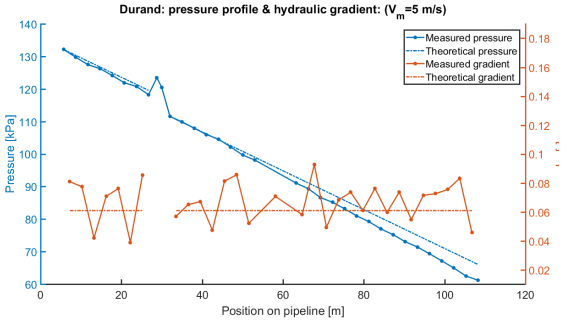

(a) Experiment #7

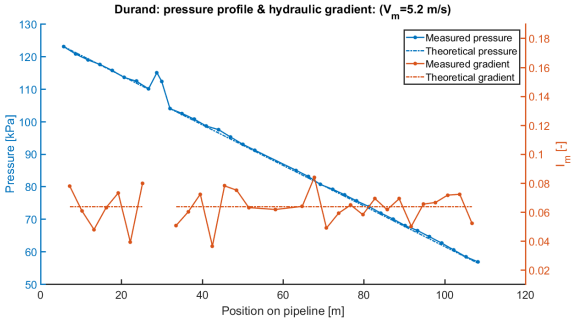

(b) Experiment #8

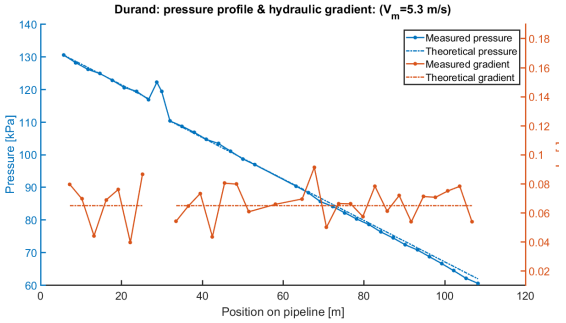

(a) Experiment #9

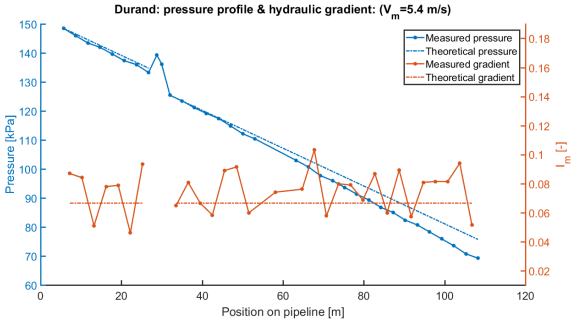

(b) Experiment #10

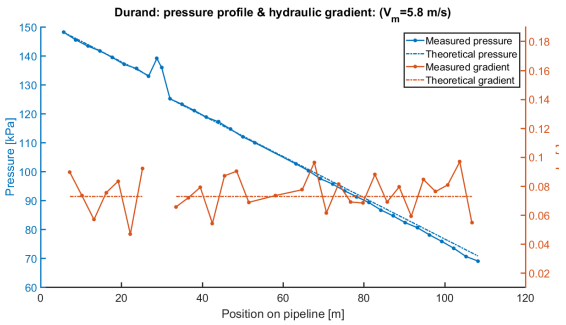

(a) Experiment #11

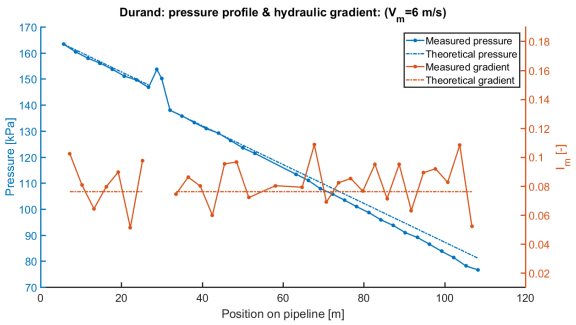

(b) Experiment #12

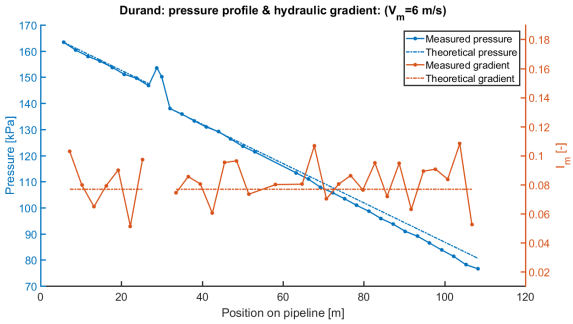

(a) Experiment #13

Result: 8% concentration

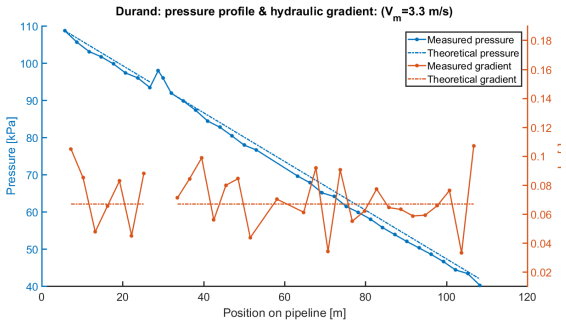

(a) Experiment #1

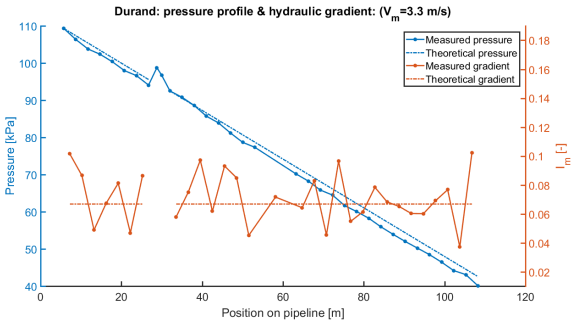

(b) Experiment #2

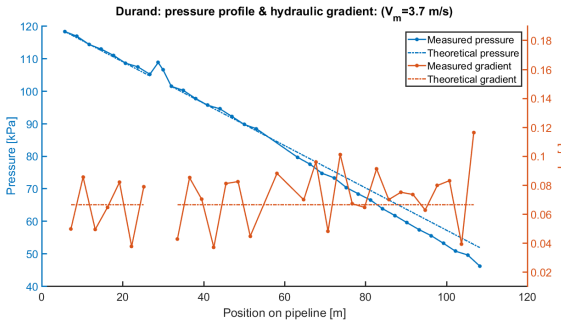

(a) Experiment #3

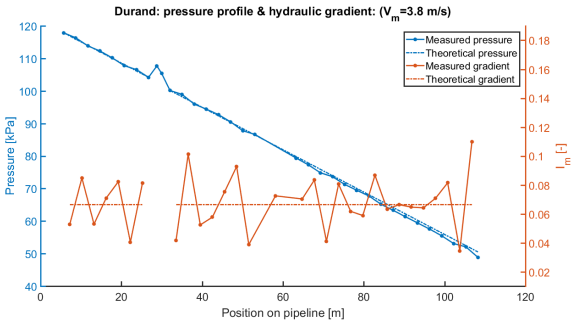

(b) Experiment #4

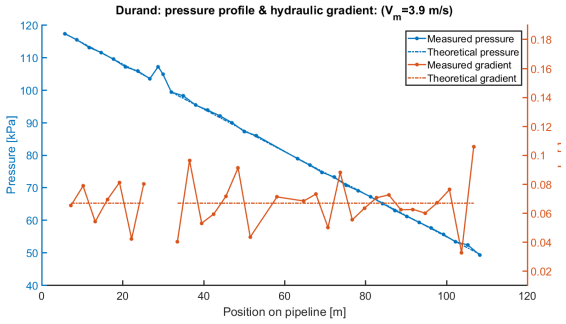

(a) Experiment #5

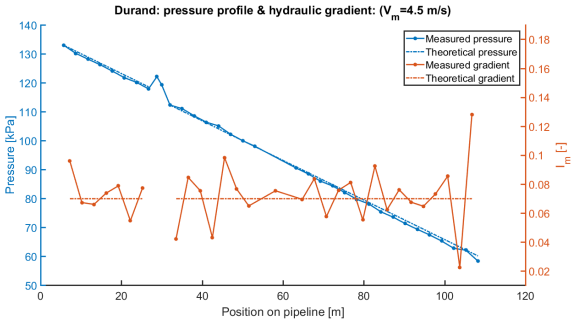

(b) Experiment #6

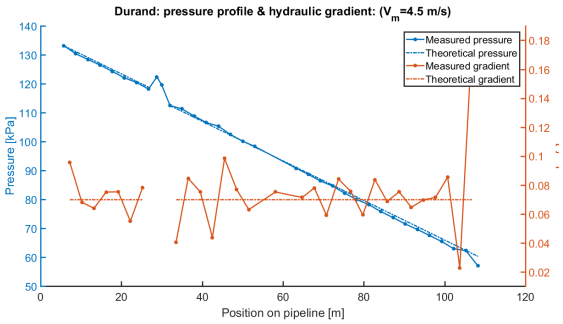

(a) Experiment #7

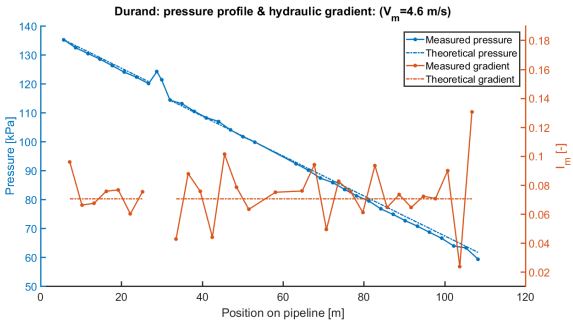

(b) Experiment #8

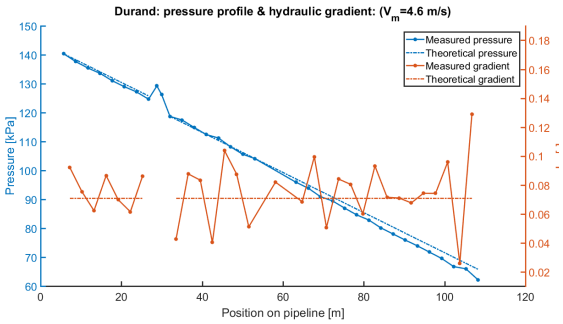

(a) Experiment #9

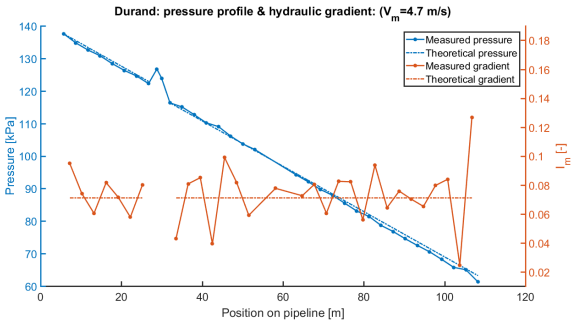

(b) Experiment #10

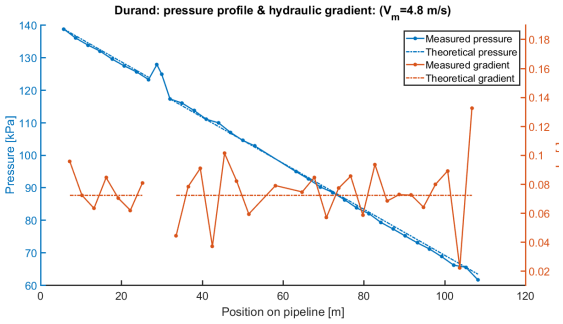

(a) Experiment #11

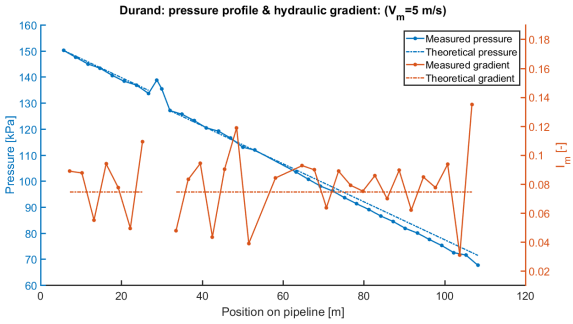

(b) Experiment #12

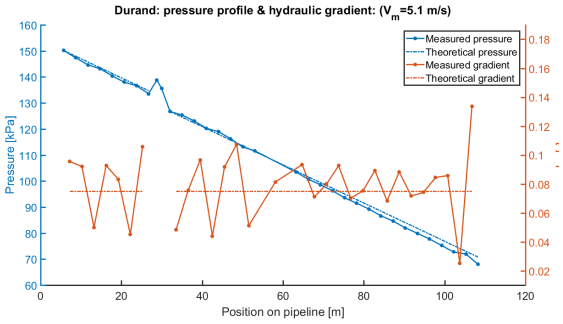

(a) Experiment #13

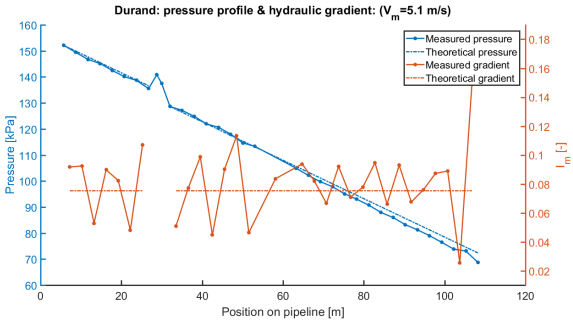

(b) Experiment #14

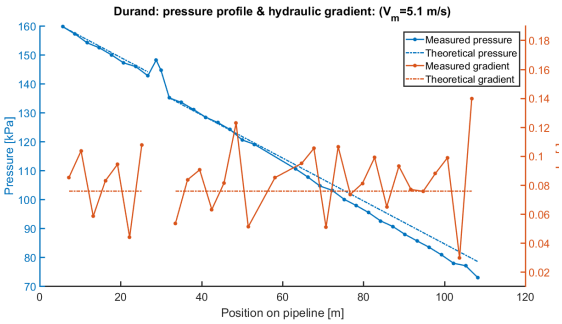

(a) Experiment #15

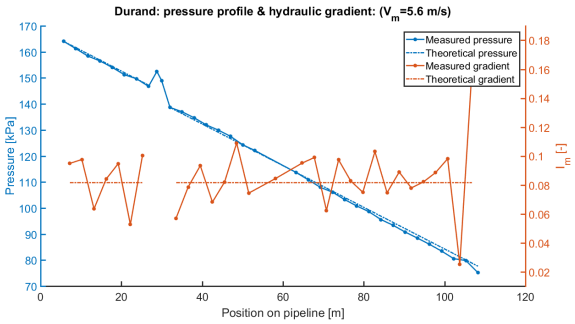

(b) Experiment #16

M

Result: 12% concentration

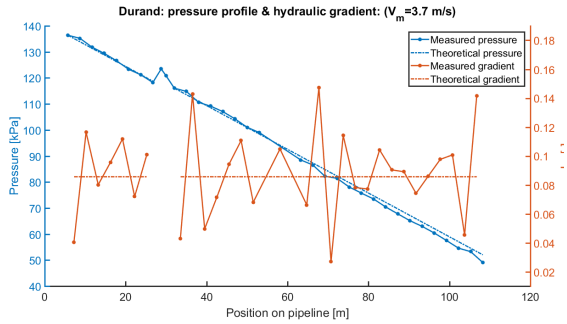

(a) Experiment #1

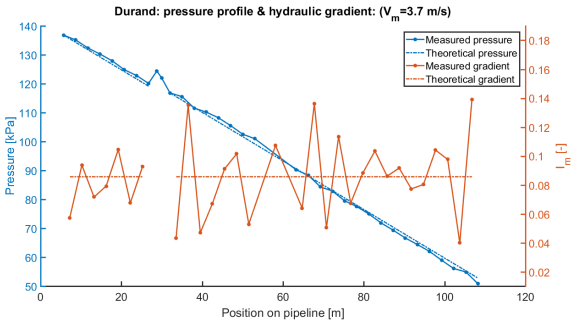

(b) Experiment #2

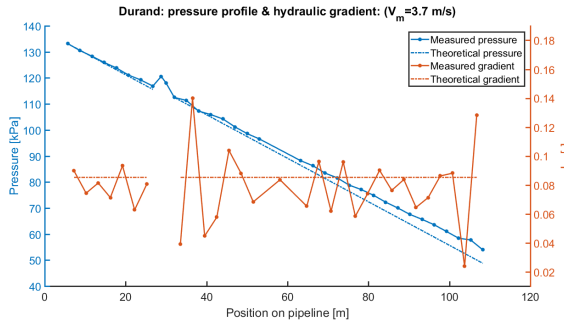

(a) Experiment #3

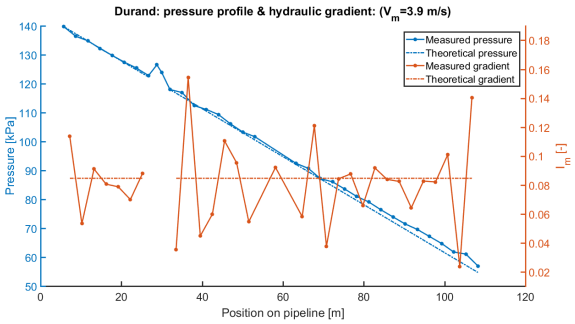

(b) Experiment #4

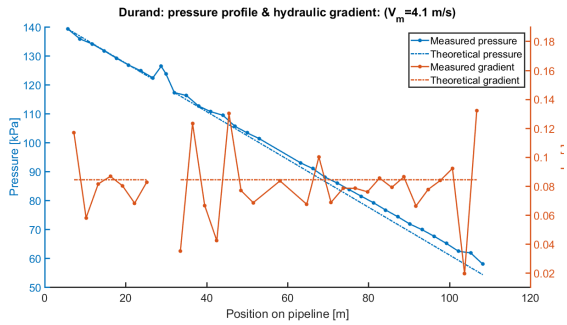

(a) Experiment #5

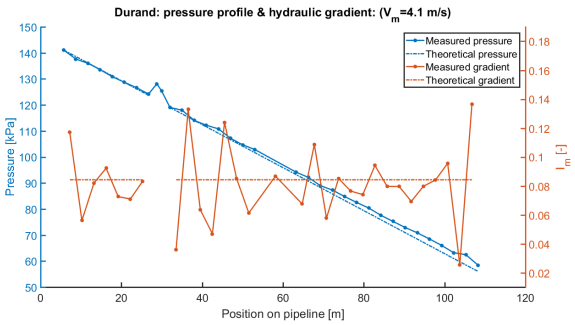

(b) Experiment #6

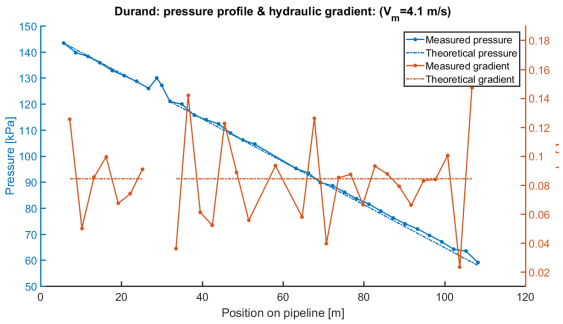

(a) Experiment #7

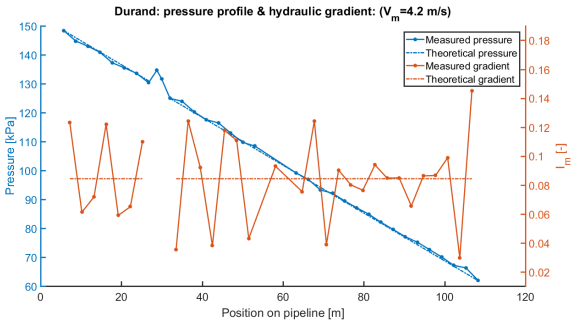

(b) Experiment #8

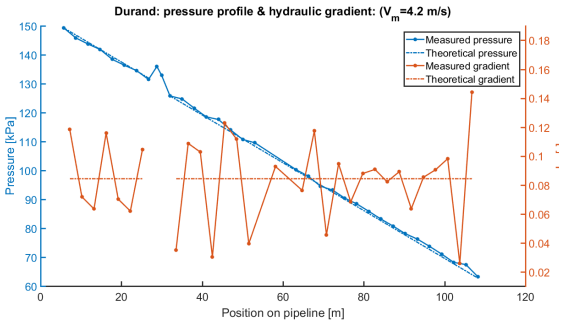

(a) Experiment #9

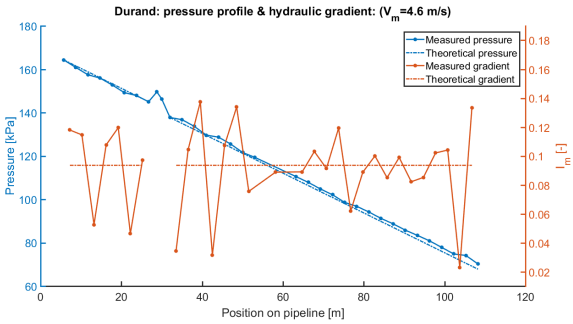

(b) Experiment #10

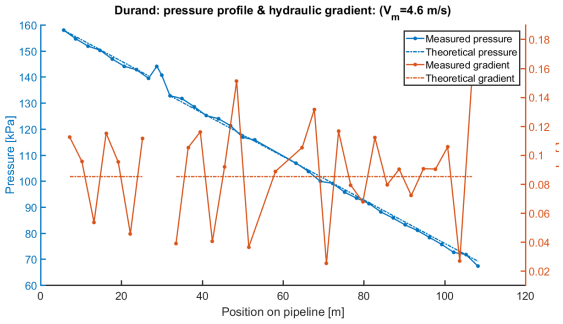

(a) Experiment #11

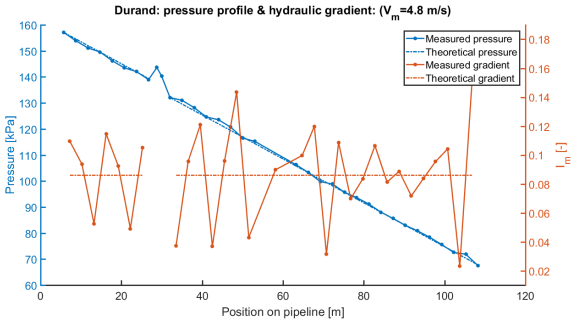

(b) Experiment #12

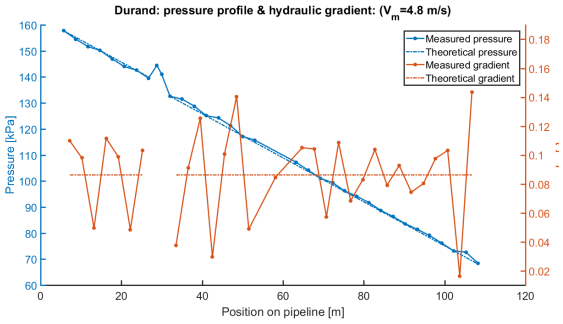

(a) Experiment #13

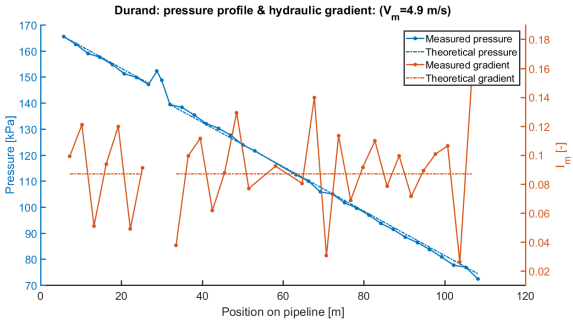

(b) Experiment #14

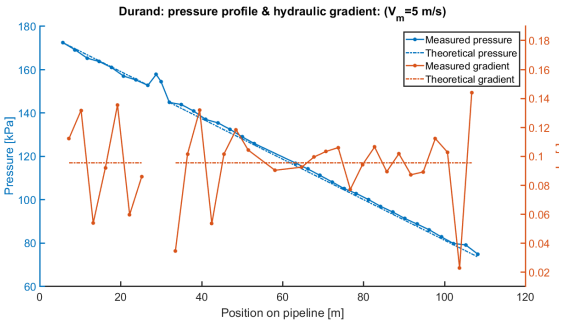

(a) Experiment #15

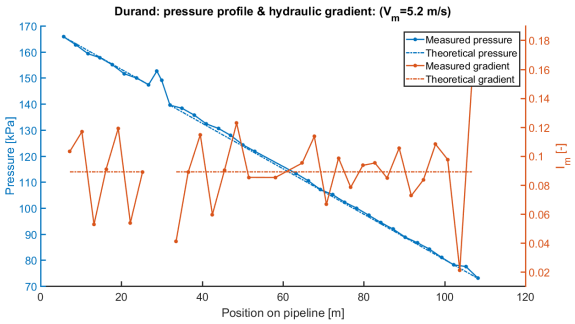

(b) Experiment #16

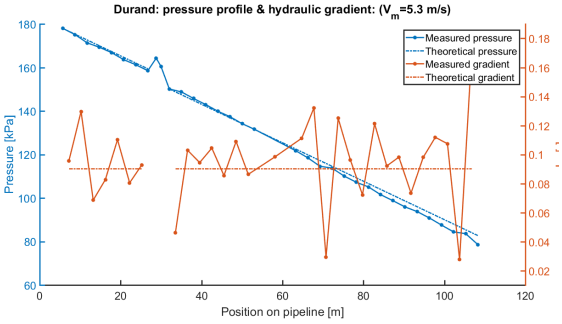

(a) Experiment #17

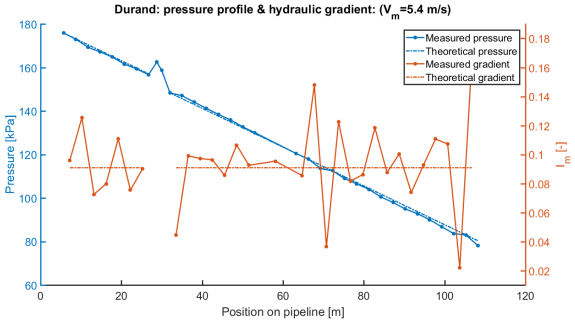

(b) Experiment #18

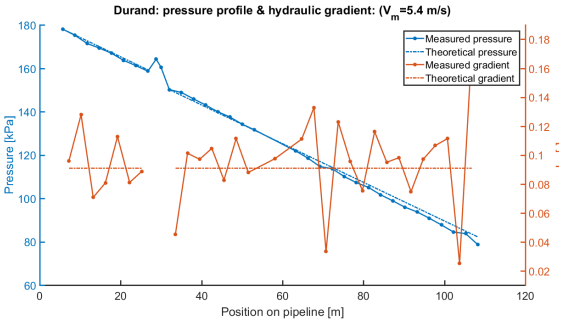

(a) Experiment #19

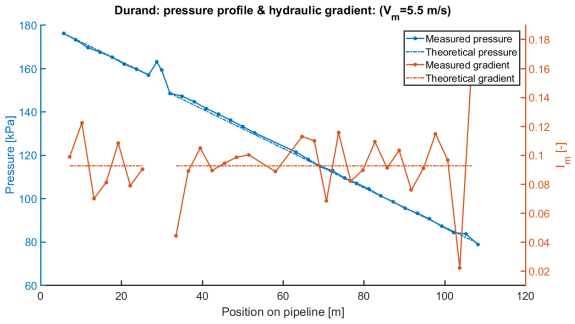

(b) Experiment #20

Result: 15% concentration

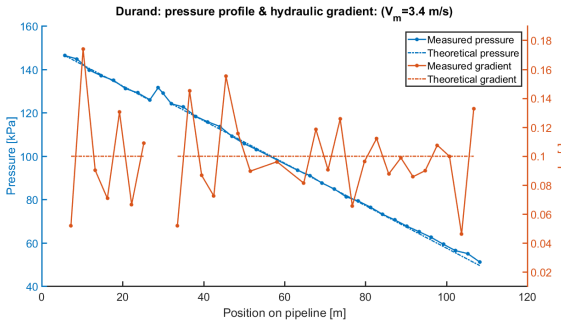

(a) Experiment #1

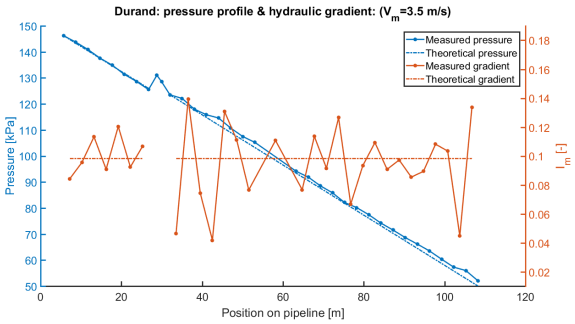

(b) Experiment #2

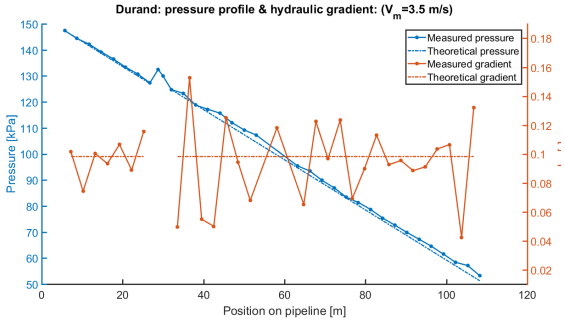

(a) Experiment #3

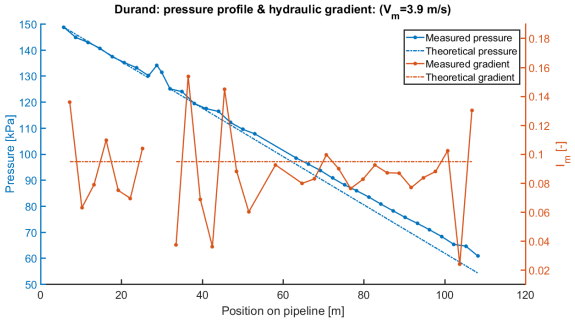

(b) Experiment #4

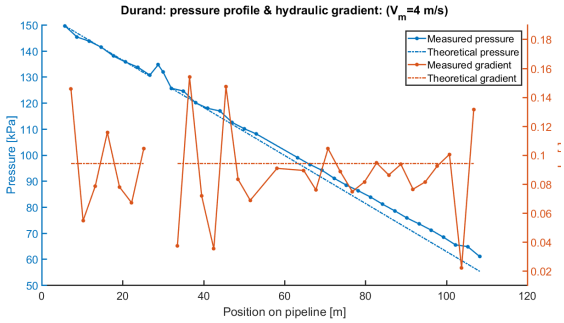

(a) Experiment #5

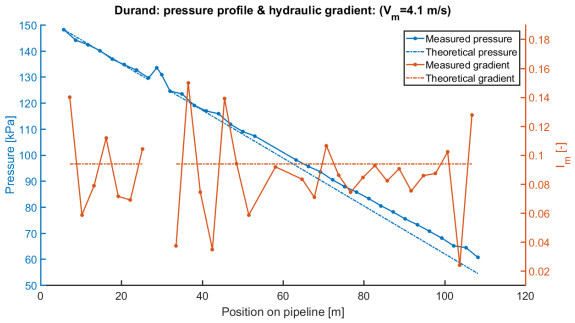

(b) Experiment #6

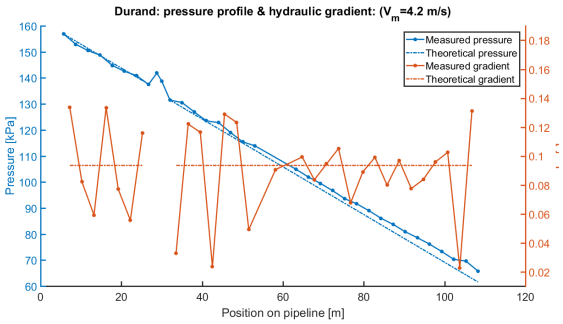

(a) Experiment #7

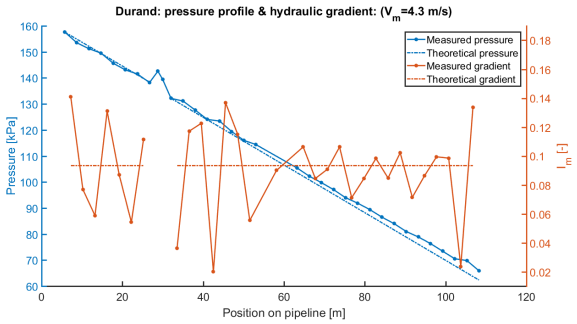

(b) Experiment #8

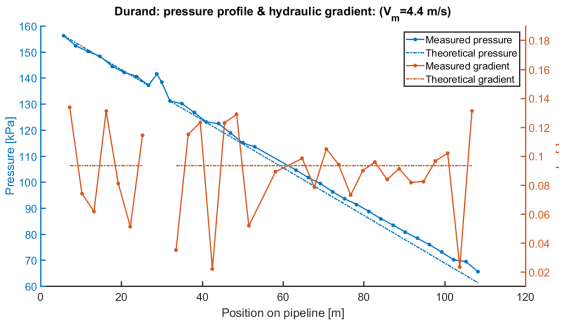

(a) Experiment #9

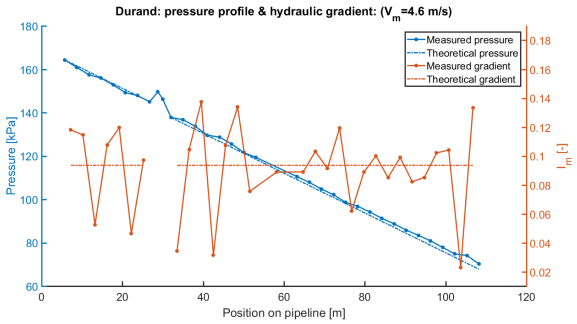

(b) Experiment #10

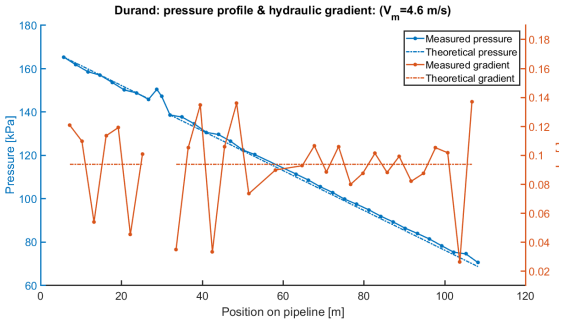

(a) Experiment #11

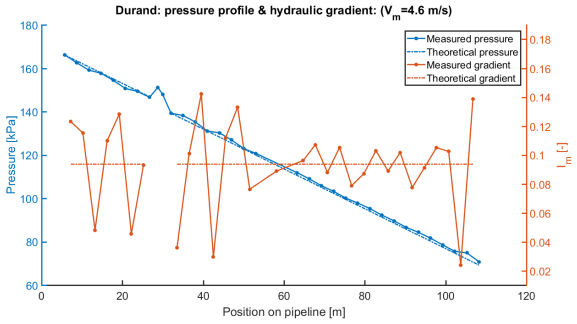

(b) Experiment #12

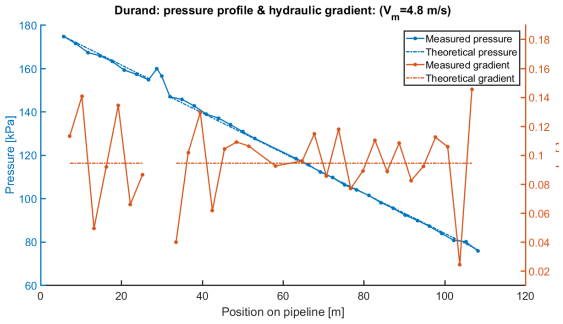

(a) Experiment #13

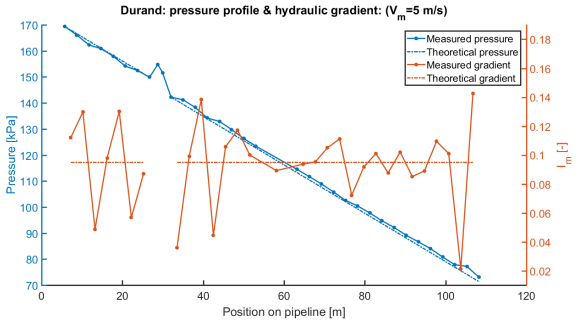

(b) Experiment #14

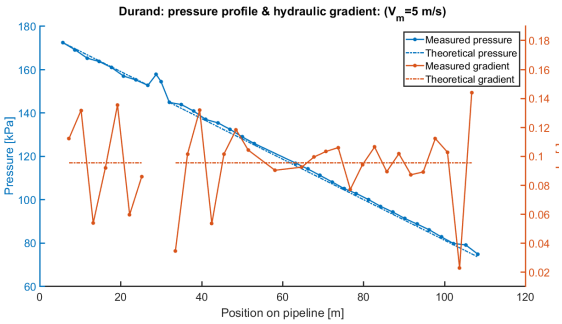

(a) Experiment #15

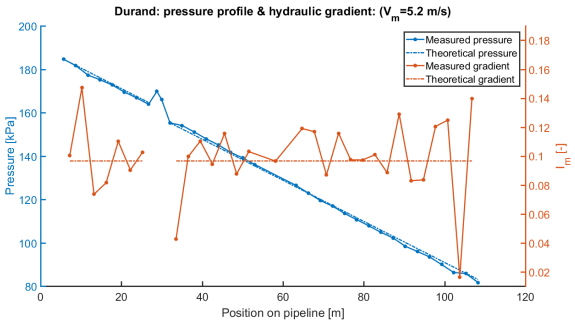

(b) Experiment #16

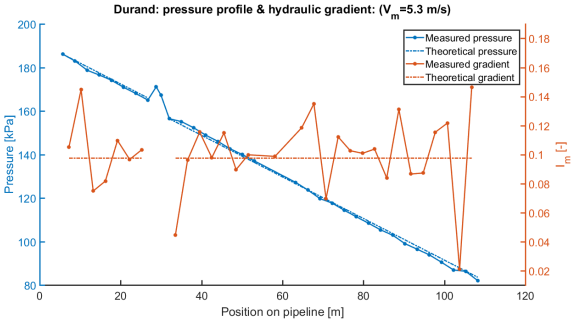

(a) Experiment #17

O

Dynamic waves: ultrasonic concentration measurement

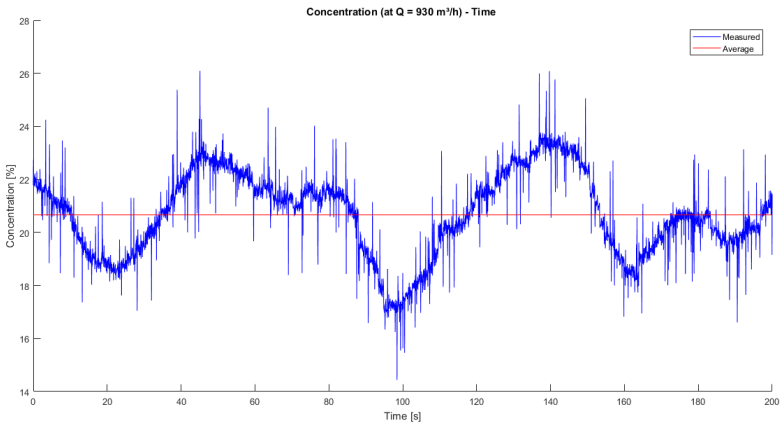

Figure O.1: Concentration: C=12%, V_m=3.7

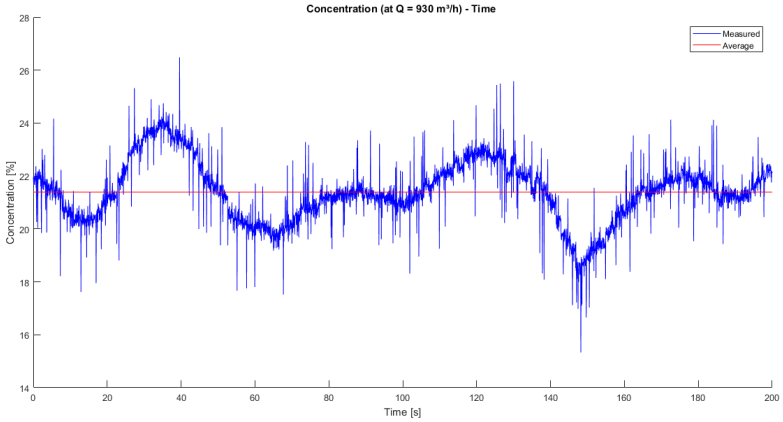

Figure O.2: Concentration: C=12%, V_m=3.7

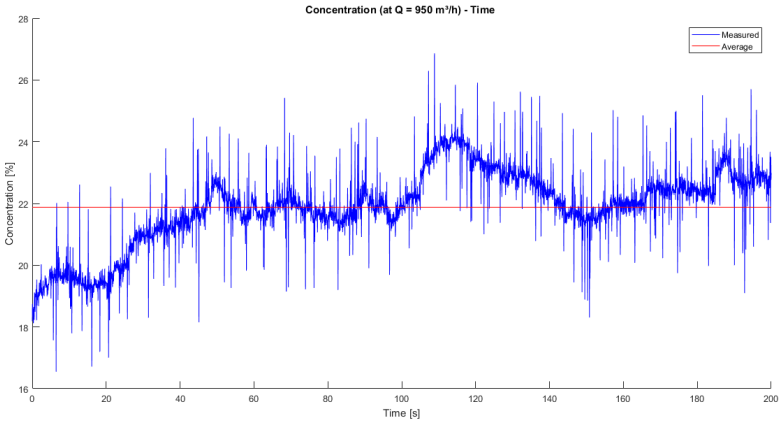

Figure O.3: Concentration: C=12%, V_m=3.7

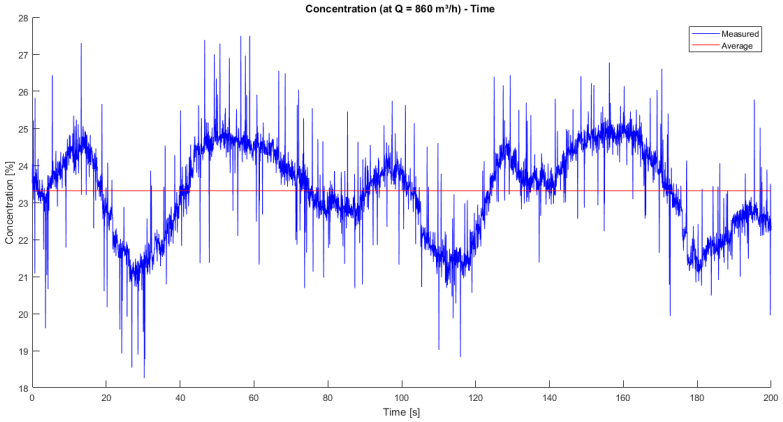

Figure O.4: Concentration: C=15%, V_m=3.4

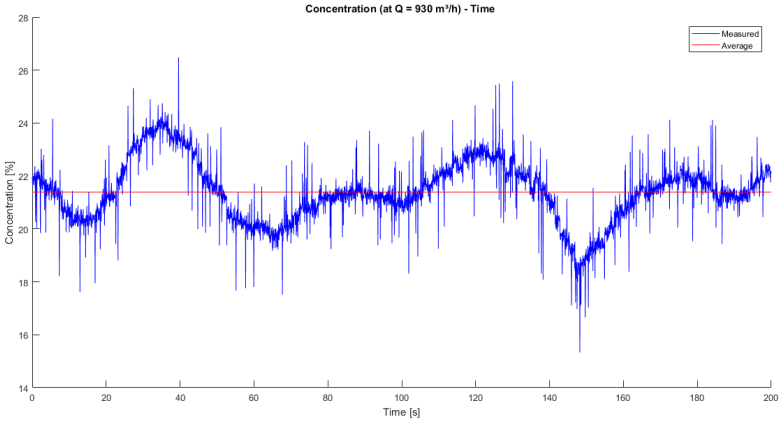

Figure O.5: Concentration: C=12%, V_m=3.4

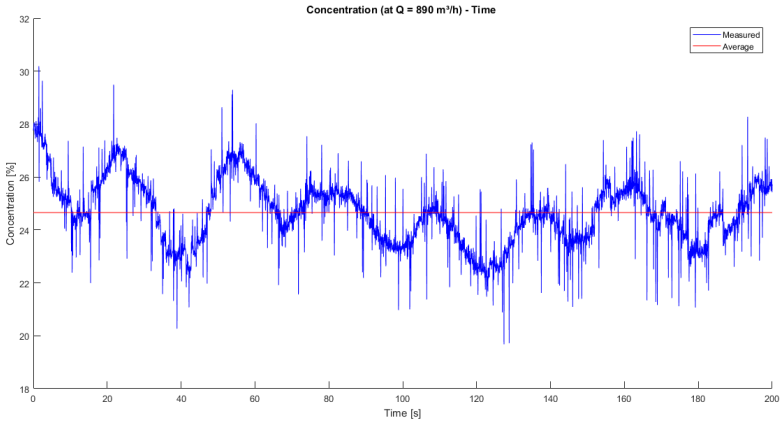

Figure O.6: Concentration: C=12%, V_m=3.5

Bibliography

S.W. Churchill. Friction-factor equation spans all fluid-flow regimes. *Chemical Engineering Journal*, 84: 94–95, 1977. ISSN 00092460.

R. Clift and D.H.M. Clift. Continuous measurement of the density of flowing slurries. *International Journal of Multiphase Flow*, 7(5):555–561, oct 1981. doi: 10.1016/0301-9322(81)90058-6.

C.F. Colebrook. Turbulent flows in pipes, with particular reference to the transition region between the smooth and rough pipe laws. *Journal of the Institution of Civil Engineers*, 11(4):133–156, feb 1939. doi: 10.1680/ijoti.1939.13150.

B. Cook, T. Bancroft (Directors), and P. Coats (Producer). Mulan. film, June 1998.

M.A. de Vreede. Hydraulic transport in inclined large diameter pipelines. mathesis, Delft University of Technology, April 2018.

R. Durand. Basic relationships of the ransportation of solids in pipes - experimental research. In *Minnesota International Hydraulics Convention*, pages 89–103, September 1953.

R.I. Ferguson and M. Church. A simple universal equation for grain settling velocity. *Journal of Sedimentary Research*, 74(6):933–937, November 2004. doi: 10.1306/051204740933.

A. Führböter. Uber die förderung von sand-wasser-gemischen in rohrleitungen. phdthesis, Technische Hochschule Hannover, 1961.

M. Gu, R. Liu, F. Ni, and L. Xu. Hydraulic transport of coarse gravel - a laboratory investigation into flow resistance. *18th World Dredging Congress*, pages 703–710, May 2007.

Hergé. *Le Lotus Bleu*. Les Adventures de Tintin. Casterman, 1936. ISBN 90-303-2510-0.

Hergé. *Tintin au Tibet*. Les Adventures de Tintin. Casterman, 1960. ISBN 90-303-2504-6.

A.P. Jufin and N.A. Lopatin. O projekte tuin na gidrotransport zernistych materialov po stalnym truboprovodam. -, 1966.

I.J. Karassik, J.P. Messina, P. Cooper, and C.C. Heald. *Pump Handbook: Third Edition*, pages 8.53–8.56. McGraw-Hill Professional, 3rd edition, 2000. ISBN 9780070340329.

A. Linder. This is officially the hottest day in shanghai in at least 145 years, July 2017. URL `http://shanghaiist.com/2017/07/21/shanghai-record-high-heat.php`.

V. Matoušek. *Flow mechanism of sand-water mixtures in pipelines*. phdthesis, Delft University of Technology, 1997.

V. Matoušek. Pressure drops and flow patterns in sand-mixture pipes. *Experimental Thermal and Fluid Science*, 26(6-7):693–702, aug 2002. doi: 10.1016/s0894-1777(02)00176-0.

V. Matoušek. Dredge pumps and slurry transport, September 2004a.

V. Matoušek. Dredge pumps and slurry transport, September 2004b.

V. Matoušek. personal communication, 2018.

V. Matoušek and J. Krupička. Different types of unsteady flow of solids generated in laboratory slurry pipe loop. *16th Int. conf. Transport & Sedimentation of Solid Particles*, pages 19–32, 2013.

H. Mees. *The Chinese Birdcage: How China's Rise Almost Toppled the West*, chapter Introduction, pages X–XVI. Palgrave Macmillan, 2016. ISBN 978-1-137-58888-3.

S.A. Miedema. An analytical approach to explain the führböter equation. *Proceedings of the Institution of Civil Engineers - Maritime Engineering*, 167(2):68–81, June 2014. doi: 10.1680/maen.13.00023.

S.A. Miedema. *Slurry Transport Fundamental, A Historical Overview & The Delft Head Loss & Limit Deposit Velocity Framework*. SAM-Consult, 2nd edition, December 2016a. ISBN 978-94-6186-690-5.

S.A. Miedema. *Slurry Transport Fundamental, A Historical Overview & The Delft Head Loss & Limit Deposit Velocity Framework*, chapter Chapter 2: Dimensionless Numbers & Other Parameters., page 17. SAM-Consult, 2nd edition, December 2016b. ISBN 978-94-6186-690-5.

L.F. Moody. Friction factors for pipe flow. *Transactions of the American Society of Mechanical Engineers*, 66:671–681, 1944.

C. Ransmayr. *Cox of het verglijden van de tijd*. Prometheus, 1st edition, April 2017. ISBN 978-90-4463-294-1.

L. Rich, J. Wilcox, G. Foster, D. Sellers (Producers), and C. Cain (Director). The amazing panda adventure. film, August 1995.

A. Sellgren, R. Visintainer, J. Furlan, and V. Matoušek. Pump and pipeline performance when pumping slurries with different particle gradings. *The Canadian Journal of Chemical Engineering*, 94(6):1025–1031, apr 2016. ISSN 0008-4034. doi: 10.1002/cjce.22489.

P.K. Swamee and A.K. Jain. Explicit equations for pipe flow problems. *Journal of hydraulics division*, 102(5):659–660, 1976a.

P.K. Swamee and A.K. Jain. Explicit equations for pipe flow problems. *Journal of the hydraulics division*, 102(5):657–664, 1976b.

A.M. Talmon. Self excitation of concentration fluctuations in dredge pipelines. In *WODCON XVII: "Dredging in a Sensitive Environment"*, 2004.

A.M. Talmon. Stationary waves measured behind a bend in heterogeneous transport. *17th Int. conf. Transport & Sedimentation of Solid Particles*, 2015. ISSN 0867-7964.

A.M. Talmon. Dredge pumps and slurry transport. Presentation, March 2017.

A.M. Talmon, L. Aanen, and R. Bakker-Vos. Laboratory tests on self-excitation of concentration fluctuations in slurry pipelines. *Journal of Hydraulic Research*, 45(5):653–660, sep 2007. doi: 10.1080/00221686.2007.9521801.

R. Terlou. Langs de oevers van de yangtze: De chinese droom, February 2016. URL https://www.vpro.nl/programmas/yangtze/kijk/afleveringen/2016/1.html.

R. Terlou and M. Krijgsman. Langs de oevers van de yangtze, February 2016.

H. van Es and J. Boone. Stationary waves in slurry pipe flow. resreport, Delft University of Technology, June 2015.

K.C. Wilson, G.R. Addie, A. Sellgren, and R. Clift. *Slurry transport using centrifugal pumps*, pages 173–177, 305–308. Springer Science+Business Media, Inc., 3rd edition, 2006a. ISBN 978-03-8723-262-1.

K.C. Wilson, G.R. Addie, A. Sellgren, and R. Clift. *Slurry transport using centrifugal pumps*. Springer Science+Business Media, Inc., 3rd edition, 2006b. ISBN 978-03-8723-262-1.